Rheological Properties of Cemented Paste Backfill with Iron Oxide and Aluminum Oxide Nanoparticles

Raouf Kaviani

A thesis submitted to the University of Ottawa
in partial fulfillment of the
requirements for the degree of
Master of Applied Science
in Civil Engineering

under the supervision of
Dr. Mamadou Fall
Department of Civil Engineering
Faculty of Engineering
University of Ottawa

Abstract

Among the various options for managing mining waste, cemented paste backfills (CPB) have become important in mining operations worldwide due to their technical, economic, and environmental advantages. CPBs are cementitious materials produced by mixing residues with a solid percentage ranging from 70 to 85%, fresh water or water from mineral processing, and a hydraulic binder, typically representing 3 to 7% of the weight. Typically, these elements are blended and mixed on the surface before being moved (either by gravity or by pumping) to underground mining voids, or cavities, where CPBs can be utilized for waste residue management, maximizing mineral recovery, and supporting underground mines. The key properties of CPBs include mechanical stability (usually assessed through strength), cost (dependent on binder consumption), transportability (dependent on rheological properties), durability, and environmental performance (usually measured by leachability, permeability, and reactivity). The most commonly used binder in CPB preparation is Portland cement (PC). PC is not only an expensive binder, but its production also consumes a significant amount of energy, thus generating a substantial amount of CO_2. Cement consumption can account for up to 80% of the CPB cost. The aforementioned factors have compelled mining companies to seek alternatives to cement that enhance CPB strength, reduce cement content, and decrease the carbon footprint of the mining industry. Iron oxide (Fe_2O_3) and aluminum oxide (Al_2O_3) nanoparticles represent the latest additive suggested to reduce the binder content of cemented backfills, increase their strength and improve their environmental footprint. However, the rheological properties of CPBs containing Fe_2O_3 and Al_2O_3 nanoparticles are not well understood. It is necessary to address this knowledge gap. Therefore, the primary objective of this research is to study the evolution of rheological properties (yield stress, viscosity) of CPBs containing Fe_2O_3 and Al_2O_3 nanoparticles. The investigation also involves measuring the materials' pH and Zeta potential, microstructural studies (TG/DTG and XRD), and electrical conductivity (EC). The findings show that adding Iron oxide (Fe_2O_3) and aluminum oxide (Al_2O_3) nanoparticles to CPB significantly changes its rheological properties, which in turn affects flowability. The yield stress and viscosity of CPB samples are greatly increased by the incorporation of nanoparticles, with the degree of influence varying based on variables including water content, curing duration, and type of binder. Because of the nanoparticles-induced microstructural changes in the CPB material, the interaction of Iron oxide (Fe_2O_3) and aluminum oxide (Al_2O_3) nanoparticles and a larger fraction of nanoparticles, along with an increase in curing time, raises rheological characteristics and decreases paste flowability. The results of EC, DTG, and XRD, which show that binder hydration rises with nanoparticles dosage, corroborate this. Furthermore, as nanoparticles increases, the zeta potential decreases in magnitude, which lowers flowability and repulsion force. However, EC, XRD, and DTG experiments indicate that the addition of 0.125% superplasticizer is identified as a compensator for the lower flowability caused by nanoparticles. These tests also suggest that the superplasticizer causes a drop-in cement hydration rate at very high ages. Additionally, it has been found that increasing the slag percentage from 0% to 50% and 75% of the binder content effectively increases yield stress while only marginally decreasing viscosity. The results of this research could significantly benefit the mining industry and enable a more environmentally friendly design of CPBs and improved residue management practices.

DEDICATION

To my beloved sister Moha

ACKNOWLEDGMENTS

I would want to thank my supervisor, Dr. Mamadou Fall, from the bottom of my heart. Honestly, I could not have finished this thesis without his help, direction, and encouragement in both my personal and research endeavors.
A special thank you to Jean Claude Célestin and all of my friends for their unwavering support and encouragement during my academic career.
Lastly, I would like to express my gratitude to F. Hasari and M. Kavani, my inspirational parents, for their unwavering love and support throughout the years.
Finally, but just as importantly, I would like to sincerely thank and admire my amazing sister Moha.

List of Symbols and Abbreviations

CH: Calcium hydroxide
CPB: Cemented paste backfills
C-S-H: Calcium silicate hydrate
DTG: Differential thermogravimetry
EC: Electrical conductivity
hrs: Hours
min: Minutes
MIP: Mercury intrusion porosimetry
9MT: Nine mine tailings
OPC: Ordinary Portland cement
PC: Portland cement
PCI: Portland Cement – Type I
PSD : Particle size distribution
Sec : Seconds
Slag: Blast furnace slag
ST: Silica tailings
TGA: Thermogravimetric analysis
Temp.: Temperature
TG: Thermal gravimetry
w/c: Water-to-cement ratio
wt.%: Percentage of total dry weight
nFeO: nano Iron Oxide particles
nAlO: nano Aluminum Oxide
nP: nano particle
SP: Superplasticizer
XRD: X-ray diffraction
Nanop: nano particle

Table of Contents

Table of Figures

Table of Tables

Table of equations

1 Chapter 1. Introduction

1.1. General Statement

The mining industry stands as a cornerstone of modern civilization, furnishing indispensable minerals and metals essential for contemporary life. Across the globe, this sector plays a pivotal role in economic advancement, employment generation, and overall societal development. In Canada, particularly, the mining industry serves as the backbone of the national economy, contributing billions of dollars annually and sustaining hundreds of thousands of jobs.

However, amidst the prosperity it brings, the mining sector grapples with significant environmental challenges and safety hazards stemming from conventional waste management practices. The extraction and processing of mineral resources yield substantial waste, including tailings and waste rock, while large-scale underground mining operations can trigger geotechnical issues such as ground subsidence and instability.

Traditional methods of waste disposal, like surface tailings ponds and dams, pose environmental risks such as acid mine drainage and jeopardize neighboring communities' well-being. The failure of these techniques can lead to disastrous consequences, both environmentally and financially.

In response to these challenges, modern mining practices are witnessing a paradigm shift towards more sustainable and technologically advanced solutions, particularly in North America. One such innovation is mine backfilling, which involves relocating extracted material underground to enhance ground conditions, mitigate environmental impact, and ensure worker safety.

Among the various backfilling techniques, cemented paste backfilling (CPB) emerges as a promising approach. CPB, comprising tailings, water, and binders, is mixed on the surface (often) and then transported underground to fill stopes or voids. This not only provides essential support for underground operations but also reduces surface-level waste exposure and lowers construction costs for surface tailings storage facilities.

The widespread adoption of CPB is driven by its manifold benefits, including environmental sustainability, enhanced safety, and economic efficiency. Engineering design factors such as cost, transportability, and mechanical stability are meticulously considered to optimize CPB performance. Uniaxial compressive strength (UCS) testing and rheological analysis are employed to assess structural integrity and flow characteristics, respectively, ensuring operational efficacy and productivity. Key rheological properties of CPB include yield stress and viscosity.

As mining endeavors continue to evolve, the utilization of innovative technologies like CPB represents a crucial step towards achieving sustainable resource extraction practices. By prioritizing environmental stewardship, worker safety, and economic viability, the mining industry can uphold its vital role in global development while minimizing its ecological footprint.

1.1 Problem Statement

Portland cement (PC) is the most often used binder in CPB. The research states that up to 8% of global carbon dioxide (CO_2) emissions are currently attributed to the cement sector ([1]-[3]). Cement can make up as much as 80% of the backfill materials, and CPB can represent as much as 20% of the overall mining expenses ([4]- [5]). Accordingly, 1.6 to 2% of the total mining costs might be decreased with a 1% decrease in cement content [6]. The aforementioned factors have compelled mining companies to seek alternatives to cement that enhance CPB strength, reduce cement content, and decrease the carbon footprint of the mining industry. Thus, in recent decades, the use of binder composed of Portland cement and supplementary cementitious material, such as blast furnace slag (slag), also known as binary cement, has been increasingly

adopted in CPB technology and practice [7-14]. However, supplementary cementitious materials, such as slag, have some shortcomings. Although the addition of slag to Portland cement can lead to an increase of the strength of CPB at advanced ages and decrease the carbon footprint of CPB, it slows down the hydration of the cement at early ages, and thus decreases the mechanical strength and suction development in the CPB at early ages, which is negative for the mechanical stability of the CPB, the mining cycle and the safety of mine workers. Therefore, iron oxide (Fe_2O_3) and aluminum oxide (Al_2O_3) nanoparticles (nP) represent the latest additive suggested to reduce the binder content of cemented backfills, increase their strength and strength increase rate, and improve their environmental footprint as well as to address the shortcomings associated with the use of Slag. However, the rheological properties of CPBs containing Fe_2O_3 and Al_2O_3 nanoparticles are not well understood. It is necessary to address this knowledge gap. Moreover, how much the addition of superplasticizer to CPB systems with nanoparticles can improve their rheological properties is not well known.

1.2 Research Objectives

The primary objective of this research is to study the evolution of rheological properties (yield stress, viscosity) of CPBs containing Fe_2O_3 and Al_2O_3 nanoparticles.
The specific objectives of this research are:

- Influence of Nano-Iron Oxide (nFeO) and Nano-Aluminum Oxide (nAlO) on the rheological properties of CPB made of Portland cement.
- Influence of Nano-Iron Oxide (nFeO) and Nano-Aluminum Oxide (nAlO) on the rheological properties of CPB that contains Slag.
- Influence of Nano-Iron Oxide (nFeO) and Nano-Aluminum Oxide (nAlO) on binder hydration in CPB.
- Impact of superplasticizer on the rheological properties of CPB with nFeO or nAlO.
- electric conductivity in CPB samples with different dosages of cement slag and, nP and superplasticizer.

1.3 Research Approach and Methodology

The research approach and methodology adopted in this research are displayed in Figure 1.1. The first section provides a detailed introduction to the theoretical and technical foundation of CPB.

Additionally, a program of experiments to investigate the impact of nP and superplasticizer on the characteristics of CPB in its fresh states is presented. To investigate the influence of the nP and superplasticizer on fresh properties, the program is further split into two sections. Tests are done in the initial phase to gain a better understanding of the yield stress and viscosity of CPB, with a focus on its rheological behavior. Binary binders with a PCI/Slag ratio of 50/50 and 75/25 are used to prepare the two groups of control CPB samples. Furthermore, CPB samples with a (PCI-Slag) are cast by partially substituting nP (0, 1, and 3 weight percent of the total binder) for slag in increasing amounts. Additionally, we added 0.125 percent of the binder as superplasticizer. The yield stress and viscosity of the freshly prepared samples are further examined at room temperature for curing durations of 0, 0.33, 1, 2, and 4 hours, respectively. In order to comprehend the rheological behavior of the previously described samples, electrical conductivity (EC) monitoring experiments, XRD and TG/DTG analyses are carried out. Chapters 3 and 4 include the experimental program's specifics. Ultimately, a discussion of all the study's findings is held, conclusions are reached, and suggestions for further research are made in order to advance the existing work.

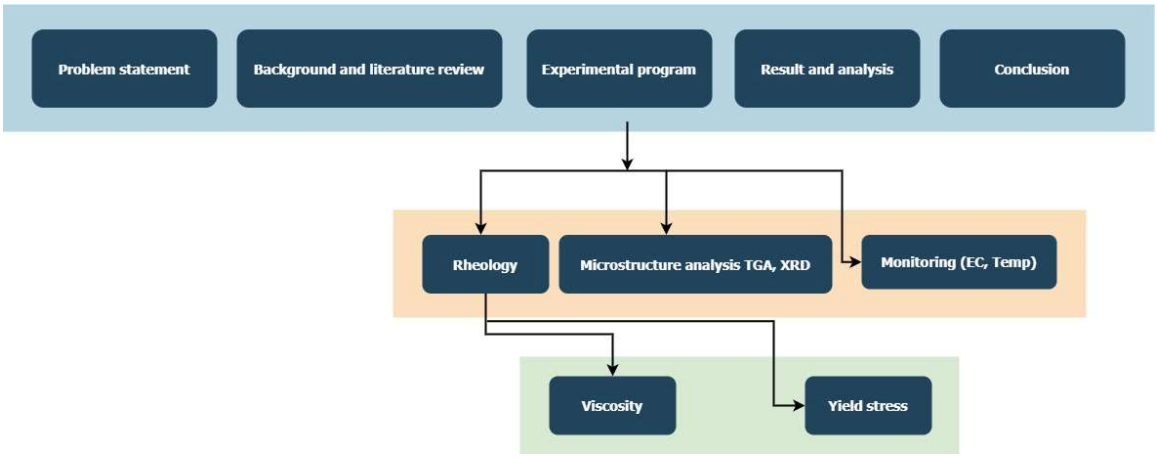

Figure 1.1 Experimental program and research methodology

1.4 Thesis Organization

The thesis manuscript is organized as follows:

Chapter 1 gives a succinct overview of the research and contains the general statement. It explains the problem statement, the goals of the investigation, and the research techniques used.

Chapter 2 includes review of background information on mining, mine backfill, CPB technology and CPB rheology. The significance of researching the fresh properties of CPB is emphasized in this chapter. In addition, a review is carried out to examine the binders that are frequently used to prepare CPB, the impact of nanoparticles on cement hydration and the properties of cementitious materials.

Chapter 3 includes the Technical Paper I. The primary focus of this paper is to examine how the affects the rheological characteristics of CPB while it is fresh. Section 3.3 discusses the impact of using a binary cement blend (PCI-Slag-nFeO-SP) on the rheological properties.

Chapter 4 presents the Technical Paper II. The primary focus of this paper is to examine how the affects the rheological characteristics of CPB while it is fresh. Section 4.3 discusses the impact of using a binary cement blend (PCI-Slag-nAlO-SP) on the rheological properties.

Chapter 5. gives an overview of the findings from this investigation and sheds light on how the usage of nP affects the properties of CPB while it's fresh; and environmental performance are then covered. This chapter also presents the key conclusions of this research and recommendations for future studies.

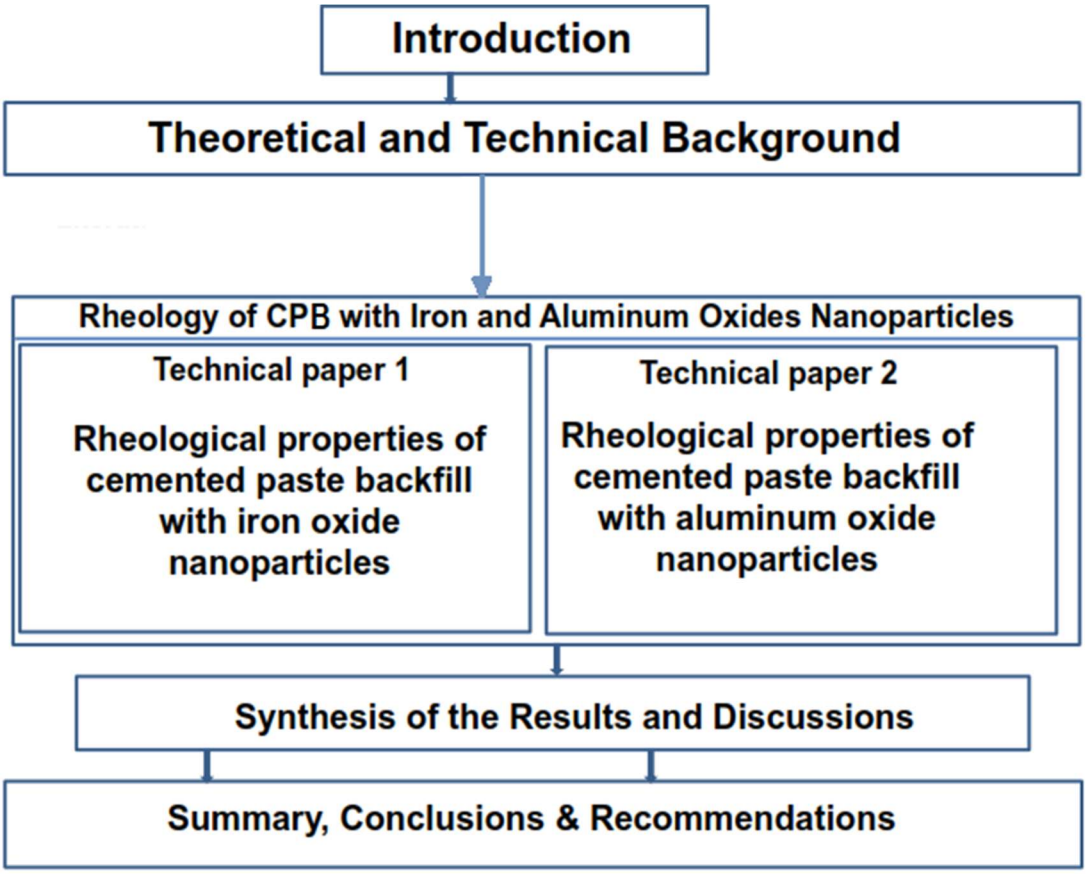

Figure 1.2 Flowchart for organizing a thesis

1.5 References

[1]. Filippo, J. D., Karpman, J., & DeShazo, J. R. (2019). The impacts of policies to reduce CO2 emissions within the concrete supply chain. Cement and Concrete Composites, 101, 67–82. https://doi.org/10.1016/j.cemconcomp.2018.08.003

[2]. Gartner, E., & Hirao, H. (2015). A review of alternative approaches to the reduction of CO2 emissions associated with the manufacture of the binder phase in concrete. Cement and Concrete Research, 78, 126–142. https://doi.org/10.1016/j.cemconres.2015.04.012

[3]. Kajaste, R., & Hurme, M. (2016). Cement industry greenhouse gas emissions – management options and abatement cost. Journal of Cleaner Production112, 4041–4052. https://doi.org/ 10.1016/j. jclepro. 20 15.07.055

[4]. Benzaazoua, M., et al. (2010). "Advances in Paste Backfill Technology for Underground Mining." Canadian Geotechnical Journal, 47(9), 931-949.

[5]. Grice, A. (1998). Underground Mining With Backfill. Proceedings of the 2nd Annual Summit-Mine Tail- ings Disposal Systems, 216, 234–239, 7.

[6]. Sadrossadat, E., Basarir, H., Luo, G., Karrech, A., Durham, R., Fourie, A., & Elchalakani, M. (2020). Multi- objective mixture design of cemented paste backfill using particle swarm optimisation algorithm. Minerals Engineering, 153, 106385. https://doi.org/10.1016/j.mineng.2020.106385

[7]. Vance, K., Aguayo, M., Oey, T., Sant, G., & Neithalath, N. (2013a). Hydration and strength development in ternary portland cement blends containing limestone and fly ash or metakaolin. Cement and Con- crete Composites, 39, 93–103. https://doi.org/10.1016/j.cemconcomp.2013.03.028

[8]. Zheng, J., Zhu, Y., & Zhao, Z. (2016). Utilization of limestone powder and water-reducing admixture in cemented paste backfill of coarse copper mine tailings. Construction and Building Materials, 124, 31–36. https://doi.org/10.1016/j.conbuildmat.2016.07.055

[9]. Courard, L., & Michel, F. (2014). Limestone fillers cement based composites: Effects of blast furnace slags on fresh and hardened properties. Construction and Building Materials, 51, 439–445. https://doi.org/10.1016/j.conbuildmat.2013.10.076

[10]. Carrasco, M. F., Menéndez, G., Bonavetti, V., & Irassar, E. F. (2005). Strength optimization of "tailor-made cement" with limestone filler and blast furnace slag. Cement and Concrete Research, 35(7), 1324–1331. https://doi.org/10.1016/j.cemconres.2004.09.023

[11]. Li, W., & Fall, M. (2018). Strength and self-desiccation of slag-cemented paste backfill at early ages: Link to initial sulphate concentration. Cement and Concrete Composites, 89. https://doi.org/ 10.10 16/j.cemconcomp.2017.09.019

[12]. Li, W., & Fall, M. (2016). Sulphate effect on the early age strength and self-desiccation of cemented paste backfill. Construction and Building Materials, 106, 296–304. https://doi.org/10.1016/j. conbuildmat. 2015.12.124

[13]. Fall, M., & Pokharel, M. (2010). Coupled effects of sulphate and temperature on the strength development of cemented tailings backfills: Portland cement-paste backfill. Cement and Concrete Composites, 32(10), 819–828. https://doi.org/10.1016/j.cemconcomp.2010.08.002

[14]. Solismaa, S., Torppa, A., Kuva, J., Heikkilä, P., Hyvönen, S., Juntunen, P., Benzaazoua, M., & Kauppila, T. (2021). Substitution of Cement with Granulated Blast Furnace Slag in Cemented Paste Backfill: Evalua- tion of Technical and Chemical Properties. Minerals, 11(10), 1068. https://doi.org/ 10. 33 90/min11101068

[15]. Haruna, S., & Fall, M. (2020). "Utilization of Cemented Paste Backfill for Underground Mining Applications: State-of-the-Art Review." Minerals, 10(6), 512.

[16]. Wu, D., Fall, M., & Cai, S. J. (2013). Coupling temperature, cement, hydration and rheological behaviour of fresh cemented paste backfill. Minerals Engineering, 42, 76–87. https://doi.org /10.1016 /j. mine- ng.2012.11.011

[17]. Xiao, B., Wen, Z., Wu, F., Li, L., Yang, Z., & Gao, Q. (2019). A simple L-shape pipe flow test for practical rheological properties of backfill slurry: A case study. Powder Technology, 356, 1008–1015. https://doi.org/10.1016/j.powtec.2019.09.012

2 Chapter 2 Technical Background and Literature Review

2.1 Introduction

Focusing on CPB, this chapter covers the basics of mining (section 2.2) and an introduction to mine backfill technology (section 2.3). Section 3 provides background information on the flowability and rheology of CPB. In addition, section 2.5 explains the hydration processes of the main binders commonly used in CPB, as well as the impact of nanoparticles on cement hydration and cementitious material properties. Section 2.7 describes the main experimental tests and analytical techniques used in the present research. The background information and literature review provided in this chapter will facilitate understanding of the experimental programs carried out as part of this research and the results obtained.

2.2 Mining

Major economic activity and a multibillion-dollar industry, mining is found in many nations, including Australia, Canada, China, India, and South Africa. To reach, remove, and handle important mineral ores from the Earth's crust, the mining industry employs a variety of techniques [1]. While underground mining is used to extract deep mineral resources, open-pit mining is utilized to collect shallow minerals. Mining is currently expanding into deeper levels, which can be as deep as 4350 m (Mponeng Gold Mine, South Africa), due to the paucity of surface minerals and technological developments in the search for lucrative minerals [2]. Globally, mining products are extracted in the millions of metric tons. However, large volumes of mining waste, such as tailings, and large subterranean voids are produced when ore is removed from the ground [3]. The waste-to-product ratio in metal mining is typically 100:1, although it can occasionally reach 1,000,000:1 ([4]; [5]). Traditional tailings disposal techniques, such as piling, stacking in tailings dams, and surface impoundment, may have detrimental effects on the environment and geotechnical hazards, such as groundwater contamination and AMD in certain situations ([6]; [7]). These geotechnical hazards include tailings dam failure and large voids that may collapse [8].

2.3 Mine backfilling and main types of mine backfills

Backfilling is the process of filling subterranean cavities with waste material for engineering or disposal purposes. It is a widely utilized technique in Canadian metal mines [10]. The most effective method for getting rid of mining waste, establishing a secure workplace, and assisting with underground activities is backfilling [9]. Backfill assistance has been employed in some capacity by about 69% of all underground mining operations in Ontario, or 65% of all operations in Canada [12]. Three primary backfill kinds are typically utilized, as described in ([13]; [9]). These are rock, hydraulic, and cemented paste backfills. Their qualities, along with economic considerations and future mine-related objectives, determine the type of backfill that is used [15].

2.3.1 Hydraulic backfill

Tailings, river or crushed sand, rock fragments, etc. combined with water and a binder is known as hydraulic backfill ([15]; [9]). It is processed on the mine's surface or below ground, and water is used as the transportation medium to move it via the hydraulic head produced by gravity or pipeline distribution systems. Hydraulic backfill, also known as slurry backfill, can be either cemented or non-cemented and has a high permeability of between 10^{-5} and 10^{-6} m/s and a low density of between 40-50% and 60-70% of solids by weight [17].

The following are some benefits of hydraulic backfill:

i. Easy to set up and use,

ii. More easily managed backfill material, and

iii. Less expensive transportation by gravity.

But with hydraulic backfilling, drainage either mechanical or gravity is necessary to eliminate extra water

from the backfill material. Thus, one of the most economical mining techniques is hydraulic backfilling with non-cemented minerals when small waste particles are available [16]. Additionally, hydraulic backfill is more likely to liquefy, which poses a serious risk to worker safety in underground mines. Disadvantages of this backfilling technique include cement washing, cement segregation from the solid phase and a substantial amount of excess water ([105]; [21]).

2.3.2 Rock backfill

Waste rocks, stone, gravel, and tailings are among the materials found in rock backfill; these materials can be utilized either in their cemented or uncemented condition [22]. Usually, 4% to 8% cement is applied when using cemented backfill. Before being placed, waste rock can be combined with cement paste via pipelines. Typically, the particle size distribution (PSD) pattern is followed when crushing, screening, and mechanical mixing are used to produce the raw material. This approach is practical and economical, offering advantages including turning large amounts of waste into useable land by moving them underground, lessening pollution to the environment, boosting site stability, and lowering the risk of land subsidence by adding more support. On the other hand, rock backfilling has the following drawbacks ([22]; [26]):

i. It uses costly equipment and requires a lot of labor.
ii. Challenging to maintain effective quality control and segregation management.
iii. Plant structure is complex and efficiency is low.

2.3.3 Cemented paste backfill (CPB)

Cement paste backfilling was initially employed in 1957 at the Bad Grund Mine in Germany [28]. The method reduced solid waste on the mine surface by using up to 60% of the mined material below as the main support element. Next, at its Lucky Friday Mine in the United States, the Hecla Mining Company used cement paste backfilling. CPB was effectively employed in Australian and Canadian mines in the 1990s to replace rock and hydraulic fills ([6]; [11]; [29]-[34]). CPB as a new cementitious material composed of tailings (70–85% wt.%), water (fresh or processed), and a minimal dosage of hydraulic binder (2–8 wt.%) ([29]-[34]).

Because of the non-Newtonian fluid behavior of this mixture and the reduced water needed for preparation, strength growth can occur more quickly [17]. The CPB mix is typically made in the backfill plant on the mine's surface and then piped to the subterranean stopes (Figure 2.1). In order to prevent water and tailings particle segregation and settlement during transportation, the mixture should consist of 70–85% solids by total mass. The backfill must contain at least 15% of particles smaller than 20 μm ([35]; [21], [18]). In underground mines ([36]; [31]; [19]), CPB is cured and as it reaches the stopes, ultimately providing support to the neighboring stopes [20].

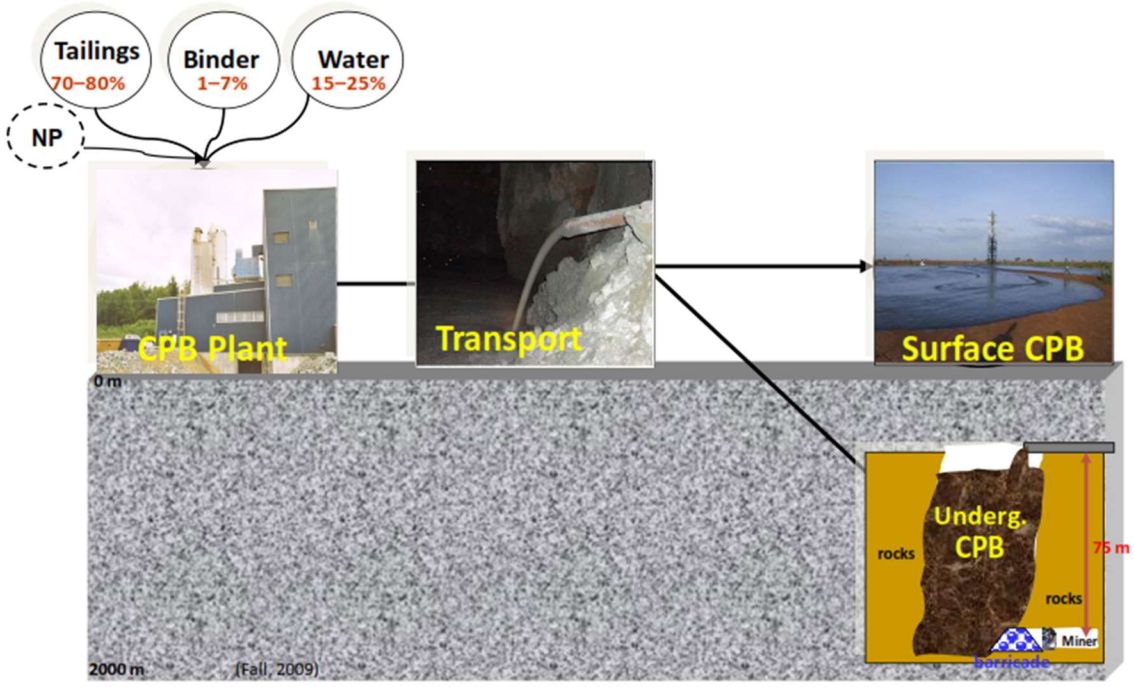

Figure 2.1 The basic arrangement for placing the CPB underground [75].

Because of CPB's advantages in terms of technology, economy, and environment, both industry and academia are becoming more interested in it. Among the benefits are:

i. CPB reduces the dangers of tailings pond failure and contamination of surface and subsurface water [5].
ii. CPB maximizes mine tailings density while minimizing the environmental impact of surface tailings ponds.
iii. CPB reduces the mining cycle, which increases the rate of ore recovery ([29]; [30]; [37]).
iv. It increases the safety, efficiency, and productivity of mining by increasing the stability (local and regional) of subterranean voids ([6]; [11]; [39]-[41]).
v. It enables the co-disposal of wastes and industrial byproducts that pose a chemical challenge, hence minimizing adverse effects on the environment ([8]; [29]; [30]).
vi. Not like hydraulic filling, which requires water drainage [42].

2.4 Flow ability and rheology of CPB

As previously indicated, CPB mixtures are carried underground by pumping, gravity, or a combination of the two after being prepared in a paste backfill plant, which is normally found on the mine's surface ([43]; [45]). The quantity of energy needed to convey the combination determines which delivery technique is used. Furthermore, as technology develops, the mining sector is growing to new heights. As a result, the effective and practical transportation of CPB is difficult and financially significant for the CPB plant's entire operation [43]. Because of this, one of the main concerns when transporting CPB to the mine stope is its flowability. It is essential because insufficient flowability can lead to pipeline blockages, which can delay transportation and result in losses of money ([46]; [47]). The fresh CPB mix's flowability, which depends on its rheological properties, determine how well CPB is transported. The study of how materials flow and deform in response to stresses or outside pressures is known as rheology [49]. The primary rheological factors that govern the flowability, pumpability, and pourability of backfill are the yield stress and viscosity of fresh paste backfills ([44]; [39]; [45]; [46]).

Because CPB mixes behave in a non-Newtonian manner, the rheological characteristics of CPB are examined using the Bingham plastic flow model. Particle characteristics, including size and distribution (also known as particle-size distribution, or PSD), surface area, diameter, particle distance, packing fraction, and solid volume fraction, all have a significant impact on the rheology of concentrated suspensions, including cemented paste backfill ([9]; [10]; [50]; [51]). Interparticle interactions have also been found to dominate the rheology of the paste in a number of studies.

2.5 Binder System Hydration Mechanisms

Among the various binders used in CPB, Portland cement (PC) stands out as the most widely utilized due to its accessibility and adaptability ([14]; [41]). As a binder, PC not only imparts compressive and tensile strength, but also enhances stiffness and cohesion in CPB. Furthermore, it is instrumental in shaping the microstructure of CPB, affecting consolidation, settlement, porosity, and hydraulic permeability ([70]; [71]).

However, PC is not only an expensive binder but also requires significant energy for its production, leading to substantial CO_2 emissions. Cement consumption can account for up to 80% of the cost of CPB. These factors have driven mining companies to seek alternatives that reduce cement content and decrease the carbon footprint of the mining industry. One such alternative is the use of ground blast furnace slag (Slag) as a partial substitute for PC in CPB technology. Slag is cost-effective and can improve the microstructure and strength of CPB systems at later ages. It is one of the most commonly added supplementary materials in CPB as a partial replacement for cement. This substitution not only reduces cement costs but also decreases the overall energy required for cement production, thereby lowering the mining industry's carbon footprint. Slag has a significantly lower embodied carbon content compared to PC—67 kg/tonne versus 913 kg/tonne, according to a 2014 technical datasheet [107]. Additionally, by enhancing the microstructure and strengthening the CPB mix at older ages, slag improves the overall long-term performance of the mix.

However, since slag is a latent hydraulic product, it can negatively affect the early strength of the CPB. Early strength gain is crucial for the mechanical stability of underground mine cavities and the timely opening of barricades, which is essential for shortening operating cycles and increasing mine productivity. To address these limitations, the addition of nanoparticles to the CPB binder system is being explored. Nanoparticles such as iron oxide (Fe2O3) and aluminum oxide (Al2O3) are currently being considered in CPB research to counterbalance the limitations of slag and increase the early strength of CPB.

In the following sections, the hydration mechanisms of Portland cement (PC) and PC/Slag systems will be described and analyzed. Following this, the impact of nanoparticles on binder hydration will be examined. These discussions aim to enhance the understanding of the results presented in this thesis.

2.5.1 PCI hydration mechanism

Ordinary Portland Cement (OPC) is produced by grinding clinkers, which are typically composed of calcium carbonate ($CaCO_3$), some gypsum (CSH2, 2-8%), and calcium sulphate, and heating them to a temperature above 1450ºC. The five chemical components that makeup OPC are silicon dioxide (SiO_2), calcium oxide (CaO), iron oxide (Fe_2O_3), aluminum oxide (Al_2O_3), and sulfur trioxide (SO_3). The OPC hydration process consists of four phases, involving a heterogeneous mixture, as described in detail below [72]. Tricalcium silicate (C_3S, also known as alite) is the main mineral component. It forms calcium silicate hydrate (C-S-H) and portlandite (CH), which greatly increase the cement paste's overall strength.

$$C_3S + 6H_2O \rightarrow C_3S_2.3H_2O + 3Ca(OH)_2$$

Equation 2.1

Di-calcium silicate, also known as belite or acetylene sulfide (C_2S), is the secondary mineral component. It yields the same hydration products as C_3S but with less CH. Furthermore, C_2S contributes more to strength development later in life but less to early-age development because of its lower solubility and slower rate of hydration compared to C_3S.

$$C_2S + 4H_2O \rightarrow C_3S_2.3H_2O + 3Ca(OH)_2$$

Equation 2.2

Lastly, the final two mineral components of the heterogeneous mixture are represented by tricalcium aluminate ($Ca_3Al_2O_3$), also known as C_3A, and calcium aluminoferrite ($Ca_4Al_2Fe_2O_{10}$), also known as C_4AF. Cement typically contains a smaller percentage of C_3A than silicates (C_3S). In contrast to the silicates, C_3A reacts more quickly and dissolves more readily. Aluminates react with cement as soon as water is added, causing flash setting and potentially affecting cementitious mixes' workability [73]. CSH2 is added to the cement in order to avoid these problems. CSH2 dissolves instantly, interacts with the hydration products to form ettringite, and releases calcium and sulphate ions into a solution in the pores.

Additionally, ettringite reacts with C_3A to generate monosulphoaluminates since CSH2 is insufficient to react with all of the C_3A present. Tetra-calcium alumino-ferrite (C4AF) regulates the pace of heat changes during hydration, while C_3A starts the chemical processes in cement (which contains silicate) ([73]; [42]).

$$4C_4AF + 2Ca(OH)_2 + 10H_2O \rightarrow C_3A.6H_2O + 3C_3F.6OH_2$$

Equation 2.3

When exposed to water, PC, the reactive phase of CPB, experiences a hydration reaction. Moreover, the main products generated during hydration are (a) C-S-H ($3CaO\bullet 2SiO_2\bullet 3H_2O$), which accounts for 60–70% of the hydration products, (b) CH, or calcium hydroxide (Ca (OH)2), which accounts for 20–25% of the hydration products, and (c) CSH2, ettringite, and calcium aluminate, which account for 15–20% of the hydration products [41]. The remaining solid products are tricalcium aluminate monosulphate hydrate (C3A•CaSO4•12H2O) or monosulphate (AFm phase) and tricalcium aluminate trisulphate hydrate (C3A•3CaSO4•32H2O) or ettringite (AFt phase) ([72]; [74]).

Five steps make up the cement hydration process: the initial mixing reaction, which takes 15 to 30 minutes; the induction or dormant period, which lasts for 1 to 3 hours; the acceleration period, which occurs 3 to 17 hours after mixing cement and water; the deceleration period, which lasts for 18 to 48 hours; that is, until the mixture contains both unhydrated cement grains and water; and densification, which occurs 48 hours to years ([42]; [73]; [75]; [76], [77]; [105]). For further information, the stages are as follows.

(i) First mixing reaction: The early hydration reactions involve the dissolution of PC grains, wherein highly reactive aluminates and CSH2 dissolve quickly. This leads to the release of ions into the pore fluid, along with Ca2+, silicates, aluminate Al3+, hydroxide OH-, sulphate SO4 2-, and alkali ions like K^+ and Na^+ ([78]; [42]);

(ii) The induction, also known as the inactive period, is characterized by the formation of a semi-permeable protective membrane (a gel of Al, Si, Ca, and S) around the cement particles and the hydrating cement grains, which inhibits additional hydration. Water enters the cement particle when the membrane around it bursts due to the calcium silicates' interaction (C_3S and C_2S). The material is mainly in a colloidal form and is known as the gel phase, even though initial crystallization begins ([42]; [72]).

(iii) Acceleration period: During this time, the C_3S and C_2S react, forming C-S-H gel and a supersaturated Ca and OH solution in the pore solution. During this time, C-S-H rapidly grows

and makes for up to 60% of the cement hydration products' total volume. The formation of CH, calcium sulphoaluminate, or ettringite (AFt) accelerates. At the conclusion of the acceleration process, C-S-H covers bigger grains, while PC grains (<3-5 mm) are entirely dissolved ([42]; [72]).

(iv) The last stage of cement hydration, known as the "deceleration period," is when AFm is formed from the reaction of AFt and C_3A. Hydration products like C-S-H and CH continue to form throughout this time, albeit more slowly. In the hydrated PC pastes, C-S-H makes up 60% of all the hydration products, with CH and Aft making up the remaining 20%. The more stable monosulphate is produced from the less stable AFt. After reaching its peak, the heat of hydration starts to decline ([42], [72]).

(v) Densification is the gradual dissolution of the belites and alites into a solid mass of CH and C-S-H. Diffusion is used to fully control the reaction's rate. High strength, extremely low porosity, and low hydraulic conductivity may take several years to develop at this point [42].

2.5.2 Slag/PCI system hydration mechanisms

. Slag typically hydrates more slowly than cement (PC), but when water is present, it can react with lime to create cementitious materials that are insoluble. To expedite the hydration process, an alkali activator may be necessary in certain circumstances [38].

Slag contains pozzolanic qualities and is a byproduct of the iron industry. Pozzolans are amorphous materials composed of siliceous or aluminosilicate minerals. In a blast furnace that produces iron, pyrometallurgical operations yield slag. It forms concurrently with iron in the molten state, and water quickly cools it down. Melting slag is reduced to glassy granular particles by the quick cooling, which also prevents crystallization ([79]; [80]). Since this affects the hydraulic reactivity of slag, further grinding to a particular slag fineness (cement fineness or finer) is done after this [81]. Because of its glassy nature, slag's response depends on the hydroxyl ions created when cement hydrates to break down its glassy structure. Cement undergoes hydration, which releases hydration products and CH, which releases hydroxyl (OH^-) and alkali (Ca^{2+}) ions. This causes the slag's glassy structure to melt, raises the pH of the pore solutions, and causes the slag in cement-slag systems to hydrate [14].

Moreover, extra secondary C-S-H gel is formed when activated slag combines with alkali hydroxide Ca $(OH)_2$, which is liberated by the cement hydration reaction [106]. These C-S-H have a lower Ca/Si ratio than those synthesized using PC, but otherwise they are comparable [82]. The capillary pore space left by the primary cement hydration products is filled with further produced secondary C-S-H gel [82].

The glass content [84] and the physical and chemical characteristics of the slag [85] of the slag are related to the rate of hydration. Slag's reactivity, which is influenced by the grade utilized, determines how much strength it develops. As per ASTM C989 (2014) and ACI 233R-03, slag is classified into three strength classifications, which are primarily determined by the slag quality, fineness, and possible additions of calcium sulfate. Slag is divided into three basic grades, 80, 100, and 120, based on the activity index.

$SP/\mathrm{P} * 100$ is the activity index. Additionally, at all ages, the strength of Grade 80 slag is less than that of the reference cement.

In Grade 100, the strength improvement is less in the early ages of 1 to 21 days, but it increases to an equal or greater degree at the later ages. Strength in grade 120 slag decreases until the third day, but then increases starting on the seventh day (ACI 233, 2003, [55]).

Slag partial replacement of cement in CPB formulations shows promise [86]. Additionally, a 5-weight percent addition of slag results in a decrease in the pores' threshold diameter from 2 microns to 1 micron [27]. Previous studies have demonstrated that a potential binder for CPB can be produced by partially replacing cement with slag ([29]; [30]) [69]-[71]; [109]).

2.5.3 Influence of nanoparticles on cement hydration and CPB properties

The addition of nanoparticles, such as Fe_2O3, Al_2O_3, to cement mixtures has been shown to have a profound impact on the hydration kinetics and the physical properties of cement-based materials. Nanoparticles are characterized by dimensions of 1 to 100 nanometers in at least two out of three dimensions. Their minute size allows them to participate rapidly in chemical reactions due to their high specific surface area (SSA), which provides a larger interface for chemical interactions. In the context of cementitious materials, nanoparticles (NPs) can alter various properties in multiple ways. If NPs are uniformly dispersed during the cement hydration reaction, they can act as nucleation sites to speed up the hydration process. Furthermore, NPs can fill the voids between cement particles, resulting in a more refined pore structure and a denser matrix in the hardened cement material, which helps immobilize pore water pressure. Another significant effect of NPs on cement-related materials is the reduction in initial setting time, primarily due to the acceleration of the hydration process in its early stages [96-99].

Research by [110] highlights that Fe_2O_3 nanoparticles act as catalysts, accelerating the hydration reactions of Portland cement, which can significantly enhance early strength development. This acceleration is attributed to the high surface energy of Fe2O3 nanoparticles, which promotes more efficient water consumption and faster formation of calcium silicate hydrate (C-S-H) and calcium aluminate hydrate (C-A-H) phases. Additionally, studies by [111] demonstrate that these nanoparticles help in refining the microstructure of the hydrated cement matrix, leading to decreased porosity and increased density. This improvement in microstructural integrity enhances the mechanical properties and durability of the concrete, making it more resistant to environmental degradation. Such modifications are crucial for extending the lifespan of concrete structures, particularly in harsh environmental conditions.

The incorporation of Al_2O_3 nanoparticles into cement matrices has been shown to significantly influence the hydration process, enhancing both the mechanical properties and durability of the resulting cementitious composites. According to [112], the presence of nano-Al_2O_3 accelerates the hydration of Portland cement by providing additional nucleation sites that facilitate the formation of calcium silicate hydrate (C-S-H) phases more rapidly than in traditional cement mixtures. This can lead to an increase in early strength development, which is crucial for many construction applications. Furthermore, [113] observed that nano-Al_2O_3 particles modify the microstructure of hydrated cement, reducing porosity and improving the packing density of the cement paste. These changes contribute to the enhanced impermeability and sulfate resistance of the cement, making it more durable in aggressive environments. The alteration in the kinetics of cement hydration and the resultant microstructural refinements underscore the potential of nano-Al_2O_3 as a beneficial additive in modern cement formulations.

However, almost all prior research on the effects of nano-Fe_2O_3 and nano-Al_2O_3 on cementitious materials has concentrated on traditional concrete or mortar [e.g., 100-113]. Since concrete and mortar differ from CPB, the findings related to these materials are not directly applicable to CPB. Additionally, only a few studies have examined the impact of nano-Fe_2O_3 and nano-Al_2O_3 on the strength and microstructure of CPB [e.g., 119], concluding that these nanoparticles enhance CPB's strength and microstructure. The results suggest that adding these nanoparticles to CPB without superplasticizers (SP) results in lower strength due to a higher likelihood of agglomeration. Conversely, samples containing SP and these nanoparticles exhibit higher unconfined compressive strength (UCS) and more suction than the control sample at early curing stages. It has been observed that the addition of nanoparticles generates more hydration products, enhancing the interparticle friction and packing density of the CPB structure [119]. Greater strength is achieved by increasing the SP content (0.25%) with the same nanoparticle content (1%). However, previous studies have overlooked the effects of nano-Fe_2O_3 and nano-Al_2O_3 on the rheological properties or flowability of CPB. No prior research has addressed the impact of these nanoparticles on the rheological properties and fresh microstructure of CPB.

2.6 Total Carbon Dioxide Emissions from Cement Production

Cement production is a significant contributor to global CO_2 emissions, accounting for about 5-7% of anthropogenic CO_2 emissions[120]. The primary sources of emissions in cement manufacturing stem from the calcination of limestone (releasing CO_2 from calcium carbonate) and the combustion of fossil fuels to heat the kilns, making it both energy- and carbon-intensive [121]. On average, each ton of Portland cement clinker produced releases around 866 kg of CO_2 [122]. The substantial emissions arise due to the need for high temperatures (up to 1,400°C) and the calcination process, which alone contributes approximately 60% of total CO_2 emissions, with the remaining 40% from fuel.

Figure 2.2. shows that compared to other construction materials, cement has a relatively high carbon footprint due to these intrinsic production processes. For example, aluminum production is highly carbon-intensive, emitting over 10,000 g of CO_2 per kg of material, whereas steel production also has a high carbon footprint due to its reliance on fossil fuels. In contrast, materials like wood have a much lower carbon footprint due to their natural carbon storage capabilities and lower processing energy. Cement's embodied CO_2 emissions are around 600-900 g of CO_2 per kg, depending on the production method and clinker content, which is significantly higher than materials like timber but lower than metals such as steel and aluminum [123].

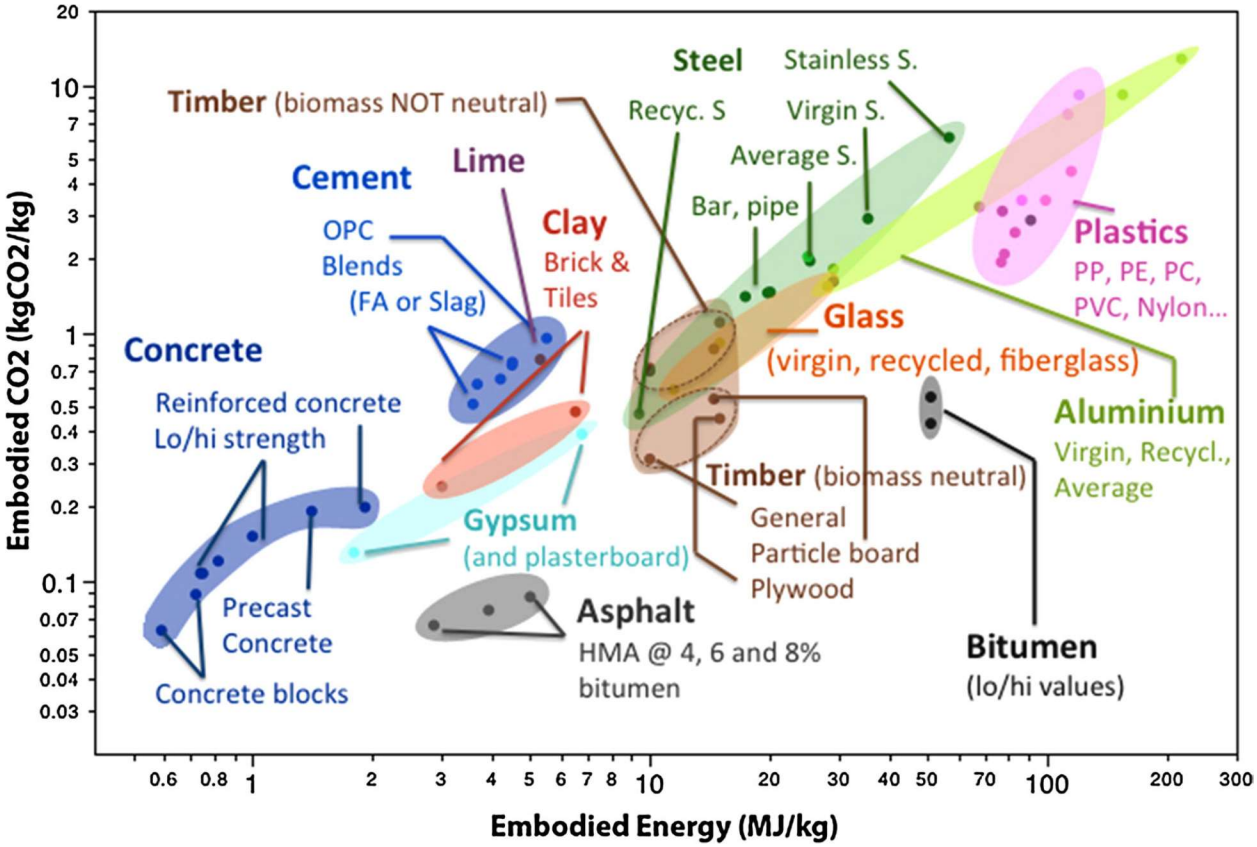

Figure 2.2 Illustration. Carbon footprint and energy consumption of commonly used construction materials. [123]

Efforts to reduce cement's carbon footprint include substituting traditional clinkers with supplementary cementitious materials (SCMs) like fly ash, slag, and pozzolans, which lower the proportion of clinker and therefore the associated CO_2 emissions. However, achieving substantial reductions requires advancing carbon capture and storage (CCS) technology, energy efficiency improvements, and exploring alternative fuels and clinker chemistries [124]. While traditional improvements can cut emissions, a significant reduction will likely depend on innovative technologies and materials, as the standard methods may not

sufficiently decrease emissions to meet climate targets [125].

2.7 Description of the test analysis techniques used in this thesis.

2.7.1 Viscosity Test

The backfill specimen viscosity was determined using a digital viscometer (Model DVE; Brookfield Engineering Laboratories Inc., Middleboro, MA, USA) equipped with an immersed rotating spindle (Figure 2.2). This apparatus enables the instantaneous measurement of viscosity by rotating a spindle at a constant speed using a calibrated spring. The viscous drag of the mixture is determined by the spring deflection caused by a rotary transducer [89]. For further insights into CPB viscosity measurements using this viscometer, refer to the work by [87].

Figure 2.3 Brookfield digital viscometer.

2.7.2 Vane Shear Test

The vane shear test was conducted to ascertain the yield stress of the samples. A vane device (Wykeham Farrance) consisting of a four-blade vane and a motor, which rotates the vane at a constant rate of 0.18 rpm through a calibrated torsion spring, was utilized in the study (Figure 2.3). Vane shear tests were performed following the ASTM D4648/D468M-13 standard. Before each test, the sample was stirred manually and then mixed with a spoon for 1 minute to ensure homogeneity and to simulate the constant shear undergone by the CPB during transport, preventing any settling of the tailing grains due to self-weight. The vane was inserted into the specimen's central surface, and the apparatus was activated. The peak torque was noted, and the corresponding yield stress was calculated using the following equation (ASTM D4648 [102]):

$$\tau_y = \frac{2T_m}{\pi D^3 \left[\frac{1}{3} + \frac{H}{D}\right]}$$

Equation 2.4 where τ represents the yield stress, Tm signifies the determined maximum torque, H denotes the length of the vane, and D represents the vane's diameter. Each test was conducted at least three times to ensure the reliability of the results.

Figure 2.4 shows the vane test method's schematic depiction

2.7.3 Microstructural Analysis

XRD, thermal gravimetry (TG), and differential thermal gravimetry (DTG) analyses were performed on CPB cement pastes to elucidate the microstructural changes in CPB specimens with and without nanoparticles. Cement paste specimens were dried at 45 °C for four days to remove free water, and then ground into powder. XRD and TG/DTG analyses were employed to determine the phase composition of the hydration products. TG/DTG analysis was conducted using a thermal analyzer (TGA Q5000 V3.15 Build 263), heating the specimens from 0 to 1000 °C in a nitrogen atmosphere at a heating rate of 10 °C/min. XRD analysis was carried out using a Rigaku Ultima-IV diffractometer, operating at 40 kV and 44 mA, scanning from 2° to 80° of 2θ range with an increment of 0.02 and a scanning rate of 0.5°/min.

2.7.3.1 pH and Zeta Potential (ZP) Measurements

pH values of the backfill specimens were determined using Metrohm 704 with an accuracy of ±0.003 Zeta potential measurements, providing insights into particle-particle interactions at the microscale [35], were conducted using the Zetasizer Nano series. The electrophoretic mobility of particles in suspension was measured based on phase analysis light scattering (PALS). ZP was determined using the Henry Equation [90]. Specimens were prepared using distilled water, and each ZP measurement was repeated five times for reliability.

Figure 2.5 Metrohm 704 with an accuracy of ±0.003

2.7.3.2 Electrical Conductivity Monitoring

To gain further insights into the cement or binder reaction processes impacting the rheological properties of CPB with varying nP contents, an EC sensor (5TE electrical conductivity) from Decagon Devices, Inc. was employed. The sensor, positioned at the center of each specimen, measured the electrical conductivity of the backfill specimens by applying an alternating current between two electrodes and calculating the resistance between them. A data logger was used to collect data from the sensor.

Figure 2.6 5TE electrical conductivity operation

2.8 Summary and Conclusion

This chapter discusses the current knowledge/findings on the hydration mechanisms of PC and PC/Slag systems, as well as the impact of nanoparticles on binder hydration. The studies reviewed indicate that while slag can improve the long-term strength and microstructure of CPB, it may negatively affect early strength. The addition of nanoparticles, particularly nano-Fe2O3 and nano-Al2O3, has shown promise in enhancing early strength and overall performance by generating more hydration products and improving the packing density of the CPB structure. However, the effects of these nanoparticles on the rheological properties and flowability of CPB are not known. Future research should focus on addressing these gaps to fully understand and optimize the use of these nanoparticles in CPB applications.

2.9 References

[1] Hussain, C. M., Paulraj, M. S., & Nuzhat, S. (2022). Chapter 10—Source reduction and waste minimization in the mining industries. In C. M. Hussain, M. S. Paulraj, & S. Nuzhat (Eds.), Source Reduction and Waste Minimization (pp. 169–176). Elsevier. https://doi.org/10.1016/B978- 0-12-824320-6.00011-3

[2] Ziegler, M., Reiter, K., Heidbach, O., Zang, A., Kwiatek, G., Stromeyer, D., Dahm, T., Dresen, G., & Hofmann, G. (2015). Mining-Induced Stress Transfer and Its Relation to a Mω 1.9 Seismic Event in an Ultra deep South African Gold Mine. Pure and Applied Geophysics, 172(10), 2557–2570. https://doi.org/10.1007/s00024-015-1033-x

[3] Kesimal, A., Yilmaz, E., Ercikdi, B., Alp, I., & Deveci, H. (2005). Effect of properties of tailings and binder on the short-and long-term strength and stability of cemented paste backfill. Materials Letters, 59(28), 3703–3709. https://doi.org/10.1016/j.matlet.2005.06.042

[4] Dudeney, A. W. L., Chan, B. K. C., Bouzalakos, S., & Huisman, J. L. (2013). Management of waste and wastewater from mineral industry processes, especially leaching of sulphide resources: State of the art. International Journal of Mining, Reclamation and Environment, 27(1), 2–37. https://doi.org/10.1080/17480930.2012.696790

[5] Qi, C., & Fourie, A. (2019). Cemented paste backfill for mineral tailings management: Review and future per- spectives. Minerals Engineering, 144, 106025. https://doi.org/10.1016/j.mineng.2019.106025

[6] Edraki, M., Baumgartl, T., Manlapig, E., Bradshaw, D., Franks, D. M., & Moran, C. J. (2014). Designing mine tailings for better environmental, social and economic outcomes: A review of alternative ap- proaches. Journal of Cleaner Production, 84, 411–420. https://doi.org/10.1016/j.jclepro.2014.04.079

[7] Yilmaz, E., & Fall, M. (2017). Introduction to Paste Tailings Management. In E. Yilmaz & M. Fall (Eds.), Paste Tailings Management (pp. 1–5). Springer International Publishing. https://doi.org/10.1007/978-3-319- 39682-8_1

[8] Bloss, M. (2014). An operational perspective of mine backfill (Y. Potvin, T. Grice, Y. Potvin, & T. Grice, Eds.; pp. 15–30). Australian Centre for Geomechanics. https://papers.acg.uwa.edu.au/p/1404_0.2_Bloss/

[9] Sivakugan, N., Veenstra, R. L., & Naguleswaran, N. (2015). Underground Mine Backfilling in Australia Using Paste Fills and Hydraulic Fills. International Journal of Geosynthetics and Ground Engineering, 1, 1–7.

[10] Rankine, R., Pacheco, M., & Sivakugan, N. (2007). Underground Mining with Backfills. Soils and Rocks, 30, 93–101. https://doi.org/10.28927/SR.302093

[11] Rankine, R. M., & Sivakugan, N. (2007). Geotechnical properties of cemented paste backfill from Cannington Mine, Australia. Geotechnical and Geological Engineering, 25(4), 383–393. https://doi.org/10.1007/s10706-006-9104-5

[12] Canadian Minerals Yearbook, 1993 Review and Outlook. Natural Resources Canada, Mining Sector, 1994. Mining Source Book, 1994. Canadian Mining Journal

[13] Nasir, O., & Fall, M. (2008). Shear behaviour of cemented pastefill-rock interfaces. Engineering Geology, 101(3–4), 146–153. https://doi.org/10.1016/j.enggeo.2008.04.010

[14] Sheshpari, M. (2015b). A review on types of binder and hydration in cemented paste backfill (CPB). Electronic Journal of Geotechnical Engineering, 20, 5949–5963.

[15] Sheshpari, M. (2015a). A review of underground mine backfilling methods with emphasis on cemented paste backfill. Electronic Journal of Geotechnical Engineering, 20, 5183–5208.

[16] Potvin, Y., Thomas, E. G., & Fourie, A. B. (2005). Handbook on Mine fill, Australian Centre for Geomechanics. University of Western Australia.

[17] Grice, A. (1998). Underground Mining with Ba ckfill. Proceedings of the 2nd Annual Summit-Mine Tailings Disposal Systems, 216, 234–239, 7.

[18] Grice, T. (2001). Recent mine developments in Australia. Proceedings of the 7th International Symposium on Mining With Backfill, 351–357.

[19] Ghirian, A., & Fall, M. (2015). Coupled Behavior of Cemented Paste Backfill at Early Ages. Geotechnical and Geological Engineering, 33(5), 1141–1166. https://doi.org/10.1007/s10706-015-9892-6

[20] Ghirian, A., & Fall, M. (2014). Coupled thermo-hydro-mechanical–chemical behaviour of cemented paste backfill in column experiments: Part II: Mechanical, chemical and microstructural processes and characteristics. Engineering Geology, 170, 11–23. https://doi.org/10.1016/j.enggeo.2013.12.004

[21] Landriault, D. (2001). Backfill in underground mining. Engineering Fundamentals and International Case Studies (2001): 601-614.

[22] Wang, Y. M., Huang, M. Q., Wu, A. X., Yao, G. H., & Hu, K. J. (2013). Rock Backfill and Hazard Control of Abandoned Stopes: A Case Study. Applied Mechanics and Materials, 368–370, 1726–1731. https://doi.org/10.4028/www.scientific.net/AMM.368-370.1726

[23] Wang, Y., Wu, A., Zhang, L., Jin, F., & Liu, X. (2018). Investigating the Effect of Solid Components on Yield Stress for Cemented Paste Backfill via Uniform Design. Advances in Materials Science and Engineering, 2018, 1–7. https://doi.org/10.1155/2018/3839174

[24] Wang, D., Shi, C., Farzadnia, N., Shi, Z., Jia, H., & Ou, Z. (2018a). A review on the use of limestone powder in cement-based materials: Mechanism, hydration and microstructures. Construction and Building Materials, 181, 659–672. https://doi.org/10.1016/j.conbuildmat.2018.06.075

[25] Wang, D., Shi, C., Farzadnia, N., Shi, Z., & Jia, H. (2018b). A review on effects of limestone powder on the properties of concrete. Construction and Building Materials, 192, 153–166. https://doi.org/10.1016/j.conbuildmat.2018.10.119

[26] Belem, T., & Benzaazoua, M. (2007). Design and Application of Underground Mine Paste Backfill Tech- nology. Geotechnical and Geological Engineering, 26, 147–174. https://doi.org/10.1007/s10706-007-9154-3

[27] Belem, T., Bussière, B., & Benzaazoua, M. (2001). The effect of microstructural evolution on the physical properties of paste Backfill. Tailings and Mine Waste', 10.

[28] Lerche, R. (1984). Development of 'pumped fill' at Grund mine, Preussag AG Metall. Proceedings of the 9th International Conference on the Hydraulic Transport of Solids in Pipes, Rome, Italy.

[29] Benzaazoua, M., Fall, M., & Belem, T. (2004). A contribution to understanding the hardening process of cemented pastefill. Minerals Engineering, 17(2), 141–152. https://doi.org/10.1016/j.mineng.2003.10.022
[35] Klein, K., & Simon, D. (2006). Effect of specimen composition on the strength development in cemented paste backfill. Canadian Geotechnical Journal, 43(3), 310–324. https://doi.org/10.1139/t06-005

[30] Benzaazoua, M., Marion, P., Picquet, I., & Bussière, B. (2004). The use of pastefill as a solidification and stabilization process for the control of acid mine drainage. Minerals Engineering, 17(2), 233–243. https://doi.org/10.1016/j.mineng.2003.10.027

[31] Fall, M., & Benzaazoua, M. (2005). Modeling the effect of sulphate on strength development of paste backfill and binder mixture optimization. Cement and Concrete Research, 35(2), 301–314. https://doi.org/10.1016/j.cemconres.2004.05.020

[32] Haruna, S., & Fall, M. (2020). Time- and temperature-dependent rheological properties of cemented paste backfill that contains superplasticizer. Powder Technology, 360, 731–740. https://doi.org/10.1016/j.pow- tec.2019.09.025

[33] Haruna, S., & Fall, M. (2021). Strength development of cemented tailings materials containing polycarboxylate ether-based superplasticizer: Experimental results on the effect of time and temperature. Canadian Journal of Civil Engineering, 48(4), 429–442. https://doi.org/10.1139/cjce- 2019-0809

[34] Jiang, H., & Fall, M. (2017). Yield stress and strength of saline cemented tailings materials in sub-zero environments: Slag-paste backfill. Journal of Sustainable Cement-Based Materials, 6(5), 314–331. https://doi.org/10.1080/21650373.2017.1280428

[35] D. Simon and M. Grabinsky, “Apparent yield stress measurement in cemented paste backfill,” International Journal of Mining, Reclamation and Environment, vol. 27, no. 4, pp. 231–256, Aug. 2013, doi: 10.1080/17480930.2012.680754.

[36] Ercikdi, B., Kesimal, A., Cihangir, F., Deveci, H., & Alp, İ. (2009). Cemented paste backfill of sulphide-rich tailings: Importance of binder type and dosage. Cement and Concrete Composites, 31(4), 268–274. https://doi.org/10.1016/j.cemconcomp.2009.01.008

[37] Fall, M., & Pokharel, M. (2010). Coupled effects of sulphate and temperature on the strength development of cemented tailings backfills: Portland cement-paste backfill. Cement and Concrete Composites, 32(10), 819–828. https://doi.org/10.1016/j.cemconcomp.2010.08.002

[38] Pokharel, M., & Fall, M. (2011). Coupled Thermochemical Effects on the Strength Development of Slag-Paste Backfill Materials. Journal of Materials in Civil Engineering, 23(5), 511–525. https://doi.org/10.1061/(ASCE)MT.1943-5533.0000192

[39] Jiang, H., Fall, M., Yilmaz, E., Li, Y., & Yang, L. (2020). Effect of mineral admixtures on flow properties of fresh cemented paste backfill: Assessment of time dependency and thixotropy. Powder Technology, 372, 258–266. https://doi.org/10.1016/j.powtec.2020.06.009

[40] Schöler, A., Lothenbach, B., Winnefeld, F., & Zajac, M. (2015). Hydration of quaternary Portland cement blends containing blast-furnace slag, siliceous fly ash and limestone powder. Cement and Concrete Composites, 55, 374–382. https://doi.org/10.1016/j.cemconcomp.2014.10.001

[41] Tariq, A., & Yanful, E. K. (2013). A review of binders used in cemented paste tailings for

underground and surface disposal practices. Journal of Environmental Management, 131, 138–149. https://doi.org/10.1016/j.jenvman.2013.09.039

[42] Simon, D.,& Grabinsky, M. (2013). Apparent yield stressmeasurement in cemented paste backfill. International Journal of Mining, Reclamation and Environment, 27(4), 231–256. https://doi.org/10.1080/17480930.2012.680754

[43] Ali, G., Fall, M., & Alainachi, I. (2021a). Time- and Temperature-Dependence of Rheological Properties of Cemented Tailings Backfill with Sodium Silicate. Journal of Materials in Civil Engineering, 33(3), 04020498. https://doi.org/10.1061/(ASCE)MT.1943-5533.0003605

[44] Ali, G. A. (2021b). Temperature Dependency of the Rheological Properties and Strength of Cemented Paste Backfill That Contains Sodium Silicate. Université d'Ottawa /University of Ottawa.

[45] Liu, S., & Fall, M. (2022). Fresh and hardened properties of cemented paste backfill: Links to mixing time. Construction and Building Materials, 324, 126688. https://doi.org/ 10.1016/j. con-buildmat.2022.126688

[46] Li, W., & Fall, M. (2018). Strength and self-desiccation of slag-cemented paste backfill at early ages: Link to initial sulphate concentration. Cement and Concrete Composites, 89. https://doi.org/10.1016/j.cemconcomp.2017.09.019

[47] Wu, D., Fall, M., & Cai, S. J. (2013). Coupling temperature, cement hydration and rheological behaviour of fresh cemented paste backfill. Minerals Engineering, 42, 76–87. https://doi.org/10.1016/j.mineng.2012.11.011

[48] Wu, D., Hou, Y., Deng, T., Chen, Y., & Zhao, X. (2017). Thermal, hydraulic and mechanical performances of cemented coal gangue-fly ash backfill. International Journal of Mineral Processing, 162, 12–18. https://doi.org/10.1016/j.minpro.2017.03.001

[49] Barnes, H. A. (2000). A handbook of elementary rheology. Aberystwyth : University of Wales. http://lib.ugent.be/catalog/rug01:002025007

[50] Mehdipour, I., Kumar, A., & Khayat, K. H. (2017). Rheology, hydration, and strength changes of interground limestone cement containing PCE dispersant and high volume supplementary cementitious materials. Ma- terials & Design, 127, 54–66. https://doi.org/10.1016/j.matdes.2017.04.061

[51] Shanahan, N., Tran, V., Williams, A., & Zayed, A. (2016). Effect of SCM combinations on paste rheology and its relationship to particle characteristics of the mixture. Construction and Building Materials, 123, 745– 753. https://doi.org/10.1016/j.conbuildmat.2016.07.094

[52] Haiqiang, J., Fall, M., & Cui, L. (2016). Yield stress of cemented paste backfill in sub-zero environments: Experimental results. Minerals Engineering, 92, 141–150. https://doi.org/10.1016/j.mineng.2016.03.014

[53] Yin, S., Wu, A., Hu, K., Wang, Y., & Zhang, Y. (2012). The effect of solid components on the rheological and mechanical properties of cemented paste backfills. Minerals Engineering, 35, 61–66. https://doi.org/10.1016/j.mineng.2012.04.008

[54] Niroshan, N., Sivakugan, N., & Veenstra, R. L. (2017). Laboratory Study on Strength Development in Cemented Paste Backfills. Journal of Materials in Civil Engineering, 29(7), 04017027.

https://doi.org/10.1061/(ASCE)MT.1943-5533.0001848

[55] Niroshan, N., Sivakugan, N., & Veenstra, R. L. (2018). Flow Characteristics of Cemented Paste Backfill. Ge- otechnical and Geological Engineering, 36(4), 2261–2272. https://doi.org/10.1007/s10706-018-0460

[56] Boger, D. V. (2013). Rheology of Slurries and Environmental Impacts in the Mining Industry. Annual Review of Chemical and Biomolecular Engineering, 4(1), 239–257. https://doi.org/10.1146/annurev-chembioeng-061312-103347

[57] Tao, C., Rosenbaum, E., Kutchko, B., & Massoudi, M. (2020). The Importance of Vane Configuration on Yield Stress Measurements of Cement Slurry (DOE/NETL--2020/2116, 1609158; p. DOE/NETL--2020/2116, 1609158). https://doi.org/10.2172/1609158

[58] Elaty, M., & Ghazy, M. (2012). Flow properties of fresh concrete by using modified geotechnical Vane shear test. HBRC Journal, 8, 159–169. https://doi.org/10.1016/j.hbrcj.2012.07.001

[59] Bauer, E., de Sousa, J. G. G., Guimarães, E. A., & Silva, F. G. S. (2007). Study of the laboratory Vane test on mortars. Building and Environment, 42(1), 86–92. https://doi.org/10.1016/j.buildenv.2005.08.016 Belem, T., & Benzaazoua, M. (2004). An overview on the use of paste backfill technology as a ground support method in cut-and-fill mines. Proceedings of the 5th Int. Symp. on Ground Support in Mining and Underground Construction, 28–30.

[60] ASTMD4648/D4648M, Test Method for Laboratory Miniature Vane Shear Test for Saturated Fine-Grained Clayey Soil, ASTM International, 2016.

[61] Bian, J., Fall, M., & Haruna, S. (2021). Sulfate-induced changes in rheological properties of fibre-reinforced cemented paste backfill
Magazine of Concrete Research, 73(11), 574–583. https://doi.org/10.1680/jmacr.19.00311

[62] Sofra, F. (2017). Rheological Properties of Fresh Cemented Paste Tailings. In E. Yilmaz & M. Fall (Eds.), Paste Tailings Management (pp. 33–57). Springer International Publishing. https://doi.org/10.1007/978-3-319- 39682-8_3

[63] Brookfield (2014) 'Brookfield Dial Reading Viscometer with Electronic Drive: Model DV-E Operating Instructions.', [online], available: https://pim-resources.coleparmer.com/instruction-man- ual/98945-xx.pdf].

[64] H. Jiang and M. Fall, “Yield stress and strength of saline cemented tailings materials in sub-zero environments: slag-paste backfill,” Journal of Sustainable Cement-Based Materials, vol. 6, no. 5, pp. 314–331, Sep. 2017, doi: 10.1080/21650373.2017.1280428.

[65] Roshani, A., & Fall, M. (2020). Rheological properties of cemented paste backfill with nano-silica: Link to curing temperature. Cement and Concrete Composites, 114, 103785. https://doi.org/10.1016/j.cemcon- comp.2020.103785

[66] Z. Li, H. Wang, S. He, Y. Lu, and M. Wang, “Investigations on the preparation and mechanical properties of the nano-alumina reinforced cement composite,” Materials Letters, vol. 60, no. 3, pp. 356–359, Feb. 2006, doi: 10.1016/j.matlet.2005.08.061.

[67] L. Senff, D. Hotza, S. Lucas, V. M. Ferreira, and J. A. Labrincha, “Effect of nano-SiO2 and nano-

TiO2 addition on the rheological behavior and the hardened properties of cement mortars," Materials Science and Engineering: A, vol. 532, pp. 354–361, Jan. 2012, doi: 10.1016/j.msea.2011.10.102.

[68] ASTM, Standard test method for laboratory miniature vane shear test for saturated fine-grained clayey soil. American Society for Testing and Materials West Conshohocken, PA, 2016.

[69] Hassani, F. A., Fathipour, M., & Mehran, M. (2007). A comparison study between double and single gate p-IMOS. AFRICON 2007, 1–7. https://doi.org/10.1109/AFRCON.2007.4401526

[70] Ouellet, S., Bussière, B., Aubertin, M., & Benzaazoua, M. (2007). Microstructural changes of cemented paste backfill: Mercury intrusion porosimetry test results. Cement and Concrete Research, 37(12), 1654–1665. https://doi.org/10.1016/j.cemconres.2007.08.016

[71] Yilmaz, E., Belem, T., Bussière, B., & Benzaazoua, M. (2008). Consolidation characteristics of early age ce- mented paste backfill. 8.

[72] Saleh, H. M., & Eskander, S. B. (2020). Innovative cement-based materials for environmental protection and restoration. In New Materials in Civil Engineering (pp. 613–641). Elsevier. https://doi.org/10.1016/B978- 0-12-818961-0.00018-1

[73] Neville, A. M. (2011). Properties of concrete (5th ed.). Pearson.

[74] Tariq, A. (2012). Synergistic and Environmental Benefits of Using Cement Kiln Dust with Slag and Fly Ash in Cemented Paste Tailings. ProQuest Dissertations Publishing.

[75] Bullard, J. W., Jennings, H. M., Livingston, R. A., Nonat, A., Scherer, G. W., Schweitzer, J. S., Scrivener, K. L., & Thomas, J. J. (2011). Mechanisms of cement hydration. Cement and Concrete Research, 41(12), 1208–1223. https://doi.org/10.1016/j.cemconres.2010.09.011

[76] Marchon, D., & Flatt, R. J. (2016). 8—Mechanisms of cement hydration. In Science and Technology of Concrete Admixtures (pp. 129–145). Elsevier Ltd.

[77] Soroka, I. (Itzhak). (1979). Portland cement paste and concrete. Macmillan.

[78] Benzaazoua, M., Peyronnard, O., Belem, T., Stephant, A., & Dublet, G. (2010). Key issues related to behaviour of binders in cemented paste backfilling. 345–363. https://doi.org/10.36487/ACG_rep/1063_30Benazzaoua

[79] Bouzoubaa, N., & Foo, S. (2004). Use of fly ash and slag in concrete: A Best Practice Guide. Materials and Technology Laboratory, MTL, 16.

[80] Duran Atiş, C., & Bilim, C. (2007). Wet and dry cured compressive strength of concrete containing ground granulated blast-furnace slag. Building and Environment, 42(8), 3060–3065. https://doi.org/10.1016/j.build- env.2006.07.027

[81] ACI Committee 233R (2000) Ground granulated blast furnace slag as a cementitious constituent in con- crete. American Concrete Institute (ACI), Farmington Hills, Michigan.

[82] Hooton, R. D. (2000). Canadian use of ground granulated blast-furnace slag as a supplementary cementing material for enhanced performance of concrete. Canadian Journal of Civil Engineer- ing, 27(4),

754–760.

[83] C. Astm, “494,” Standard Specification for Chemical Admixture for Concrete, 2004.

[84] Tanaka, H. (1983). “Property after being heated and re-hydrated of hardened cement paste”,. Cement & Concrete Research, April: 34-40.

[85] Roy, D. M. (1982, November). Hydration, structure, and properties of blast furnace slag cements, mortars, and concrete. In Journal Proceedings (Vol. 79, No. 6, pp. 444-457).

[86] Benzaazoua, M., Belem, T., & Bussière, B. (2002). Chemical factors that influence the performance of mine sulphidic paste backfill. Cement and Concrete Research, 32(7), 1133–1144. https://doi.org/10.1016/S0008-8846(02)00752-4

[87] J. D. Clogston and A. K. Patri, “Zeta Potential Measurement,” in Characterization of Nanoparticles Intended for Drug Delivery, S. E. McNeil, Ed., Totowa, NJ: Humana Press, 2011, pp. 63–70. doi: 10.1007/978-1-60327-198-1_6.

[88] De Souza, E. M. (1997). Glassfill an environmental alternative for waste glass disposal. CIM Bull. 1010, 58e64.

[89] S. Haruna and M. Fall, “Time- and temperature-dependent rheological properties of cemented paste backfill that contains superplasticizer,” Powder Technology, vol. 360, pp. 731–740, Jan. 2020, doi: 10.1016/j.powtec.2019.09.025.

[90] “Brookfield.” [Online]. Available: https://pim-resources.coleparmer.com/instruction-manual/98945-xx.pdf

[91] A. Roshani and M. Fall, “Rheological properties of cemented paste backfill with nano-silica: Link to curing temperature,” Cement and Concrete Composites, vol. 114, p. 103785, Nov. 2020, doi: 10.1016/j.cemconcomp.2020.103785.

[92] H. F. Taylor, Cement chemistry, vol. 2. Thomas Telford London, 1997.

[93] B. Xiao, M. Fall, and A. Roshani, “Towards Understanding the Rheological Properties of Slag-Cemented Paste Backfill,” International Journal of Mining, Reclamation and Environment, vol. 35, no. 4, pp. 268–290, Apr. 2021, doi: 10.1080/17480930.2020.1807667.

[94] A. Roshani and M. Fall, “Flow ability of cemented pastefill material that contains nano-silica particles,” Powder Technology, vol. 373, pp. 289–300, Aug. 2020, doi: 10.1016/j.powtec.2020.06.050.

[95] Cui, L., and M. Fall. 2018. "Impact of Nano-Additives on the Hydration Kinetics and Mechanical Properties of Cemented Paste Backfill." Journal of Sustainable Mining 17, no. 4: 226-234.

[96] H. Du, S. Du, and X. Liu, “Durability performances of concrete with nano-silica,” Construction and Building Materials, vol. 73, pp. 705–712, Dec. 2014, doi: 10.1016/j.conbuildmat.2014.10.014.

[97] F. Lavergne, R. Belhadi, J. Carriat, and A. Ben Fraj, “Effect of nano-silica particles on the hydration, the rheology and the strength development of a blended cement paste,” Cement and Concrete Composites, vol. 95, pp. 42–55, Jan. 2019, doi: 10.1016/j.cemconcomp.2018.10.007.

[98] J. Chen, S. Kou, and C. Poon, “Hydration and properties of nano-TiO2 blended cement composites,”

Cement and Concrete Composites, vol. 34, no. 5, pp. 642–649, May 2012, doi: 10.1016/j.cemconcomp.2012.02.009.

[99] J. Björnström, A. Martinelli, A. Matic, L. Börjesson, and I. Panas, “Accelerating effects of colloidal nano-silica for beneficial calcium–silicate–hydrate formation in cement,” Chemical Physics Letters, vol. 392, no. 1–3, pp. 242–248, Jul. 2004, doi: 10.1016/j.cplett.2004.05.071.

[100] Xiao, B., Fall, M., & Roshani, A. (2021). Towards Understanding the Rheological Properties of Slag-Cemented Paste Backfill. International Journal of Mining, Reclamation and Environment, 35(4), 268–290. https://doi.org/10.1080/17480930.2020.1807667

[101] P. Pereira, L. Evangelista, J. De Brito, The effect of superplasticisers on the workability and compressive strength of concrete made with fine recycled concrete aggregates. Constr. Build. Mater., 28 (1) (2012), pp. 722-729.

[102] X. J. Deng, B. Klein, J. X. Zhang, D. Hallbom, and B. De Wit, “Time-dependent rheological behaviour of cemented backfill mixture,” International Journal of Mining, Reclamation and Environment, vol. 32, no. 3, pp. 145–162, 2018.

[103] J. Plank, D. Vlad, A. Brandl, P. Chatziagorastou, Colloidal chemistry examination of the steric effect of polycarboxylate superplasticizers. Cem. Int., 3 (2) (2005), pp. 100-110.

[104] L. Huynh, D.A. Beattie, D. Fornasiero, J. Ralston, Effect of polyphosphate and naphthalene sulfonate formaldehyde condensate on the rheological properties of dewatered tailings and cemented paste backfill. Miner. Eng., 19 (1) (2006), pp. 28-36

[105] Ghirian, A. (2016). Coupled Thermo-Hydro-Mechanical-Chemical (THMC) Processes in Cemented Tailings Backfill Structures and Implications for their Engineering Design. Université d’Ottawa/University of Ottawa.

[106] Neville, A. M., & Brooks, J. J. (2010). Concrete technology (2nd ed.). Prentice Hall.

[107] Solismaa, S., Torppa, A., Kuva, J., Heikkilä, P., Hyvönen, S., Juntunen, P., Benzaazoua, M., & Kauppila, T. (2021). Substitution of Cement with Granulated Blast Furnace Slag in Cemented Paste Backfill: Evaluation of Technical and Chemical Properties. Minerals, 11(10), 1068. https://doi.org/10.3390/min11101068

[108] Lee, J.H., Kim, H.G., and Park, S.M. (2019). "Impact of Superplasticizers on the Hydration and Microstructure of Portland Cement." Cement and Concrete Research, 124, 105834.

[109] Patel, T.K., and Morris, J. (2020). "Enhancing Concrete Performance with Superplasticizers: Rheology, Setting, and Strength." Journal of Construction and Building Materials, 230, 117062.

[110] Zhang, H., Kodur, V., Qi, S., Cao, L., & Wu, B. (2016). "Influence of nano-Fe2O3 on the hydration properties of Portland cement." Cement and Concrete Composites, 70, 83-92.

[111] Kumar, P., & Singh, S. (2018). "Effects of nano-Fe2O3 particles on the durability and mechanical properties of concrete." Construction and Building Materials, 168, 485-493.

[112] Li, Z., Zhou, X., & Shen, W. (2014). "Effect of nano-Al2O3 on the hydration and microstructure of Portland cement." Cement and Concrete Research, 58, 128-136.

[113] Maravelaki-Kalaitzaki, P., Agioutantis, Z., & Karatasios, I. (2015). "Nanostructured materials for the restoration and preservation of historic masonry in urban buildings." Materials and Structures, 48(9), 2997-3008.

[114] John, E., & Lothenbach, B. (2023). Cement hydration mechanisms through time – a review. Journal of Materials Science, 58, 9805–9833.

[115] Mechanisms of carbonation hydration hardening in Portland cements.

[116] Some Mechanical Features of the Hydration of Portland Cement and the Making of Concrete.

[117] Hydration Mechanisms of Portland Cement: Topochemical or Through-Solution Reaction.

[118] The initial stages of cement hydration at the molecular level.

[119] Saremi, A., Fall, M (2023). Strength and suction development of nano-cemented paste backfill. Cleaner Materials 8: 100190.

[120] International Energy Agency. Energy Technology Transitions for Industry: Strategies for the Next Industrial Revolution. Paris: International Energy Agency, 2009. ISBN 978-92-64-06858-2.

[121] U.S. Global Change Research Program. Global Climate Change Impacts in the United States: A State of Knowledge Report. Cambridge, MA: Cambridge University Press, 2009. ISBN 978-0-521-14407-0.

[122] World Business Council for Sustainable Development. Cement Industry Energy and CO2 Performance: Getting the Numbers Right. Concrete Sustainability Initiative, 2009. ISBN 978-3-940388-48-3.

[123] Hammond, G., and C. Jones. Embodied Carbon: The Inventory of Carbon and Energy (ICE). BSRIA, 2011. ISBN 978-0-86022-703-8.

[124] Enkvist, P., J. Dinkel, and C. Lin. Impact of the Financial Crisis on Carbon Economics: Version 2.1 of the Global Greenhouse Gas Abatement Cost Curve. McKinsey & Company, 2010.

[125] Barcelo, L., and J. Kline. “The Cement Industry Roadmap to Reduce Carbon Emissions.” In Proceedings of the 2012 Carbon Management Technology Conference, Orlando, 2012.

3 Technical Paper 1: Rheological Properties of Iron Oxide Nanoparticle-Modified Cemented Paste Tailings Materials

Raouf Kaviani, Mamadou Fall

Abstract:
The rheological characteristics of Cemented Paste Backfill (CPB) materials incorporating iron oxide nanoparticles (nFeO) remain uninvestigated, with no existing studies addressing this aspect. Understanding the yield stress and viscosity of CPB containing nFeO during the early stages is essential, particularly for implementing nano-CPB technology in underground mines. This study aims to investigate in depth the impact of nFeO on the rheological properties of CPB and its evolution as a function of time. CPB samples of various compositions (e.g. nFeO content, binder type, superplasticizer content) are subjected to yield stress and viscosity measurements at 0 min, 20 min, 1 h, 2 h and 4 h intervals. In addition, the study includes monitoring electrical conductivity (EC), performing microstructural analyses (TG/DTG and XRD), pH and Zeta potential measurements on the samples. The results reveal that incorporation of nFeO into CPB leads to significant alterations in its rheological characteristics, affecting its flowability. Incorporation of nFeO significantly increases the yield stress and viscosity of CPB samples, the degree of influence depending on factors such as binder type, curing time and water content. The interaction of nFeO and a larger portion of nFeO, together with an increase in curing time, increases rheological properties, leading to a decrease in paste flowability, due to the nFeO-induced microstructural changes occurring in the CPB material. This is confirmed by EC, DTG and XRD results, which indicate an increase in binder hydration as nFeO dosage increases. In addition, increasing nFeO reduces the magnitude of the zeta potential, leading to a decrease in repulsion force and flowability. However, the addition of 0.125% superplasticizer is identified as a compensator for the reduced flowability induced by nFeO, as shown by EC, XRD and DTG tests which reveal a decrease in cement hydration rate at very high ages due to the superplasticizer. Furthermore, increasing the slag content from 0% to 50% and 75% of the binder content proves effective in slightly decreasing viscosity but significantly increasing yield stress. The new insights presented in this study help to advance nano-CPB technology, offering valuable implications for its effective application in underground mine backfill operations. They not only shed light on the rheological behavior of nano-CPB materials, but also hold promise for advancing the application of the nano-CPB technology in underground mine backfill operations.

Keywords: Cemented paste backfill, Tailings, Mine, Rheology, Nano-particles, Cement, Iron oxide

3.1 Introduction

The use of cemented paste backfill (CPB) material for filling mine cavities has grown significantly in recent decades. CPB, a combination of tailings, binder, and water, plays a critical role in enhancing ground control and creating a safe working environment. Additionally, it facilitates the effective disposal of mine waste, thereby reducing the potential risks associated with tailings dam failures, and tailings-induced environmental contamination and promoting optimal resource recovery [1-6].

The stability of the underground CPB structure is of paramount importance in ensuring the safety of personnel and equipment in underground mining operations. Thus, the CPB structure must achieve sufficient mechanical strength. Moreover, achieving CPB design strength as quickly as possible is an objective shared by all stakeholders involved in backfilling operations. This early strength gain is crucial for timely actions, such as the opening of barricades, scheduling mining activities in the neighboring stope, and, ultimately, shortening the mining cycle to enhance overall productivity and profitability.

However, the traditional components used in CPB preparation, including the binder, water, and tailings, are not inherently designed to promote rapid early CPB strength gain. Typically, ordinary Portland cement (OPC) remains the most commonly used binder in CPB preparation. The use of ordinary Portland cement (OPC) as a binding agent in CPB not only contributes to increased costs but also limits the rate of early CPB strength gain. Furthermore, the production of OPCs leads to the emission of a substantial volume of greenhouse gases. The current production rate, exceeding 4 billion tonnes of OPC annually, contributes to 7% of global CO2 emissions [7]. As the mining industry increasingly gravitates towards a sustainable future, the excessive use of OPC in CPB technology runs counter to this objective.

In response to cost considerations, supplementary cementitious materials (SCMs), notably blast furnace slag (BFS), have been frequently used to partially replace ordinary OPC in CPBs. While this practice contributes to cost reduction and helps lower the carbon footprint associated with CPBs, the drawback lies in the slag's slower early hydration, resulting in a noticeable drop in early-age strength and rate of strength development in CPBs incorporating slag. This slowdown poses productivity challenges for mines. As a result, the mining industry has been prompted to look for alternative approaches aimed at accelerating the strength development and reducing the carbon footprint of CPBs [8-9].

The incorporation of nanoparticles, in particular iron oxide nanoparticles (nFeO), as additives in CPBs is an emerging avenue in CPB technology. This innovative approach aims to enhance the mechanical properties and reduce the carbon footprint of CPBs by incorporating Fe_2O_3 nanoparticles into the CPB mixes while reducing its OPC content [2]. This trend is inspired by the successful application of nano-particles in producing high-performance concrete with improved early-age strength and strength enhancement rates [10-20]. The incorporation of nano-particles in concrete or cement-based materials (CBMs) has garnered significant attention in recent years. Studies have demonstrated that the inclusion of nano-particles can substantially enhance the mechanical properties of conventional concrete or mortar materials, owing to their physical (e.g., filler effect) and chemical (e.g., enhancement of the cement hydration) effects. Notably, nano-Fe_2O_3 has been extensively investigated in the context of CBMs. In the realm of construction materials, particularly in the context of cement and concrete research, extensive investigation has underscored the efficacy of incorporating nano-iron Oxide (nFeO) particles. These studies have pointed towards the considerable enhancement of both strength and strength gain rate in concrete or mortar composition (e.g., [21-28]). Iron oxide's role as a filler contributes to reduced porosity, thus fostering the formation of a denser cementitious matrix.

However, beyond the imperative focus on strength, another critical design consideration in the context of CPB is the flow ability or transportability of the fresh material. Ensuring suitable flow ability is essential to facilitate smooth pumping and delivery to mine cavities (stopes). Insufficient flow ability can lead to complications such as pipe blockages, ultimately incurring significant economic setbacks for mining operations (e.g.[10], [13], [29-32]). Unfortunately, the specific impact of nFeO particles on the flow ability of CPB remains a relatively unexplored area. Evaluation of flow ability typically entails the examination of CPB's rheological properties, involving the analysis of viscosity and yield stress, representing the material's resistance to deformation and initiation of flow, respectively [33-34].

Nevertheless, several fundamental questions about the interplay between nFeO and CPB's rheological properties remain unanswered. These include inquiries into the influence of nFeO on CPB yield stress, its impact on the viscosity of fresh CPB, variation in viscosity and yield stress during the curing and transportation phases, the resulting changes in CPB's microstructure due to nFeO, and the potential interactions with superplasticizers or mineral admixtures Slag. Addressing these critical knowledge gaps is imperative for the successful integration and application of nano-CPB technology. Thus, this study encompasses an array of experimental methodologies, including comprehensive rheological tests, microstructural analyses, chemical evaluation, and an extensive monitoring program, aiming to provide crucial insights into the effects of nFeO particles on CPB's rheological, microstructural, and chemical properties across different binder types, with or without superplasticizers, over varying timeframes.

3.2 Experimental Approach

3.2.1 Specimen Preparation and Materials

3.2.1.1 Tailings

The study employed synthetic silica tailings (ST) characterized by their non-reactive and non-acid generating properties, ensuring result reliability. ST mainly consists of quartz minerals, mirroring the mineral composition of natural tailings from numerous hard rock mines in Canada. The medium-sized ST exhibited a grain size distribution similar to that of tailings from various mines in eastern Canada (see Figure 3.1 and Table 3.1).

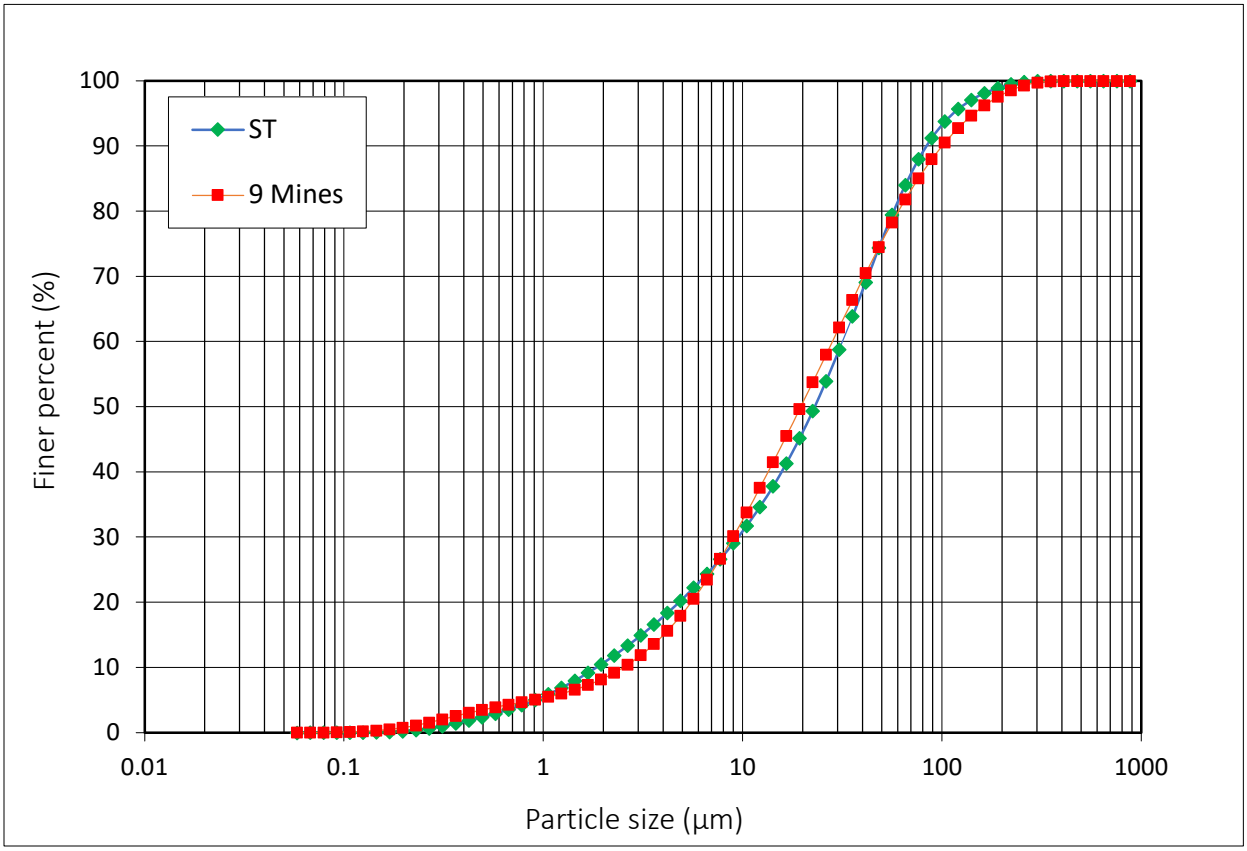

Figure 3.1 Distribution of silica tailings (ST) grain sizes and average grain sizes of tailings from nine Eastern Canadian mines.

Table 3.1 Physical characteristics of the tailings used.

Element	Gs	D_{10} (µm)	D_{30} (µm)	D_{50} (µm)	D_{60} (µm)	Ss (cm^2/g)
ST	2.7	1.9	9.0	22.5	31.5	3600
An average of 9 mines	–	1.8	9.1	20.0	30.8	–

Gs: specific gravity; Ss: specific surface area.

3.2.1.2 Binders and water

Ordinary PC type I (PCI) served as the primary binder with a specific gravity of 3.2. Additionally, select CPB specimens were prepared using a blend of PC and slag at a 50/50 and 25/75 weight ratio, a common practice in Canadian CPB plants, with a binder content of 4.5% by weight [12, 26]. Table 3.2 provides the physical properties and chemical composition of the binders, determined primarily through X-ray fluorescence (XRF). Distilled water, with a water-to-cement ratio of 7.8, was utilized for the preparation of all backfill samples.

Table 3.2 Primary chemical and physical properties of the Portland cement and Slag used.

	Na_2O	MgO	Al_2O_3	SiO_2	K_2O	CaO	TiO_2	MnO	Fe_2O_3	Relative density	Specific surface area (cm^2/g)
PCI	0.34	2.58	4.81	20.38	0.96	62.70	0.23	0.05	3.61	3.2	1300
Slag	0.28	11.78	10.60	35.57	0.48	39.21	0.47	0.30	0.62	2.8	2100

3.2.1.3 Nano-Iron Oxide

Utilized in various concentrations (0%, 1%, and 3% by total mass of binder materials), nano-iron Oxide, an amorphous Fe_2O_2 with high purity and a large specific surface area, was sourced in colloidal form from Dow Corning, Inc. Table 3.3 shows the chemical and physical characteristics of the employed nFeO particles.

Table 3.3 Chemical and physical specifications of the nano-particles used.

Nano-Fe_2O_3		
	Purity (%)	0.98
	APS	20-40 nm
	SSA	40–60 m^2/g
	PH	5-7
	Color	Red-brown
	Bulk density	1.2 g/cm^3

Data obtained from suppliers.

3.2.1.4 Superplasticizer

Certain CPB samples were supplemented with a superplasticizer (0.125% by weight of the mixture). Master Glenium 7500 (Master G) from BASF, meeting ASTM specifications for high-range water-reducing admixtures, was the selected superplasticizer [35-36].

3.2.2 Specimen Preparation

Various CPB mixtures with differing nFeO proportions were prepared alongside reference samples devoid of nFeO (0% nFeO). Maintaining a consistent water-to-binder ratio (W/B) of 7.8 and binder content of 4.5 wt%, the dry ingredients were thoroughly blended for 5 minutes, followed by the addition of water and nFeO, mixed for an additional 5 minutes using a mechanical mixer. The CPB was then transferred into 10 cm height and 5 cm diameter plastic cylinders, with larger cylinders of 10 cm in diameter and 20 cm in height used for monitoring purposes. After eliminating trapped air through manual vibration, the CPB cylinders were sealed and cured at room temperature for specific durations to mimic various transportation times. The mix proportions for the prepared CPBs are outlined in Table 3.4. Additionally, cement paste samples for microstructure analysis were prepared using a consistent W/B ratio of 1. Post-curing, various tests and analyses were conducted on the CPB and CP specimens (Table 3.5).

Table 3.4 Mix composition of the specimens prepared for rheological tests.

Sample name	Nano-Fe_2O_3 [(a)] (%)	Binder (%)	Binder type	w/b	Superplasticizer (%)
CPB-PCI-0%nFeO	0	4.5	PCI	7.8	0
CPB-PCI-1%nFeO	1	4.5	PCI	7.8	0
CPB-PCI-3%nFeO	3	4.5	PCI	7.8	0
CPB-PCI 1%nFeO-SP	1	4.5	PCI	7.8	0.125
CPB-PCI 3%nFeO-SP	3	4.5	PCI	7.8	0.125
CPB-50%PCI/50%Slag 0%nFeO	0	4.5	PCI/Slag (50/50)[b]	7.8	0
CPB-50%PCI/50%Slag 1%nFeO	1	4.5	PCI/ Slag (50/50)	7.8	0
CPB-50%PCI/50%Slag 3%nFeO	3	4.5	PCI/ Slag (50/50)	7.8	0
CPB-25%PCI/75%Slag 0%nFeO	0	4.5	PCI/Slag (25/75)	7.8	0
CPB-25%PCI/75%Slag 1%nFeOCPB	1	4.5	PCI/Slag (25/75)	7.8	0
CPB-25%PCI/75%Slag 3%nFeOCPB	3	4.5	PCI/Slag (25/75)	7.8	0

a) by the mass of the binder; b) PC/Slag (50/50) = the blend weight ratio of Portland cement to Slag is 50/50

Table 3.5 Summary of the mix composition of the specimens prepared for XRD, TG/DTG analyses.

Sample Nomenclat-eure	Binder Conte-nt %	%PCI in the binder	%Slag in the binder	SP %	Taili-ngs type	$\frac{W}{C}$ Ra-tio	Mixi-ng Wate-r	Nanap Content %	Nanop type	Curi-ng time (hrs)
CPB-PCI 0	-	100	0	0	none	1	DW	0	none	2
CPB-PCI 1	-	100	0	0	none	1	DW	1	nFeO	2
CPB-PCI 3	-	100	0	0	none	1	DW	3	nFeO	2
CPB-PCI/Slag 3	-	50	50	0	none	1	DW	3	nFeO	2
CPB-PCI 3-SP	-	100	0	0.125	none	1	DW	3	nFeO	2

DW: distilled water; SP: superplasticizer; Nanop: nanoparticles

3.2.3 Methods of Testing and Analysis

3.2.3.1 Viscosity Test

The backfill specimen viscosity was determined using a digital viscometer (Model DVE; Brookfield Engineering Laboratories Inc., Middleboro, MA, USA) equipped with an immersed rotating spindle. This apparatus enables the instantaneous measurement of viscosity by rotating a spindle at a constant speed using a calibrated spring. The viscous drag of the mixture is determined by the spring deflection caused by a rotary transducer [37]. For further insights into CPB viscosity measurements using this viscometer, refer to the work by [36]. Samples were assessed at specific curing times of 0 min, 20 min, 1 h, 2 h, and 4 h, with tests conducted twice to ensure result repeatability.

3.2.3.2 Vane Shear Test

The vane shear test was conducted to ascertain the yield stress of the samples. A vane device (Wykeham Farrance) consisting of a four-blade vane and a motor, which rotates the vane at a constant rate of 0.18 rpm through a calibrated torsion spring, was utilized in the study. Vane shear tests were performed at 0 min, 20 min, 1 h, 2 h, and 4 h post-mixing, following the ASTM D4648/D468M-13 standard. Before each test, the sample was stirred manually and then mixed with a spoon for 1 minute to ensure homogeneity and to simulate the constant shear undergone by the CPB during transport, preventing any settling of the tailing grains due to self-weight. The vane was inserted into the specimen's central surface, and the apparatus was activated. The peak torque was noted, and the corresponding yield stress was calculated using the following equation (ASTM D4648 [38]):

$$\tau_y = \frac{2T_m}{\pi D^3 \left[\frac{1}{3} + \frac{H}{D}\right]}$$

Equation 3.1 Where τ represents the yield stress, T_m signifies the determined maximum torque, H denotes the length of the vane, and D represents the vane's diameter. Each test was conducted at least three times to ensure the reliability of the results.

3.2.3.3 Microstructural Analysis

XRD, thermal gravimetry (TG), and differential thermal gravimetry (DTG) analyses were performed on CPB cement pastes to elucidate the microstructural changes in CPB specimens with and without nFeO. Cement paste specimens were dried at 45 °C for four days to remove free water, and then ground into powder. XRD, and TG/DTG analyses were employed to determine the phase composition of the hydration products. TG/DTG analysis was conducted using a thermal analyzer (TGA Q5000 V3.15 Build 263), heating the specimens from 0 to 1000 °C in a nitrogen atmosphere at a heating rate of 10 °C/min. XRD

analysis was carried out using a Rigaku Ultima-IV diffractometer, operating at 40 kV and 44 mA, scanning from 2° to 80° of 2θ range with an increment of 0.02 and a scanning rate of 0.5°/min.

3.2.3.4 pH and Zeta Potential (ZP) Measurements

pH values of the backfill specimens were determined using Metrohm 704 with an accuracy of ±0.003. Each measurement was taken at least twice for result validation, and average values were recorded. Zeta potential measurements, providing insights into particle-particle interactions at the microscale [10], were conducted using the Zetasizer Nano series. The electrophoretic mobility of particles in suspension was measured based on phase analysis light scattering (PALS). ZP was determined using the Henry Equation [39]. Specimens were prepared using distilled water, and each ZP measurement was repeated five times for reliability.

3.2.3.5 Electrical Conductivity Monitoring

To gain further insights into the cement or binder reaction processes impacting the rheological properties of CPB with varying nFeO contents, an EC sensor (5TE electrical conductivity) from Decagon Devices, Inc. was employed. The sensor, positioned at the center of each specimen, measured the electrical conductivity of the backfill specimens by applying an alternating current between two electrodes and calculating the resistance between them. A data logger was used to collect data from the sensor.

3.3 Results and Discussion

3.3.1 Influence of Nano-Iron Oxide (nFeO) on the rheological properties of CPB made of Portland cement

The influence of nFeO on time-dependent changes in the rheological characteristics (yield stress, viscosity) of CPB with 100% Portland cement as binder is illustrated in Figure 3.2. This figure shows that irrespective of nanoparticle content, the yield stress and viscosity of the backfill increase with curing time. This behavior arises from the evolving process of cement hydration over time, giving rise to an augmented production of various cement hydration products, including C-S-H, ettringite, and CH, as the hydration reaction advances [40-41]. This, in sequence, promotes the agglomeration of particles and the development of more cohesive structures [10], thereby enhancing inter-frictional resistance and yield stresses of the material [12]. Additionally, with the rising degree of cement hydration, there is a concurrent increase in the size of hydration products [13, 40, 42]. Consequently, the solid volume fraction of CPB samples rises continuously, resulting in a progressive rise of viscosity [16, 41, 43]. Moreover, the cement hydration process consumes free water, leading to a reduction in the thickness of the water film surrounding the particles. This reduction in water content is directly linked to a gradual enhancement in yield stress. Clearly, this decrease in water content correlates with an augmentation in the solid volume fraction of the CPB. Higher solid volume fractions contribute to heightened levels of particle-particle interactions, consequently elevating the apparent viscosities of fresh CPB specimens, as noted by [13], [17]

The experimental findings of thermal analyses (TG/DTG) support the aforementioned notion that an extended curing time results in the generation of more cement hydration products, as evidenced by TG/DTG analyses performed on cement pastes cured for 60 minutes and 240 minutes, as depicted in Figure 3.3. This figure reveals three distinct endothermic peaks or weight losses occurring at temperature ranges of 50-200°C, 400-450°C, and 600-700°C. The weight loss between 50-200°C is primarily attributed to the evaporation of bound water and the dehydration of hydration products like C-S-H, carboaluminates, ettringite, and gypsum. The peak between 400-450°C is mainly due to the dehydroxylation of CH, and the peak between 600-700°C results from the decomposition of calcite ($CaCO_3$) ([44-48]). It is evident from Figure 3.3 that the peak at temperature ranges of 50-200°C and 400-450°C is higher in cement paste cured for 240 minutes compared to the specimen cured for 60 minutes. This observation indicates an increase in the quantity of hydration products generated in the CPB samples with prolonged curing time.

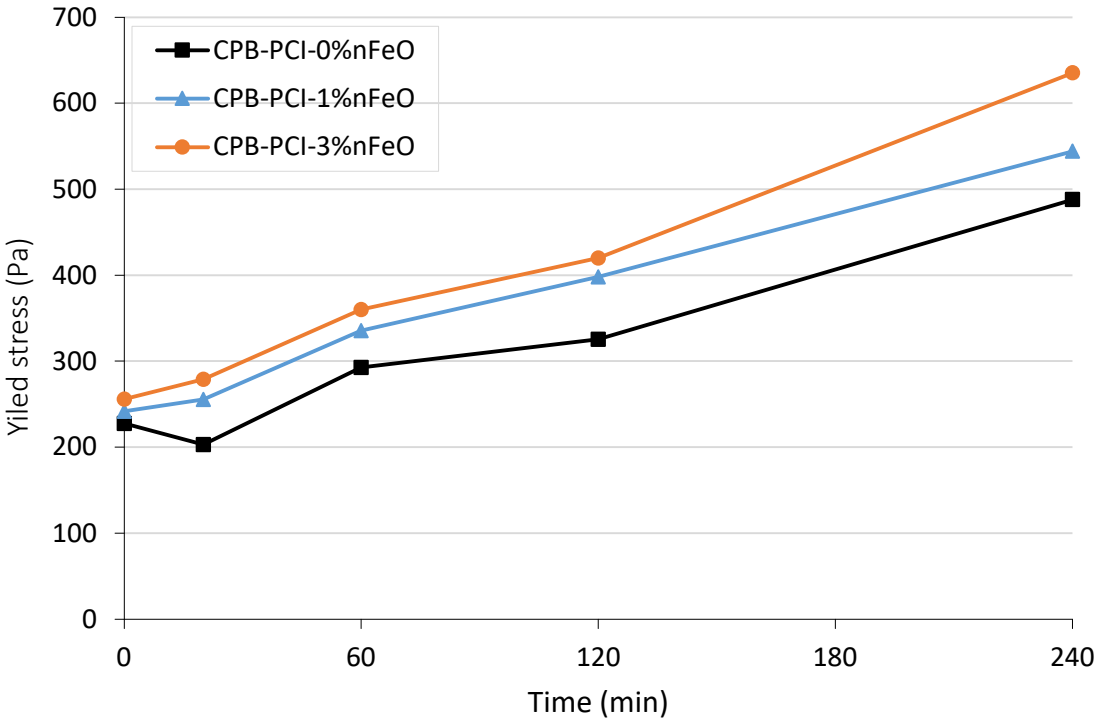

a) Yield stress

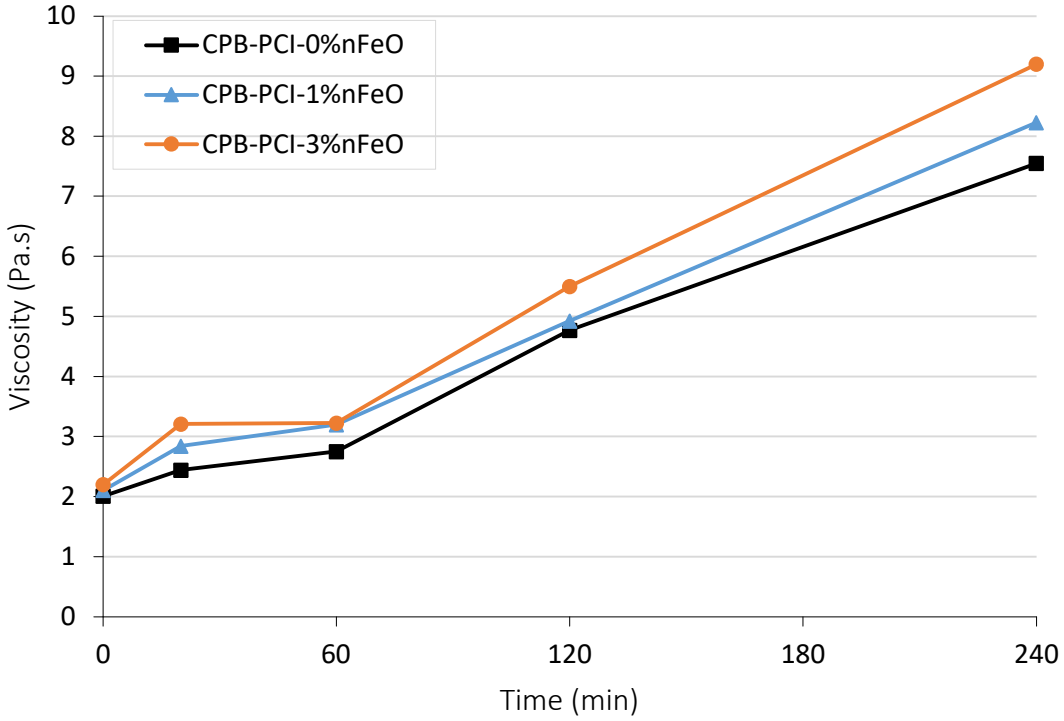

b) Viscosity

Figure 3.2 Effect of nano-Fe2O3 (nFeO) content on the evolution of the rheological properties of CPB with Portland cement: a) yield stress; b) Viscosity

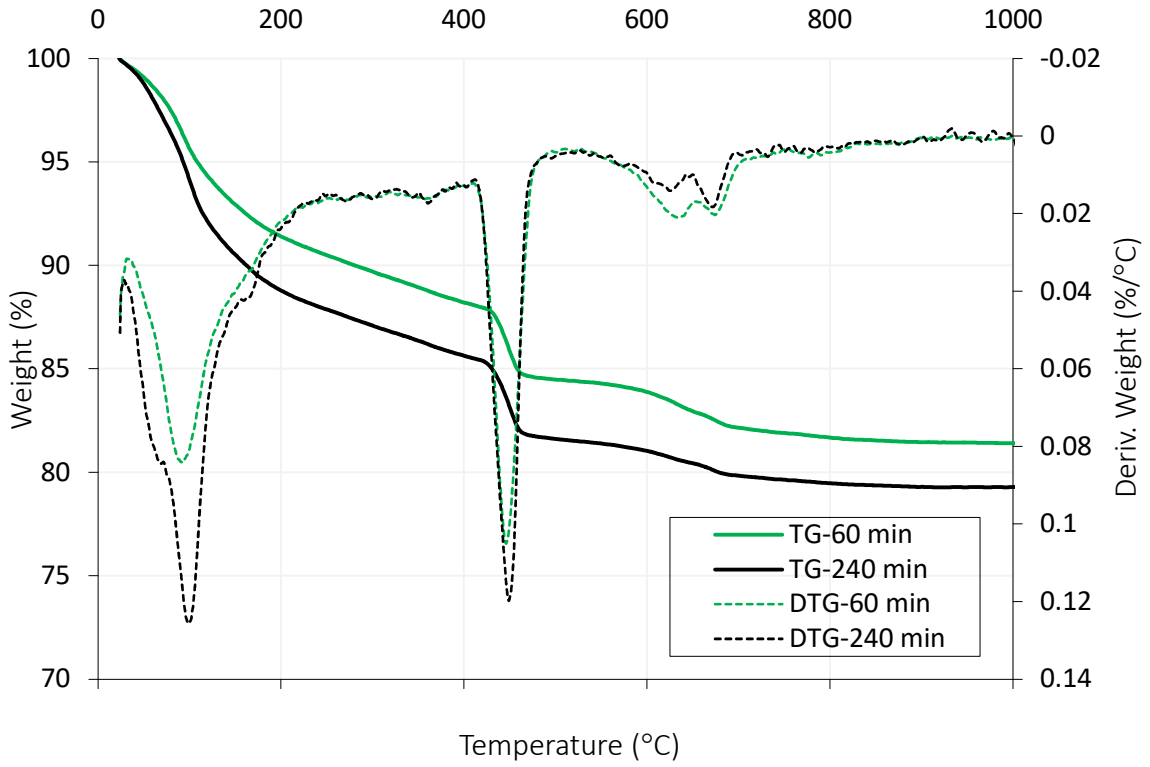

Figure 3.3 TG/DTG analysis results of cement paste samples without nFeO and cured for 60 min. and 240 min.

Additionally, Figure 3.2 indicates a significant modification in CPB's flow ability due to the addition of nano-particles. It shows a substantial increase in backfill yield stress and viscosity with the incorporation of nFeO, irrespective of the testing age. For instance, at 0 min, 20 min, 1 h, 2 h, and 4 h, the yield stress of specimen containing 3% nFeO was 256 Pa, 279 Pa, 360 Pa, 420 Pa, and 635 Pa, respectively, representing an increase of about 12%, 37%, 23%, 29%, and 30% compared to the 0% nanoparticle sample. The yield stress of samples with 1% nFeO increased by about 6%, 26%, 14%, 22%, and 12% compared to the 0% nanoparticle samples at 0 min, 20 min, 1 h, 2 h, and 4 h, respectively. Moreover, the addition of 1% and 3% nFeO resulted in a 9% and 22% increase, respectively, in viscosity at 4 h compared to the control sample. Furthermore, the influence of adding 3% nFeO on CPB viscosity at 0 h and 20 min was more pronounced than that of 1%. The decline in flowability observed in the presence of nFeO, as indicated by increased yield stress and viscosity, can be attributed to combined effects of several factors. These factors include (i) the filler effect exerted by nanoparticles, (ii) the enhancement of the cement hydration induced by nFeO, (iii) an increase in water demand due to the presence of nanoparticles, and (iv) enhanced flocculation or agglomeration of the paste owing to nFeO particles [40, 49, 50-56]. These factors collectively contribute to the altered rheological properties of CPB in the presence of nFeO, and a more in-depth discussion of these factors follows below.

- **nFeO filler effect:** It is widely recognized that nano-particles play a crucial role by partially occupying the void spaces within a cementitious medium, leading to the densification of its microstructure [42]. This in turn raises the frictional resistance between the particles and the solid volume fraction in the CPB material, and ultimately the yield stress and viscosity of the backfill material [18], [40].
- **Enhancement of the cement hydration by nFeO:** The minute dimensions of nFeO particles offer an abundance of nucleation sites, facilitating the precipitation of numerous hydration products, notably C-S-H. These nucleation sites play a pivotal role in fostering and intensifying the hydration process of essential cement compounds, including C_3S, C_2S, C_3A, and C_4AF [40, 54, 57]. The XRD analyses

conducted on 2-hour-old cement pastes of CPB, which included 0%, 1%, and 3% nFeO particles (depicted in Figure 3.4), validate the enhancement of cement hydration upon the incorporation of nFeO. The XRD results show the presence of a higher quantity of hydration products in the sample containing nFeO. For example, CH intensity is higher for the sample with nFeO than for the sample without nFeO. Indeed, CH intensity at 18 and 34 degrees 2-theta for the sample containing nanoparticles (nFeO) is higher than for the sample without nFeO. This observation implies a greater formation of CH in specimens with the inclusion of nFeO, underscoring its impact on cement hydration. This conclusion regarding the generation of more hydration products due to the addition of nFeO particles aligns with the results of TG/DTG analyses done on 2h-old-cement pastes with different nFeO contents (0%, 1% and 3%) presented in Figure 3.5. These results reveal that the cement paste, when modified with nFeO, exhibits the most pronounced endothermic peaks and weight loss within the temperature range of 100°-180°C. These indicators suggest an increased formation of hydration products, leading to elevated yield stress and viscosity levels. This alignment is further supported by the congruence with the results of EC monitoring results of CPB samples with varying percentages of nFeO depicted in Figure 3.6. As depicted in this graph, the curves exhibit increasing trends initially, attributable to the dissolution phase of the cement. Following the addition of water to the cement, the dissolution of ions from the cement occurred, releasing various types of ions such as potassium, calcium Iron oxide ions, and aluminate. These free and mobile ions enhanced the electrical conductivity of the paste [57-58]. As further hydration reaction took place, hydrates like CH, C-S-H, and ettringite filled the capillary pores. Consequently, the decrease in both ion mobility and concentration led to a reduction in EC [59]. As presented in Figure 3.6, during the early stage (up to 2 hours or 120 min), the EC for the samples containing nFeO was higher compared to those without nFeO. Additionally, there was a distinct shift of the EC peaks to shorter hydration times with the incorporation of nFeO, suggesting accelerated hydration reaction rates with nFeO inclusion. Indeed, the conductivity peaks occurred at 3.5 hours (210 min), 3.7 hours (220 min), and 5.8 hours (350 min) for the specimens containing 3%, 1%, and 0% nFeO, respectively. This rapid acceleration of cement hydration during the initial phases aligns with the observations presented in Figure 3.2 concerning yield stress and viscosity.

- **nFeO-induced increase in water demand:** The incorporation of nFeO into the CPB directly affected the water demand of the CPB mixture to achieve suitable flowability. It is well-known that nano-particles increase water demand [60-61]. The higher water demand in the presence of nanoparticles is attributed to their high surface area (386 m^2/g), which adsorbs the free water on their surface. Finer particles mean more surface area to be wetted. Consequently, a higher amount of water is required to maintain the workability or flowability of the CPB at an acceptable level [62].
- **Enhanced flocculation or agglomeration of the paste owing to nFeO particles:** The inclination towards agglomeration or flocculation subsequent to introducing nFeO particles corresponds with the outcomes of zeta potential (ZP) measurements conducted on the CPBs containing varying amounts of nFeO particles (Figure 3.7). ZP determination, a method utilized for assessing the surface charge and potential stability of suspended particles, indicates that a higher ZP magnitude is associated with increased electrostatic repulsion between charged particles, resulting in enhanced dispersion. ZP represents the electrostatic surface charge, dictating the extent of repulsion or attraction between colloidal particles [57]. Consequently, the dispersal process of nFeO particles in an alkaline environment of Portland cement paste (Figure 3.7) can be discerned through ZP. Figure 3.8 portrays the pH trend over time for PCI-CPB samples incorporating 0% and 3% nFeO. The formation of $Ca(OH)_2$ due to cement hydration establishes an alkaline condition (high pH) in all CPB samples. After a 20-minute curing period, pH values for specimens with 0% and 3% nFeO were 12.79 and 12.93, respectively. Furthermore, after 2 hours of aging, pH values increased to 13.03 and 13.06 for samples with 0% and 3% nFeO, respectively. As evident in Figure 3.8, the pH of CPB with 3% nFeO surpasses that of CPB without nFeO, aligning with the discussed fact that nFeO particles enhance cement compound hydration, releasing more alkali ions into CPB pore water and consequently elevating the pH value. Figure 3.7 displays ZP measurement results for CPB with 100% PCI,

incorporating 1% and 3% nFeO, in comparison with the control sample. The ZP of the CPB decreases as the nFeO percentage increases, indicating a greater electronic double-layer repulsive force in the absence of nFeO. Reduced repulsion and low ZP lead to altered rheology and increased water demand, consistent with the results of yield stress and viscosity, as discussed earlier [14].

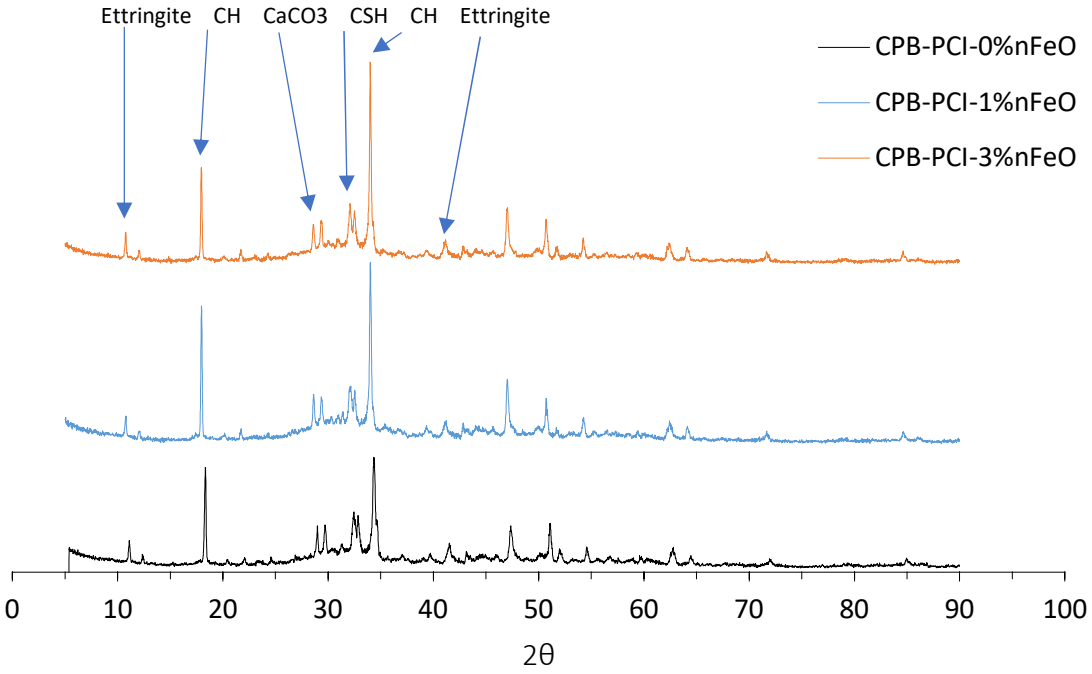

Figure 3.4XRD results of cement paste of PCI-CPB with 0,1 and 3 percentage of nFeO inclusion after 2 h.

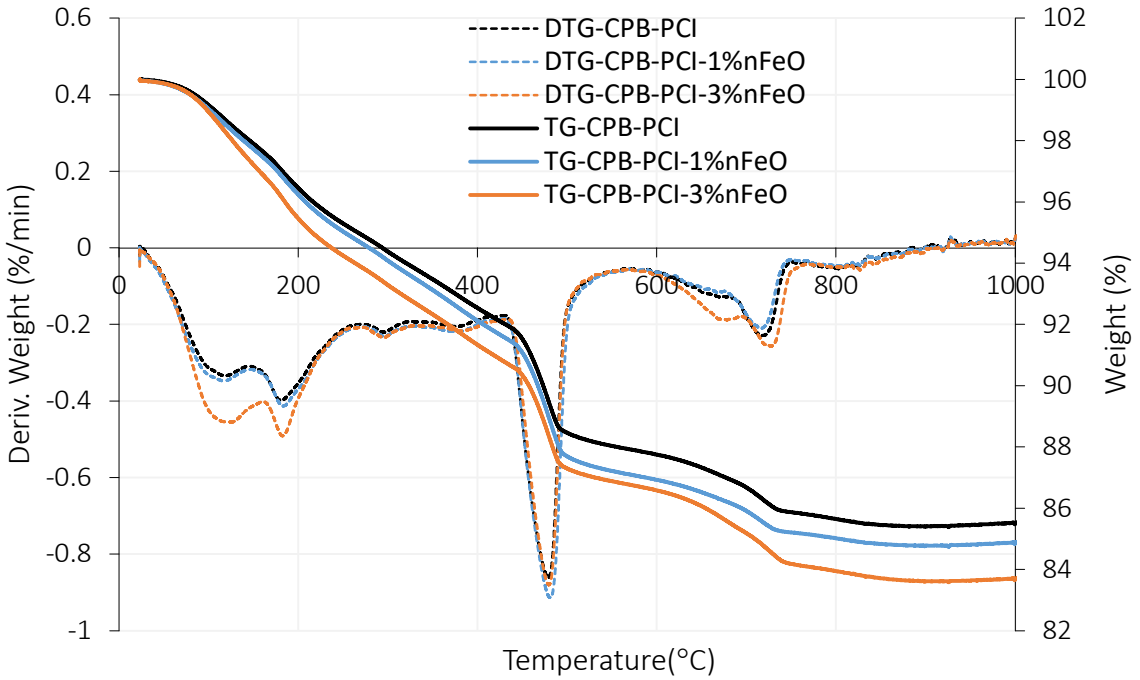

Figure 3.5 TG/DTG diagrams for cement pastes with 100% PCI cured for 2 h and containing 0%, 1%, and 3% of nFeO particles

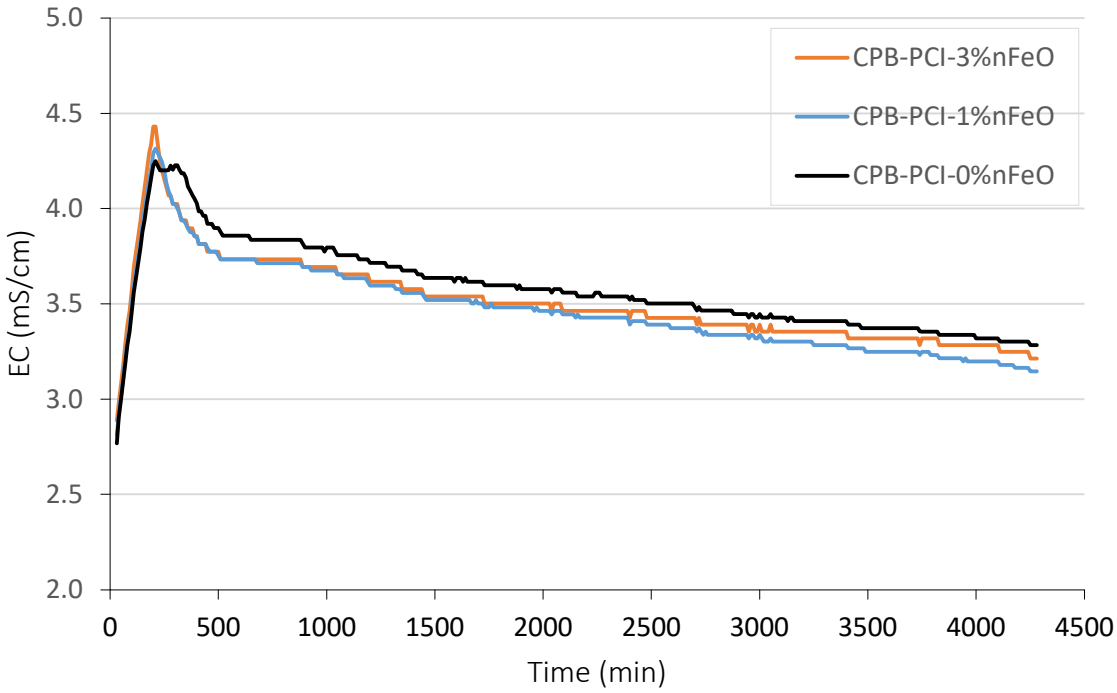

.

Figure 3.6 Changes in electrical conductivity of PCI-CPB specimens.

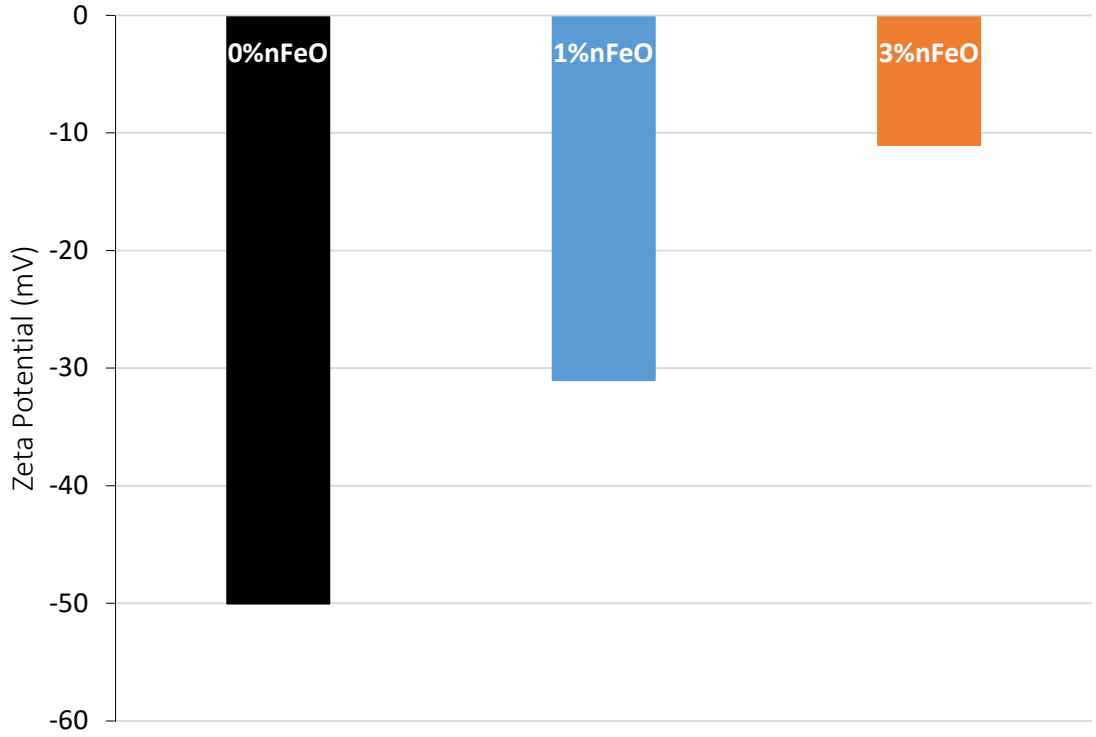

Figure 3.7 Zeta potentials of 2 hours old CPB with 0% nFeO vs 1%nFeO vs 3% nFeO.

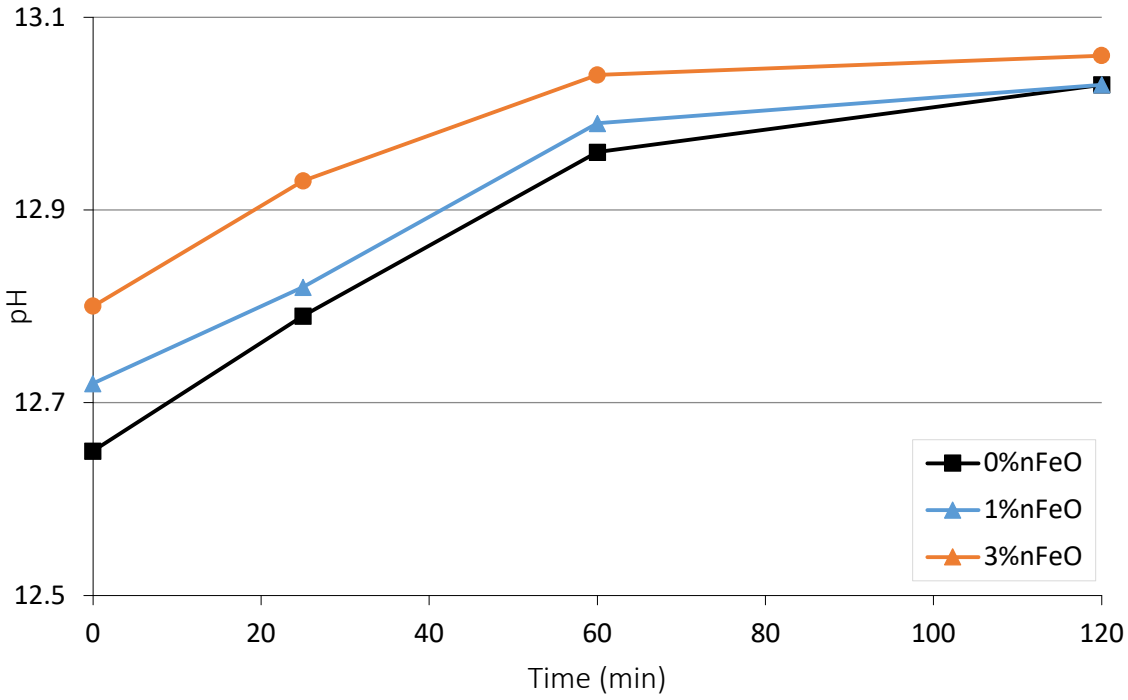

Figure 3.8 pH evolution of CPBs with 0% nFeO vs 1%nFeO vs 3%nFeO.

3.3.2 Influence of Nano-Iron Oxide (nFeO) on the rheological properties of CPB with Slag

In recent years, blending cement with a mineral mixture, such as Slag, has been widely employed in cemented backfill. Blended cement results in a cost decrease of CPB and improves its durability [41]. Moreover, the use of Slag, which is a low-carbon binder, helps to reduce the carbon footprint of a mine, thereby promoting sustainable mining and mine waste management. Thus, further tests were carried out to assess the rheological characteristics of backfill wherein Portland cement was partially substituted with slag. Three replacement scenarios were explored: a 0% replacement denoted as PCI, a 50% replacement denoted as PCI/Slags (50/50), and a 75% replacement represented as PCI/Slags (25/75).

Figure 3.9 illustrates the impact of varying nFeO percentages on the yield stress (Figure 3.9a) and viscosity (Figure 3.9b) of backfill samples with PCI, PCI/Slag (50/50), and PCI/Slag (25/75) after a 2-hour curing period. The data reveals a consistent trend: both yield stress and viscosity exhibit show an ascending trend with increasing nFeO content and curing time across all sample types—PCI, PCI/Slag (50/50), and PCI/Slag (25/75) regardless of the binder utilized. The underlying mechanisms driving this behavior have been elucidated in the preceding section. In particular, Figure 3.9a indicates that, regardless of the presence or absence of nanoparticles, samples containing Slag consistently display higher yield stress compared to those containing only PC. Moreover, the yield stress shows a positive correlation with the proportion of Slag in the mix. To illustrate, the yield stress values for samples with 100% PCI, PCI/Slag (50/50), and PCI/Slag (25/75) after a 2-hour aging period without nFeO were 325, 423, and 683 Pa, respectively. The increased yield stress observed in samples containing PCI/Slag can be ascribed to alterations in inter-particle forces resulting from the partial replacement of PCI with Slag. The coagulation and dispersion behavior of a suspension is influenced by Van der Waals attraction and electrostatic repulsive forces. When the predominant particle interaction is attraction, aggregates form, leading to an augmentation in yield stress. Figure 3.13 displays the results of zeta potential analysis conducted on fresh CPB samples with

varying PCI-to-Slag replacement ratios, excluding nFeO. Notably, the absolute value of zeta potential is higher in the 100%PCI-CPB sample (50 mV) compared to the Slag-CPB sample (25 mV for PCI/Slag (50/50), 20 mV for PCI/Slag (25/75)), indicating a greater electric double layer repulsive force in the former. Conversely, particles in the Slag-CPB exhibit increased attractiveness, contributing to higher yield stress. Additionally, in line with DLVO theory, the reduced zeta potential in Slag-CPB suggests the potential formation of a 'secondary minimum,' characterized by a weaker and potentially reversible adhesion between particles. These weak flocs remain stable enough to withstand Brownian motion, requiring additional externally applied force for the vane blade to induce flow in the suspension [19-20].

Moreover, by examining Figure 3.9b, it becomes evident that the viscosity of the CPB exhibits a contrasting trend in comparison to the yield stress when Slag is introduced into the binder system, regardless of the presence or absence of nanoparticles. To put it differently, the introduction of Slag as a partial replacement for PC results in a reduction in the viscosity of the backfill samples. The higher viscosity of 100%PCI-CPB, in comparison to Slag-CPBs, can be rationalized through two underlying mechanisms. Firstly, the faster hydration rate of cement (compared to Slag) in the early stages leads to the formation of more hydration products, such as C–S–H gel, ettringite, and CH, effectively bonding the tailing particles and thereby increasing the solid volume fraction and particle cohesion, ultimately resulting in higher viscosity. Secondly, the reduced formation of hydration products in the Slag-CPB implies a lower specific surface area for the C–S–H gel, resulting in diminished water adsorption and consequently more free water in the Slag-CPB. This excess free water forms a water film that envelops and lubricates particles [33]. The argument regarding the increased formation of hydration products in 100%PCI-CPB samples is experimentally validated through thermal analysis (TG/DTG) test results, which are employed to ascertain the phase stability of cement and the quantity of hydrates present. Figures 3.11 and 10 illustrate the TG/DTG and XRD diagrams for cement paste (CP) specimens with Slag/PCI-CP and PCI-CP. Analyzing the TG/DTG curves for various combinations of CPs reveals that the presence of hydration products was notably elevated when the binder consisted of 100% PCI. This higher amount is favorable for the CPB hardening but alters the flow ability since C-S-H is the most important binding component of cement-based materials [11]. The formation of a greater number of cement hydration products in samples containing 100% PCI is also confirmed experimentally by the results of monitoring the EC of CPB with 100% PCI and with a mixture of PCI cement and slag (50/50), presented in figure 3.12. This figure shows that EC reached its maximum earlier in the sample with 100%PCI than in that with a cement blend, indicating faster hydration of the binder in the former case.

From Figure 3.9, it is also evident that the addition of nFeO increased the yield stress of all CPBs, irrespective of the binder type. However, the yield stress of the PCI/Slag (25/75) increased more with nFeO content than with PCI/Slag (50/50), and PCI-CPB samples. Indeed, PCI/Slag (25/75) samples showed the highest yield stress at 3% nFeO after 2 hours (912 Pa). This magnificent yield stress can be interpreted as follows. Initially, upon water addition to the mixture (pre-induction period), certain cement components such as aluminate (C_3A) and gypsum dissolve, resulting in a slight reduction of solid concentration [63-64]. Second, the early-age hydration reactions of Slag/PCI-blended binder proceed slower than that of PCI alone, leading to fewer hydration products and yield stress controlled by initial inter-particle forces in the Slag-CPB mixture[12]. This slower hydration rate is supported by electrical conductivity monitoring results, where higher values are observed in samples with higher Portland cement content (Figure 3.12). Conversely, CPBs with Slag/PCI-blended binder exhibit delayed peak electrical conductivity, indicating slower early-age hydration reactions [65-66] (Figure 3.12). As the Slag replacement percentage increases, the reactivity of CPB samples decreases due to a reduction in the alkaline activating environment provided by Portland cement hydration. Third, the consumption of calcium hydroxide (CH) by Slag activation increases the negative zeta potential of the mixture, enhancing repulsive force and flowability [67-68]. Additionally, increasing the proportion of slag in the blended binder leads to higher yield stress and viscosity of Slag-CPB [65, 69]. This is attributed to the small particle size of Slag particles, resulting in a filler effect that bridges spaces between cement particles or tailings grains, leading to denser packing within the backfill matrix [12, 15]. Denser packing increases friction between particles, thereby increasing yield

stress. Moreover, denser packing increases solid volume fraction, intensifying particle-particle interactions and viscosity according to the Krieger–Dougherty model [63].

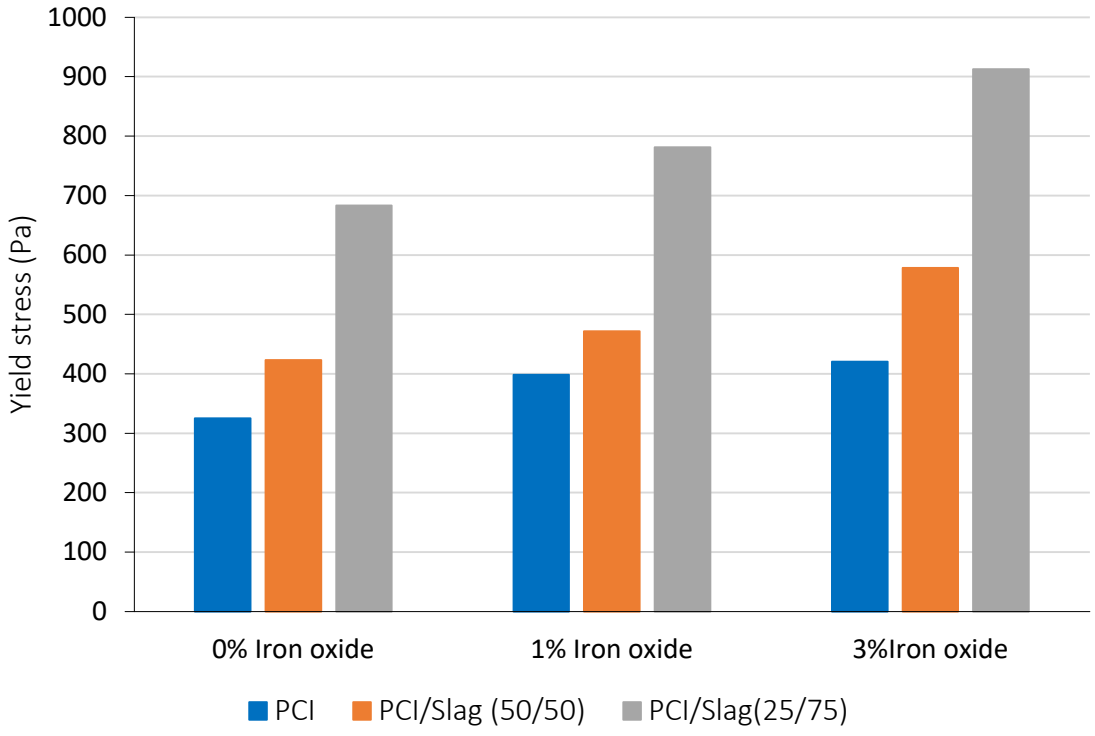

a) Yield stress

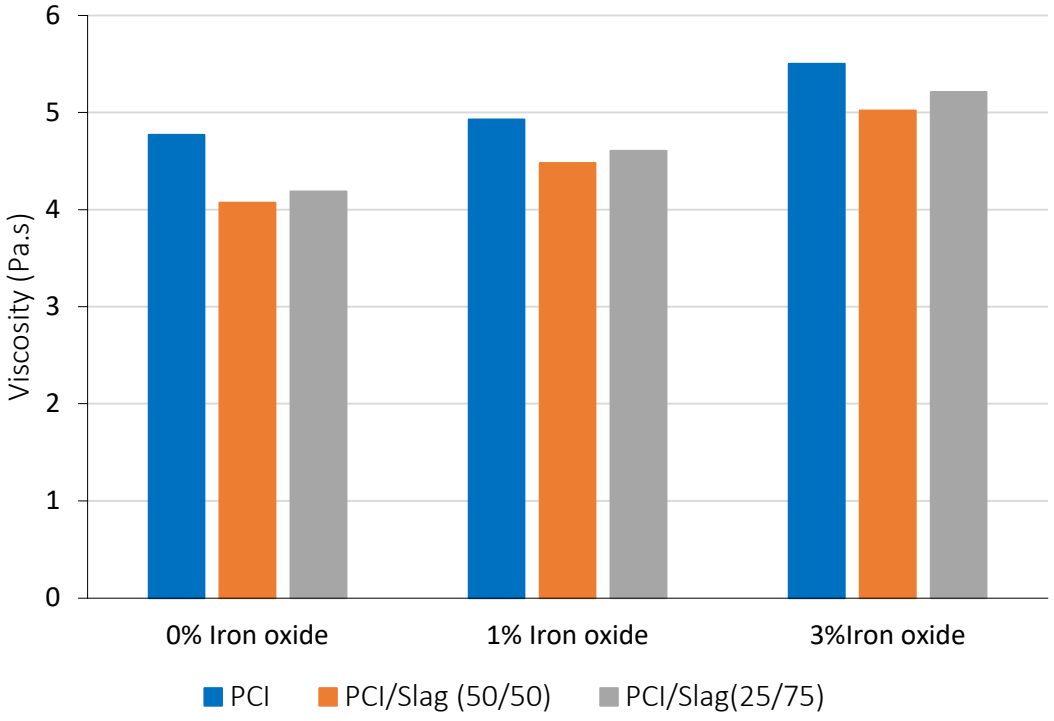

b) Viscosity.

Figure 3.9 Effect of Slag and nano-Fe2O3 and binder type on the rheological properties of 2 hr old CPB. a) yield stress; b) Viscosity

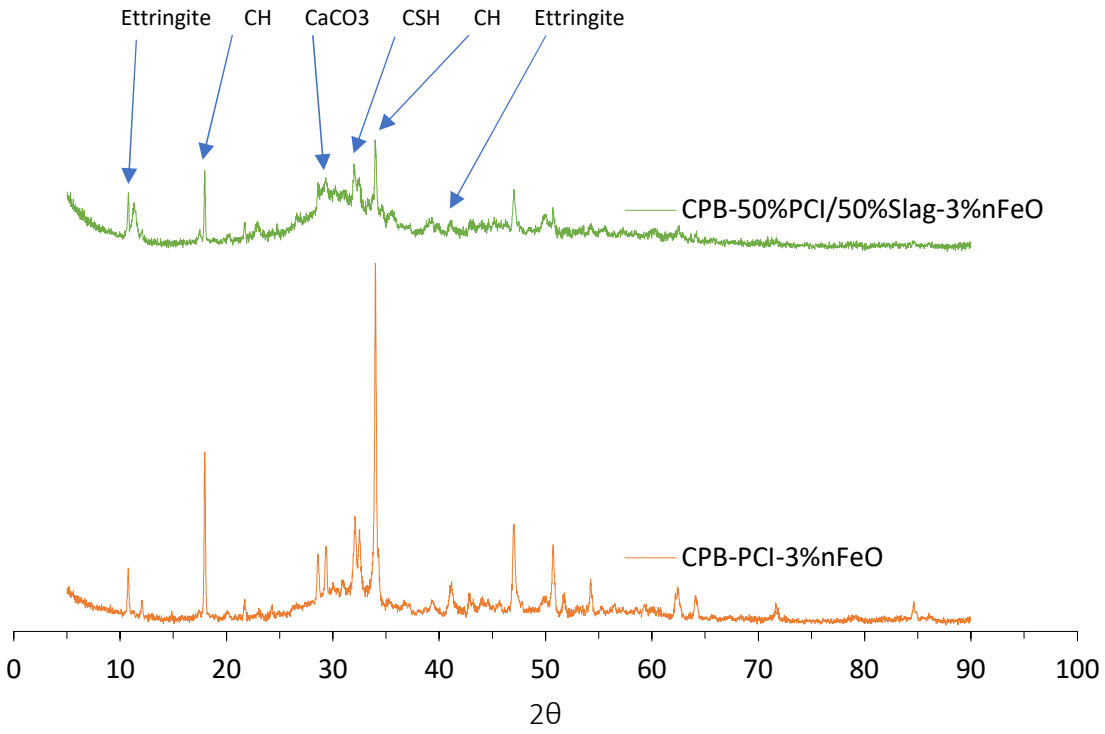

Figure 3.10 XRD results of cement paste of PCI/Slag (50/50), with the inclusion of 3% nFeO samples after 2 h.

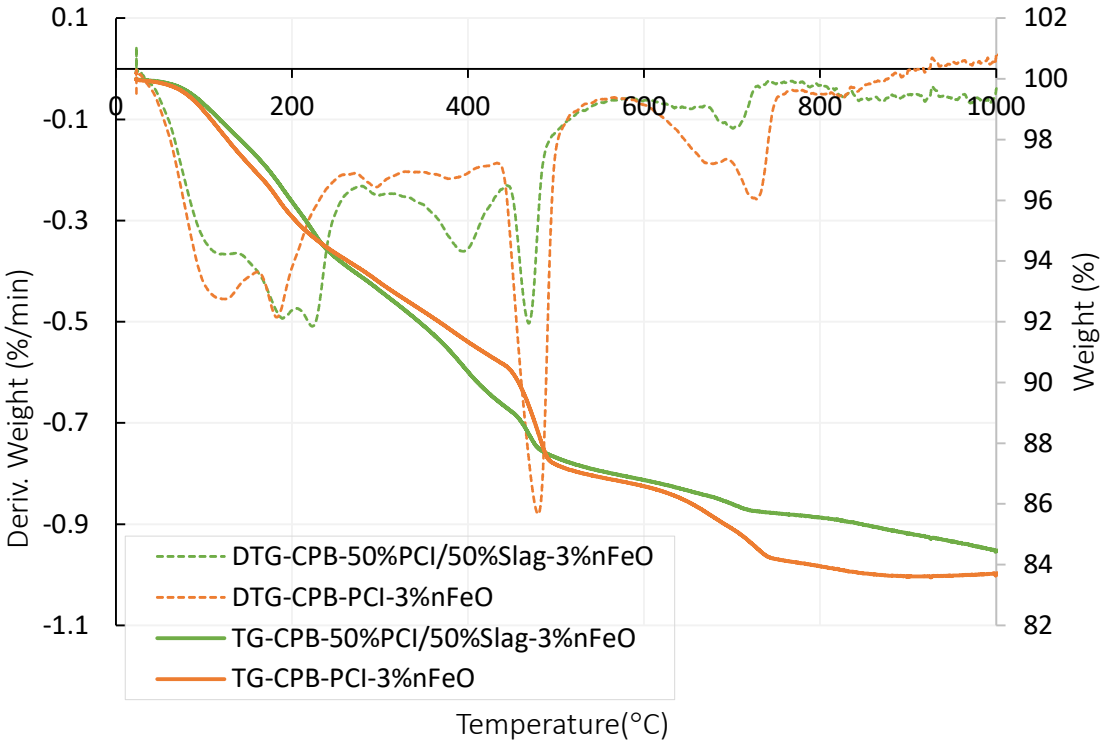

Figure 3.11 TG/DTG results of cement paste of PCI and PCI, PCI/Slag (50/50), with the inclusion of 3% nFeO samples after 2 h.

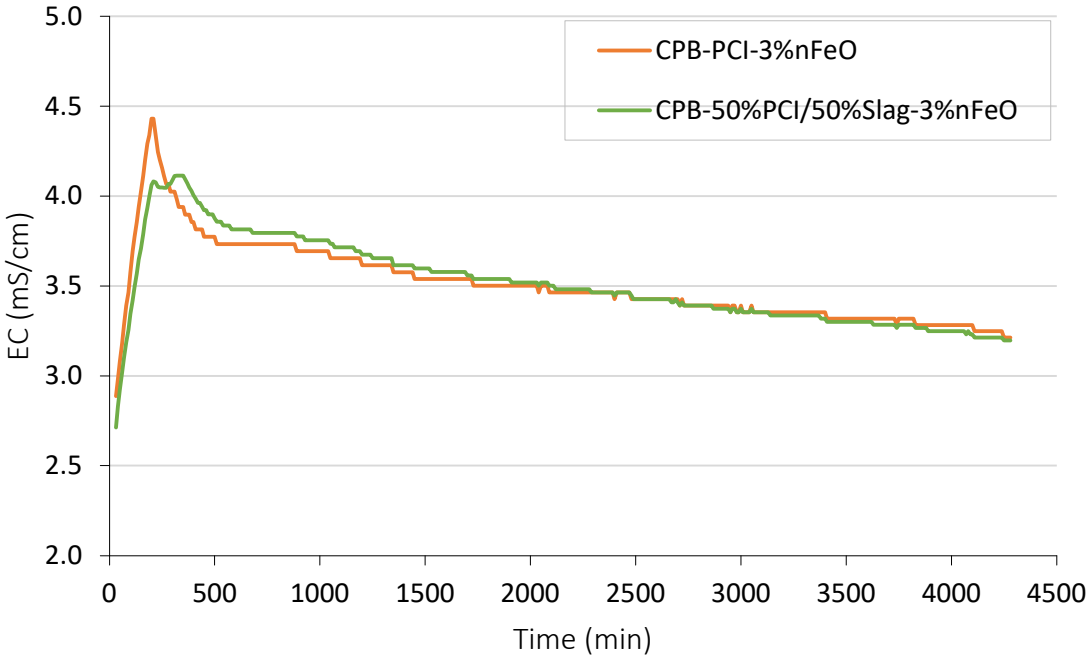

Figure 3.12 EC monitoring results of CPB samples with the PCI, PCI/Slag (50/50), with the inclusion of 3% nFeO.

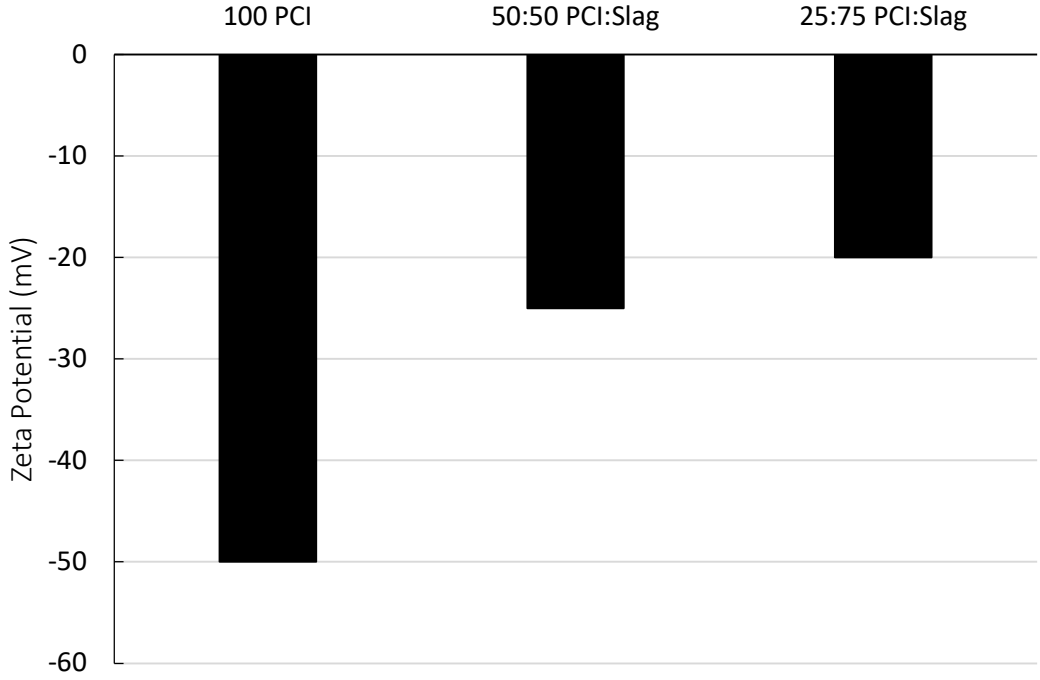

Figure 3.13 Zeta potentials of (100%) PCI-CPB vs Slag-CPB (50:50 PCI: Slag) vs Slag-CPB (25:75 PCI: Slag).

3.3.3 Impact of superplasticizer on the rheological properties of CPB with nFeO

The findings presented and analyzed earlier indicate that the introduction of nFeO particles adversely affects the flow characteristics of CPB. This may be a potential concern for ensuring the smooth transport of fresh CPBs modified with nFeO particles in practice. Consequently, a pertinent inquiry arises: can the incorporation of a superplasticizer substantially improve the flow properties of CPB containing nFeO? As such, an investigation into the impact of superplasticizer on the rheological properties of CPB with nFeO was also undertaken.

Figure 3.14 illustrates the impact of a superplasticizer (at a concentration of 0.125% by weight of the mixture) on the yield stress (Figure 3.14a) and viscosity (Figure 3.14b) of CPB aged 0, 20 minutes, 1 hour, 2 hours, and, 4 hours containing different amounts of nFeO. This figure shows that the addition of a superplasticizer to the CPB with nFeO particles resulted in a substantial improvement of the flow ability of CPB, regardless of the nanoparticle content. For example, specimens with 3% nFeO and 1% nFeO in the presence of superplasticizer showed a reduction in yield stress of 57% and 54%, respectively, after 4 hours of aging. Correspondingly the viscosity of the samples decreases too. Additionally, it can be observed from Figure 3.14a that the impact of the superplasticizer on the yield stress was more pronounced for CPB samples with higher nFeO content. This behavior suggests that the addition of a superplasticizer is even more crucial for improving the flow ability of CPB with a higher nFeO percentage. This enhancement of the flow ability of CPB with superplasticizer would obviously result in enhancing pumping efficiency, reducing energy consumption and operational costs associated with pumping the nFeO-CPB material underground.

The reduction in yield stress and viscosity resulting from the inclusion of a superplasticizer can be attributed to the combined influence of two key factors. Firstly, it originates from the dispersing effect of higher-range water-reducing admixtures (WRAs). Superplasticizers derived from carboxylic compounds, such as Master

Glenium, introduce two distinct mechanisms of repulsion between cement particles: a) electrostatic repulsion resulting from the negative charges of the carboxylic group, and b) steric repulsion associated with the long polymer chains in the compound [36, 66, 72-73]. Secondly, the superplasticizer contributes to delaying cement hydration at very early stages. As the repulsive force between cement particles intensifies, fewer hydration by-products are produced, resulting in lower solid content and reduced viscosity of the CPB. This statement is supported by TG/DTG diagrams of cement paste samples with varying superplasticizer proportions cured for 2 hours, as depicted in Figure 3.15. The diagrams indicate that more hydration products are produced within the cement paste without superplasticizer. Specifically, the initial peak at around 100-200°C, indicating the most significant weight loss, are observed in the sample containing 0% superplasticizer. The first peak corresponds to the formation of products such as calcium-silicate-hydrate (C-S-H), ettringite, and gypsum ([47], [70-72]). This lower peak observed in TG/DTG results (Figure 3.15) of the cement paste sample with superplasticizer suggest that significantly fewer solid products are formed during the hydration process in the presence of the superplasticizer. Additionally, EC monitoring results depicted in Figure 3.16 support the assertion that the superplasticizer retards the hydration reaction. The electrical conductivity of the cement paste containing 0.125% superplasticizer is notably lower than that of the paste with 0% superplasticizer, indicating higher ion mobility in the paste without the admixture. Moreover, the specimen without superplasticizer reaches its peak earlier (after 210 min) than the sample with superplasticizer (peak after 240 min), suggesting a faster rate of cement hydration in the superplasticizer-free sample.

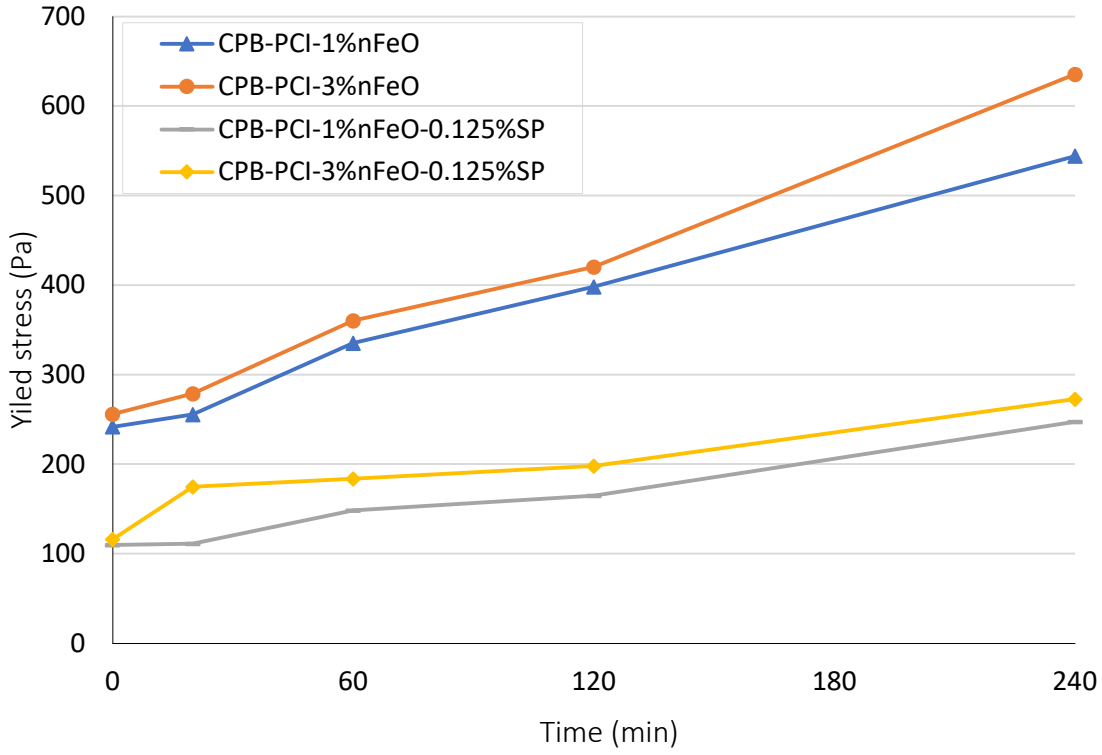

a) Yield stress

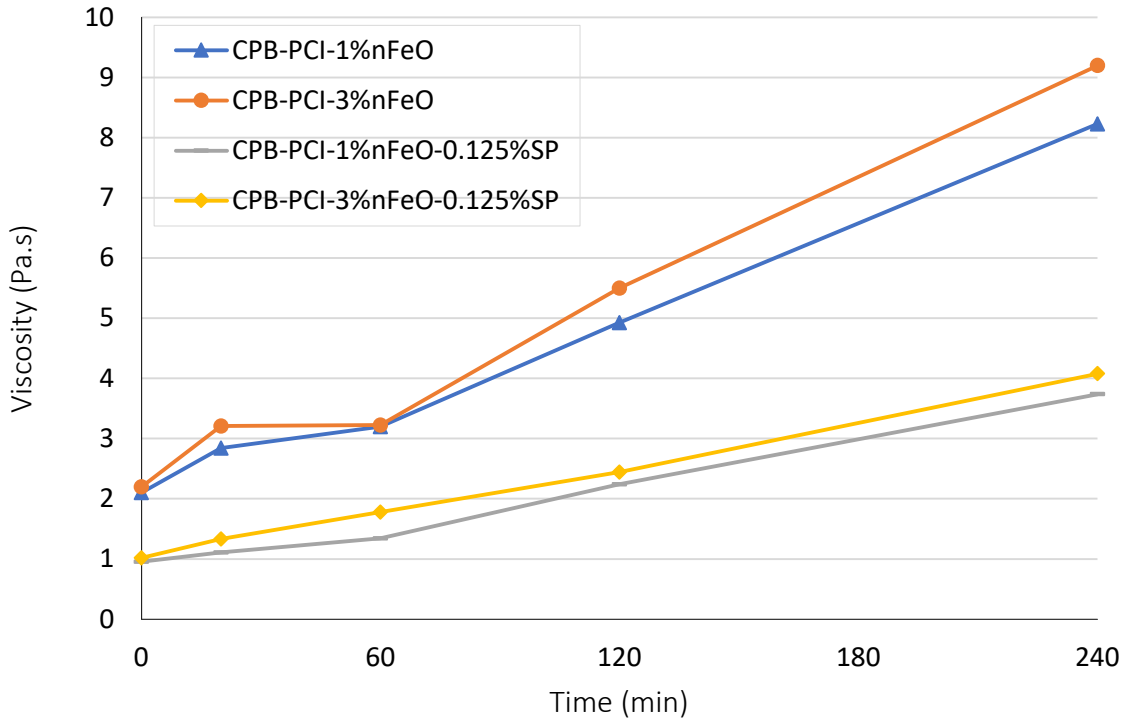

b) Viscosity.

Figure 3.14 Effect of superplasticizer versus nano-Fe2O3 on the evolution of CPB rheological properties. a) yield stress; b) Viscosity

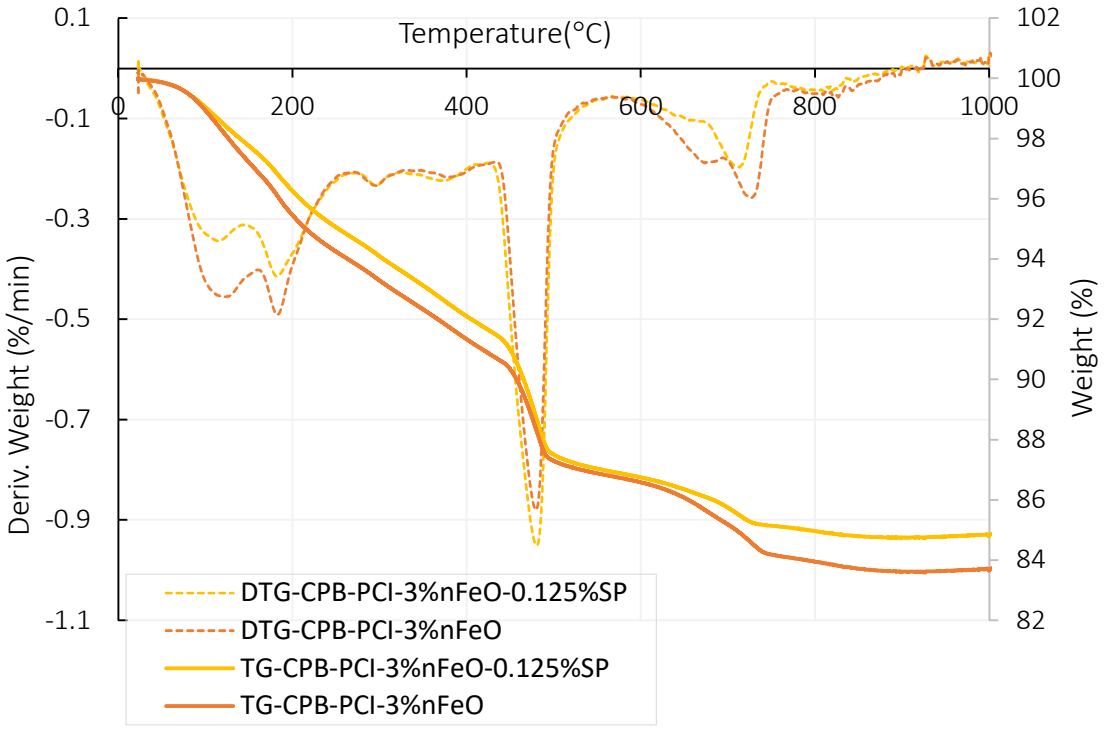

Figure 3.15 TG/DTG results of cement paste of PCI and PCI with the inclusion of 3% nFeO and 0.125% SP samples after 2 h.

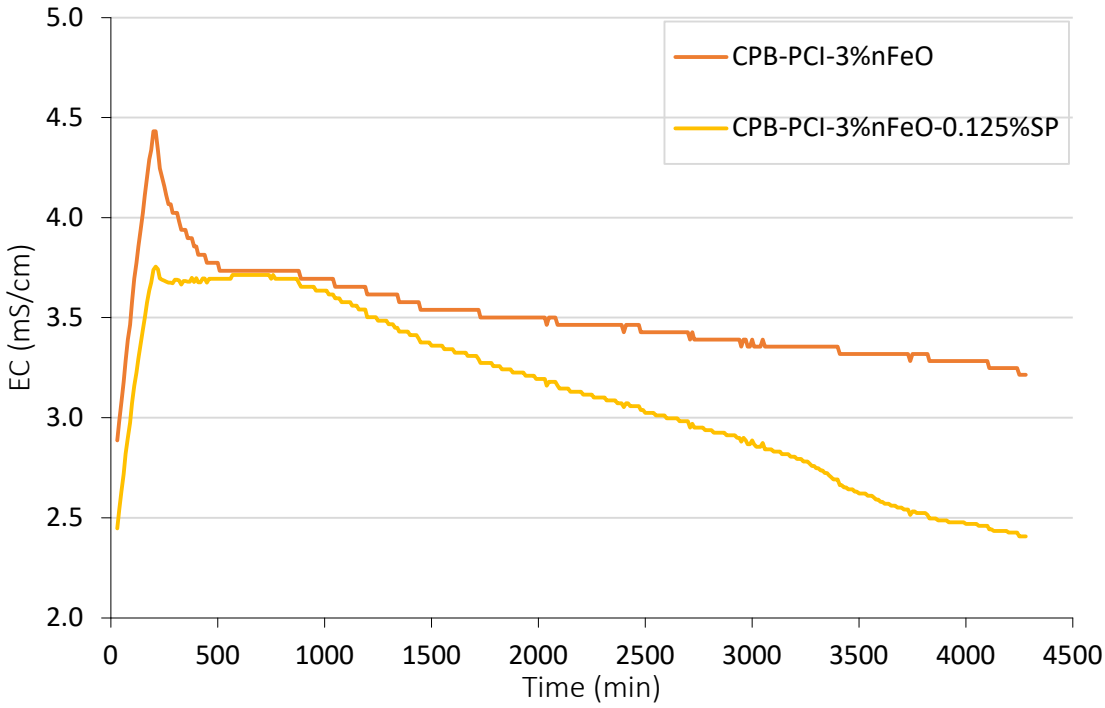

Figure 3.16 displays the EC of the PCI with the inclusion of 3% nFeO and 0.125% SP.

3.4 Conclusion

This study experimentally examined the effect of nFeO on the rheological properties of cemented paste backfill. Drawing on the findings, the subsequent deduction may be made:

- The addition of nFeO particles to CPB or increasing the dosage of nFeO leads to the alteration of the flowability of the fresh CPB, by increasing its yield stress and viscosity. The mechanisms responsible for this alteration include (i) the filler effect of nFeO; (ii) the production of more cement hydration products due to the enhancement of the cement hydration by nFeO; (iii) a nFeO-induced increase in water demand; (iv) nFeO-induced enhancement of flocculation or agglomeration of the CPB.

- The magnitude of the effect of nFeO particles on the rheological properties depends on the curing time. The nFeO-induced increase in yield stress and viscosity of CPB becomes more significant as the curing or transportation time increases. This is because the enhancement of flocculation of the CPB due to nFeO particles and the nFeO-induced formation of more binder hydration products increase with time.

- The intensity of the effect of nFeO on the flowability of CPB also depends on the type of binder employed in the preparation of CPB. The yield stress of the PCI-CPB increased slower as the nFeO content increased than that of PCI/Slag (25/75) and PCI/Slag (50/50) samples. Thus, the flowability of a PCI/Slag binder is more altered by nFeO than that of CPB without Slag as transportation time increases. The mechanism responsible for this behavior can be attributed to the friction effect of multivalent cations between nFeO particles. Moreover, denser packing increases solid volume fraction, intensifying particle-particle interactions and viscosity according to the Krieger–Dougherty model.

- The examined Slag-CPB demonstrated an increased yield stress but decreased viscosity compared to PCI-CPB. The elevated binder content contributed to reduced yield stress and viscosity when maintaining a constant water-cement ratio, primarily due to increased free water bleeding. Additionally, an augmentation in the Slag proportion in the Slag-CPB resulted in decreased flowability.

- The addition of superplasticizer to CPB with nFeO can substantially improve its flow ability or transportability due to the superplasticizer-induced increase in the electrostatic repulsion between the CPB particles. The effect of superplasticizer is more pronounced as the nFeO content increses

Lastly, while nano-engineered cemented paste backfill is assumed to have tremendous potential, scaling up the laboratory results and operating on a larger scale are of the utmost importance to analyze the cost-benefit ratio.

3.5 References:

[1] L. Cui, M. Fall. Multiphysics modeling and simulation of strength development and distribution in cemented tailings backfill structures. International Journal of Concrete Structures and Materials, 12 (1): 1-22, 2018.

[2] L. Cui, M. Fall. Modeling of pressure on retaining structures for fill mass. Tunnelling and Underground Space Technology 69:94-107, 2017.

[3] H. Du, S. Du, and X. Liu, "Durability performances of concrete with nano-silica," Construction and Building Materials, vol. 73, pp. 705–712, Dec. 2014, doi: 10.1016/j.conbuildmat.2014.10.014.

[4] A. Ghirian and M. Fall, "Coupled thermo-hydro-mechanical–chemical behaviour of cemented paste backfill in column experiments. Part I: Physical, hydraulic and thermal processes and characteristics," Engineering Geology, vol. 164, pp. 195–207, Sep. 2013, doi: 10.1016/j.enggeo.2013.01.015.

[5] J. Qiu, Z. Guo, L. Yang, H. Jiang, and Y. Zhao, "Effects of packing density and water film thickness on the fluidity behaviour of cemented paste backfill," Powder Technology, vol. 359, pp. 27–35, Jan. 2020, doi: 10.1016/j.powtec.2019.10.046.

[6] A. Aldhafeeri, M. Fall. Sulphate induced changes in the reactivity of cemented tailings backfill. International Journal of Mineral Processing 166 (10):13-23, 2017.

[7] F. Colangelo, A. Forcina, I. Farina, and A. Petrillo, "Life Cycle Assessment (LCA) of Different Kinds of Concrete Containing Waste for Sustainable Construction," Buildings, vol. 8, no. 5, p. 70, May 2018, doi: 10.3390/buildings8050070.

[8] M. Fall and M. Benzaazoua, "Modeling the effect of sulphate on strength development of paste backfill and binder mixture optimization," Cement and Concrete Research, vol. 35, no. 2, pp. 301–314, Feb. 2005, doi: 10.1016/j.cemconres.2004.05.020.

[9] A. Ghirian and M. Fall, "Strength evolution and deformation behaviour of cemented paste backfill at early ages: Effect of curing stress, filling strategy and drainage," International Journal of Mining Science and Technology, vol. 26, no. 5, pp. 809–817, Sep. 2016, doi: 10.1016/j.ijmst.2016.05.039.

[10] D. Simon and M. Grabinsky, "Apparent yield stress measurement in cemented paste backfill," International Journal of Mining, Reclamation and Environment, vol. 27, no. 4, pp. 231–256, Aug. 2013, doi: 10.1080/17480930.2012.680754.

[11] H. F. Taylor, The chemistry of cements. 1, 2. print. London: Acad. Press, 1972.

[12] J. Haiqiang, M. Fall, and L. Cui, "Yield stress of cemented paste backfill in sub-zero environments: Experimental results," Minerals Engineering, vol. 92, pp. 141–150, Jun. 2016, doi: 10.1016/j.mineng.2016.03.014.

[13] P. Xiapeng, M. Fall, and S. Haruna, "Sulphate induced changes of rheological properties of cemented paste backfill," Minerals Engineering, vol. 141, p. 105849, Sep. 2019, doi: 10.1016/j.mineng.2019.105849.

[14] F. Lavergne, R. Belhadi, J. Carriat, and A. Ben Fraj, "Effect of nano-silica particles on the hydration, the rheology and the strength development of a blended cement paste," Cement and Concrete Composites, vol. 95, pp. 42–55, Jan. 2019, doi: 10.1016/j.cemconcomp.2018.10.007.

[15] H. Jiang and M. Fall, “Yield stress and strength of saline cemented tailings materials in sub-zero environments: slag-paste backfill,” Journal of Sustainable Cement-Based Materials, vol. 6, no. 5, pp. 314–331, Sep. 2017, doi: 10.1080/21650373.2017.1280428.

[16] H. Justnes and H. V. Vikan, “Viscosity of Cement Slurries as a Function of Solids Content,” 2005. [Online]. Available: https://api.semanticscholar.org/CorpusID:89612352.

[17] D. P. Bentz, C. F. Ferraris, M. A. Galler, A. S. Hansen, and J. M. Guynn, “Influence of particle size distributions on yield stress and viscosity of cement–fly ash pastes,” Cement and Concrete Research, vol. 42, no. 2, pp. 404–409, Feb. 2012, doi: 10.1016/j.cemconres.2011.11.006.

[18] Z. Li, T. Ohkubo, and Y. Tanigawa, “Theoretical Analysis of Time-Dependence and Thixotropy of Fluidity for High Fluidity Concrete,” J. Mater. Civ. Eng., vol. 16, no. 3, pp. 247–256, Jun. 2004, doi: 10.1061/(ASCE)0899-1561(2004)16:3(247).

[19] C.-J. Chin, S. Yiacoumi, and C. Tsouris, “Probing DLVO Forces Using Interparticle Magnetic Forces: Transition from Secondary-Minimum to Primary-Minimum Aggregation,” Langmuir, vol. 17, no. 20, pp. 6065–6071, Oct. 2001, doi: 10.1021/la0015260.

[20] J. A. Fornes, “Secondary minimum analysis in the DLVO-theory,” Colloid & Polymer Sci, vol. 263, no. 12, pp. 1004–1007, Dec. 1985, doi: 10.1007/BF01410994.

[21] J. Chen, S. Kou, and C. Poon, “Hydration and properties of nano-TiO2 blended cement composites,” Cement and Concrete Composites, vol. 34, no. 5, pp. 642–649, May 2012, doi: 10.1016/j.cemconcomp.2012.02.009.

[22] G. Land and D. Stephan, “The influence of nano-silica on the hydration of ordinary Portland cement,” J Mater Sci, vol. 47, no. 2, pp. 1011–1017, Jan. 2012, doi: 10.1007/s10853-011-5881-1.

[23] Z. Li, H. Wang, S. He, Y. Lu, and M. Wang, “Investigations on the preparation and mechanical properties of the nano-alumina reinforced cement composite,” Materials Letters, vol. 60, no. 3, pp. 356–359, Feb. 2006, doi: 10.1016/j.matlet.2005.08.061.

[24] M. Oltulu and R. Şahin, “Pore structure analysis of hardened cement mortars containing silica fume and different nano-powders,” Construction and Building Materials, vol. 53, pp. 658–664, Feb. 2014, doi: 10.1016/j.conbuildmat.2013.11.105.

[25] G. Quercia, P. Spiesz, G. Hüsken, and H. J. H. Brouwers, “SCC modification by use of amorphous nano-silica,” Cement and Concrete Composites, vol. 45, pp. 69–81, Jan. 2014, doi: 10.1016/j.cemconcomp.2013.09.001.

[26] A. M. Said, M. S. Zeidan, M. T. Bassuoni, and Y. Tian, “Properties of concrete incorporating nano-silica,” Construction and Building Materials, vol. 36, pp. 838–844, Nov. 2012, doi: 10.1016/j.conbuildmat.2012.06.044.

[27] L. Senff, D. Hotza, S. Lucas, V. M. Ferreira, and J. A. Labrincha, “Effect of nano-SiO2 and nano-TiO2 addition on the rheological behavior and the hardened properties of cement mortars,” Materials Science and Engineering: A, vol. 532, pp. 354–361, Jan. 2012, doi: 10.1016/j.msea.2011.10.102.

[28] M. Zhang and H. Li, “Pore structure and chloride permeability of concrete containing nano-particles for pavement,” Construction and Building Materials, vol. 25, no. 2, pp. 608–616, Feb. 2011, doi: 10.1016/j.conbuildmat.2010.07.032.

[29] B. Bharathan, M. McGuinness, S. Kuhar, M. Kermani, F. P. Hassani, and A. P. Sasmito, “Pressure loss and friction factor in non-Newtonian mine paste backfill: Modelling, loop test and mine field data,” Powder Technology, vol. 344, pp. 443–453, Feb. 2019, doi: 10.1016/j.powtec.2018.12.029.

[30] M. Fall, M. Benzaazoua, and E. G. Saa, “Mix proportioning of underground cemented tailings backfill,” Tunnelling and Underground Space Technology, vol. 23, no. 1, pp. 80–90, Jan. 2008, doi: 10.1016/j.tust.2006.08.005.

[31] D. Wu, M. Fall, and S. J. Cai, “Coupling temperature, cement hydration and rheological behaviour of fresh cemented paste backfill,” Minerals Engineering, vol. 42, pp. 76–87, Mar. 2013, doi: 10.1016/j.mineng.2012.11.011.

[32] M. Yang, “Interparticle Potential and Sedimentation Behavior of Cement Suspensions Review and Results from Paste,” Advanced Cement Based Materials, vol. 5, no. 1, pp. 1–7, Jan. 1997, doi: 10.1016/S1065-7355(96)00076-4.

[33] H. Jiang and M. Fall, “Yield stress and strength of saline cemented tailings in sub-zero environments: Portland cement paste backfill,” International Journal of Mineral Processing, vol. 160, pp. 68–75, Mar. 2017, doi: 10.1016/j.minpro.2017.01.010.

[34] S. Hanehara and K. Yamada, “Rheology and early age properties of cement systems,” Cement and Concrete Research, vol. 38, no. 2, pp. 175–195, Feb. 2008, doi: 10.1016/j.cemconres.2007.09.006.

[35] C. Astm, “494,” Standard Specification for Chemical Admixture for Concrete, 2004.

[36] S. Haruna and M. Fall, “Time- and temperature-dependent rheological properties of cemented paste backfill that contains superplasticizer,” Powder Technology, vol. 360, pp. 731–740, Jan. 2020, doi: 10.1016/j.powtec.2019.09.025.

[37] “Brookfield.” [Online]. Available: https://pim-resources.coleparmer.com/instruction-manual/98945-xx.pdf.

[38] ASTM, Standard test method for laboratory miniature vane shear test for saturated fine-grained clayey soil. American Society for Testing and Materials West Conshohocken, PA, 2016.

[39] J. D. Clogston and A. K. Patri, “Zeta Potential Measurement,” in Characterization of Nanoparticles Intended for Drug Delivery, S. E. McNeil, Ed., Totowa, NJ: Humana Press, 2011, pp. 63–70. doi: 10.1007/978-1-60327-198-1_6.

[40] A. Roshani and M. Fall, “Rheological properties of cemented paste backfill with nano-silica: Link to curing temperature,” Cement and Concrete Composites, vol. 114, p. 103785, Nov. 2020, doi: 10.1016/j.cemconcomp.2020.103785.

[41] Y. Zhou, M. Fall, and S. Haruna, “Flow ability of cemented paste backfill with chloride-free antifreeze additives in sub-zero environments,” Cement and Concrete Composites, vol. 126, p. 104359, Feb. 2022, doi: 10.1016/j.cemconcomp.2021.104359.

[42] H. F. Taylor, Cement chemistry, vol. 2. Thomas Telford London, 1997.

[43] American Society for Testing and Materials, “Cement, concrete and aggregates,” 1979.

[44] W. Sha, E. A. O'Neill, and Z. Guo, "Differential scanning calorimetry study of ordinary Portland cement," Cement and Concrete research, vol. 29, no. 9, pp. 1487–1489, 1999.

[45] W. Li and M. Fall, "Strength and self-desiccation of slag-cemented paste backfill at early ages: Link to initial sulphate concentration," Cement and Concrete Composites, vol. 89, pp. 160–168, May 2018, doi: 10.1016/j.cemconcomp.2017.09.019.

[46] I. Pane and W. Hansen, "Investigation of blended cement hydration by isothermal calorimetry and thermal analysis," Cement and Concrete Research, vol. 35, no. 6, pp. 1155–1164, Jun. 2005, doi: 10.1016/j.cemconres.2004.10.027.

[47] Q. Zhou and F. P. Glasser, "Thermal stability and decomposition mechanisms of ettringite at< 120 C," Cement and Concrete Research, vol. 31, no. 9, pp. 1333–1339, 2001.

[48] E. Nonnet, N. Lequeux, and P. Boch, "Elastic properties of high alumina cement castables from room temperature to 1600 C," Journal of the European Ceramic Society, vol. 19, no. 8, pp. 1575–1583, 1999.

[49] B. Xiao, M. Fall, and A. Roshani, "Towards Understanding the Rheological Properties of Slag-Cemented Paste Backfill," International Journal of Mining, Reclamation and Environment, vol. 35, no. 4, pp. 268–290, Apr. 2021, doi: 10.1080/17480930.2020.1807667.

[50] Y. Zhou and M. Fall, "Investigation on rheological properties of cemented pastefill with chloride-bearing antifreeze additives in sub-zero environments," Cold Regions Science and Technology, vol. 196, p. 103506, Apr. 2022, doi: 10.1016/j.coldregions.2022.103506.

[51] Y. M. Berkmen and A. Lande, "Chest roentgenography as a window to the diagnosis of Takayasu's arteritis," Am J Roentgenol Radium Ther Nucl Med, vol. 125, no. 4, pp. 842–846, Dec. 1975, doi: 10.2214/ajr.125.4.842.

[52] E. Akbar, Z. Yaakob, S. K. Kamarudin, M. Ismail, and J. Salimon, "Characteristic and composition of Jatropha curcas oil seed from Malaysia and its potential as biodiesel feedstock feedstock," European Journal of Scientific Research, vol. 29, no. 3. pp. 396–403, 2009.

[53] Y. Cai et al., "The use of tetraethyl orthosilicate silane (TEOS) for surface-treatment of hardened cement-based materials: A comparison study with normal treatment agents," Construction and Building Materials, vol. 117, pp. 144–151, Aug. 2016, doi: 10.1016/j.conbuildmat.2016.05.028.

[54] J. Björnström, A. Martinelli, A. Matic, L. Börjesson, and I. Panas, "Accelerating effects of colloidal nano-silica for beneficial calcium–silicate–hydrate formation in cement," Chemical Physics Letters, vol. 392, no. 1–3, pp. 242–248, Jul. 2004, doi: 10.1016/j.cplett.2004.05.071.

[55] E. Akbar, Z. Yaakob, S. K. Kamarudin, M. Ismail, and J. Salimon, "Characteristic and composition of Jatropha curcas oil seed from Malaysia and its potential as biodiesel feedstock feedstock," European Journal of Scientific Research, vol. 29, no. 3, pp. 396–403, 2009.

[56] "Mechanical Properties of Concrete Incorporating High Volumes of Fly Ash From Sources in the U.S.," MJ, vol. 90, no. 6, 1993, doi: 10.14359/4426.

[57] A. Roshani and M. Fall, “Flow ability of cemented pastefill material that contains nano-silica particles,” Powder Technology, vol. 373, pp. 289–300, Aug. 2020, doi: 10.1016/j.powtec.2020.06.050.
[58] X. Wei, “Study on hydration of Portland cement with fly ash using electrical measurement,” Mater. Struct., vol. 38, no. 277, pp. 411–417, Jan. 2005, doi: 10.1617/14108.

[59] W. J. McCarter, G. Starrs, and T. M. Chrisp, “Electrical conductivity, diffusion, and permeability of Portland cement-based mortars,” Cement and Concrete Research, vol. 30, no. 9, pp. 1395–1400, Sep. 2000, doi: 10.1016/S0008-8846(00)00281-7.

[60] H. Madani, A. Bagheri, and T. Parhizkar, “The pozzolanic reactivity of monodispersed nanosilica hydrosols and their influence on the hydration characteristics of Portland cement,” Cement and Concrete Research, vol. 42, no. 12, pp. 1563–1570, Dec. 2012, doi: 10.1016/j.cemconres.2012.09.004.

[61] Y. Qing, Z. Zenan, K. Deyu, and C. Rongshen, “Influence of nano-SiO2 addition on properties of hardened cement paste as compared with silica fume,” Construction and Building Materials, vol. 21, no. 3, pp. 539–545, Mar. 2007, doi: 10.1016/j.conbuildmat.2005.09.001.

[62] M. Fall, M. Benzaazoua, and S. Ouellet, “Experimental characterization of the influence of tailings fineness and density on the quality of cemented paste backfill,” Minerals Engineering, vol. 18, no. 1, pp. 41–44, Jan. 2005, doi: 10.1016/j.mineng.2004.05.012.

[63] I. M. Krieger and T. J. Dougherty, “A Mechanism for Non-Newtonian Flow in Suspensions of Rigid Spheres,” Transactions of the Society of Rheology, vol. 3, no. 1, pp. 137–152, Mar. 1959, doi: 10.1122/1.548848.

[64] S. Panchal, D. Deb, and T. Sreenivas, “Variability in rheology of cemented paste backfill with hydration age, binder and superplasticizer dosages,” Advanced Powder Technology, vol. 29, no. 9, pp. 2211–2220, 2018.

[65] D. Manmohan and P. K. Mehta, “Influence of pozzolanic, slag, and chemical admixtures on pore size distribution and permeability of hardened cement pastes,” Cement, concrete, and aggregates, vol. 3, no. 1, pp. 63–67, 1981.

[66] İ. B. Topçu, T. Uygunoğlu, and İ. Hocaoğlu, “Electrical conductivity of setting cement paste with different mineral admixtures,” Construction and Building Materials, vol. 28, no. 1, pp. 414–420, Mar. 2012, doi: 10.1016/j.conbuildmat.2011.08.068.

[67] W. U. Di, S. Cai, and G. Huang, “Coupled effect of cement hydration and temperature on rheological properties of fresh cemented tailings backfill slurry,” Transactions of Nonferrous Metals Society of China, vol. 24, no. 9, pp. 2954–2963, 2014.

[68] X. J. Deng, B. Klein, J. X. Zhang, D. Hallbom, and B. De Wit, “Time-dependent rheological behaviour of cemented backfill mixture,” International Journal of Mining, Reclamation and Environment, vol. 32, no. 3, pp. 145–162, 2018.

[69] V. Kocaba, E. Gallucci, and K. L. Scrivener, “Methods for determination of degree of reaction of slag in blended cement pastes,” Cement and Concrete Research, vol. 42, no. 3, pp. 511–525, 2012.

[70] M. Fall, J. C. Célestin, M. Pokharel, and M. Touré, “A contribution to understanding the effects of curing temperature on the mechanical properties of mine cemented tailings backfill,” Engineering Geology, vol. 114, no. 3, pp. 397–413, 2010, doi: https://doi.org/10.1016/j.enggeo.2010.05.016.

[71] C. E. M. Gomes, O. P. Ferreira, and M. R. Fernandes, “Influence of vinyl acetate-versatic vinylester copolymer on the microstructural characteristics of cement pastes,” Materials Research, vol. 8, pp. 51–56, 2005.

[72] X. F. He, C. W. Miao, Y. H. Wu, X. X. Cao, and D. Liu, “Thermal Reaction Kinetics of Fly Ash Cement Paste at the Age of 28 Days,” Applied Mechanics and Materials, vol. 668, pp. 91–94, 2014.

[72] P. Pereira, L. Evangelista, J. De Brito, The effect of superplasticisers on the workability and compressive strength of concrete made with fine recycled concrete aggregates. Constr. Build. Mater., 28 (1) (2012), pp. 722-729.

[73] J. Plank, D. Vlad, A. Brandl, P. Chatziagorastou, Colloidal chemistry examination of the steric effect of polycarboxylate superplasticizers. Cem. Int., 3 (2) (2005), pp. 100-110.

[74] L. Huynh, D.A. Beattie, D. Fornasiero, J. Ralston, Effect of polyphosphate and naphthalene sulfonate formaldehyde condensate on the rheological properties of dewatered tailings and cemented paste backfill. Miner. Eng., 19 (1) (2006), pp. 28-36.

[75] M. Fall, Technology of cemented paste backfill. Lectures notes of geotechnical hazards and risks. University of Ottawa, 2009.

4 Technical Paper 2: Rheological Properties of Aluminium Oxide Nanoparticle-Modified Cemented Paste Tailings Materials

Raouf Kaviani, Mamadou Fall

Abstract:
There are currently no researches that examine the rheological properties of Aluminium Oxide nanoparticle (nAlO)-containing Cemented Paste Backfill (CPB) materials. Knowing the yield stress and viscosity of CPB containing nAlO is crucial, especially when applying nano-CPB technology in subterranean mines. The purpose of this work is to thoroughly examine how nAlO affects the rheological characteristics of CPB and how those characteristics change over time. Yield stress and viscosity measurements are performed on CPB samples with different compositions (e.g., nAlO content, binder type, and superplasticizer content) at intervals of 0 min, 20 min, 1 h, 2 h, and 4 h. The investigation also involves measuring the materials' pH and Zeta potential, microstructural studies (TG/DTG and XRD), and electrical conductivity (EC). The findings show that adding nAlO to CPB significantly changes its rheological properties, which in turn affects flowability. The yield stress and viscosity of CPB samples are greatly increased by the incorporation of nAlO, with the degree of influence varying based on variables including water content, curing duration, and type of binder. Because of the nAlO-induced microstructural changes in the CPB material, the interaction of nAlO and a larger fraction of nAlO, along with an increase in curing time, raises rheological characteristics and decreases paste flowability. The results of EC, DTG, and XRD, which show that binder hydration rises with nAlO dosage, corroborate this. Furthermore, as nAlO increases, the zeta potential decreases in magnitude, which repulsion forces and lowers flowability. However, EC, XRD, and DTG studies indicate that the addition of 0.125 percent superplasticizer acts as a compensator for the lower flowability caused by nAlO, as the superplasticizer causes a drop-in cement hydration rate at very high ages. Moreover, the increase of the slag percentage from 0% to 50% and 75% of the binder content slightly decreases viscosity, but greatly increases yield stress. The study's fresh perspectives contribute to the advancement of nano-CPB technology and have important ramifications for the practical use of this technology in underground mine backfill operations.

Keywords: Cemented paste backfill, Tailings, Mine, Rheology, Nano-particles, Cement, Aluminium Oxide

4.1 Introduction

In recent decades, there has been a notable increase in the usage of cemented paste backfill (CPB) material for filling mine voids. CPB, a mixture of water, binder, and tailings, is essential for improving ground control and establishing a secure working environment. It also makes it easier to properly dispose of mine waste, which lowers the danger of tailings dam collapses, tailings-induced environmental contamination, and maximizes resource recovery [1-6].

Ensuring the safety of persons and equipment in underground mining operations is contingent upon the stability of the subterranean CPB structure. Therefore, adequate mechanical strength must be achieved via the CPB structure. Moreover, everyone engaging in backfilling activities has the same goal of reaching CPB design strength as soon as feasible. This early strength gain is essential for prompt measures, like barrier opening and scheduling mining at the nearby stope, which will ultimately shorten the mining cycle and increase overall profitability and productivity.

Nevertheless, the binder, water, and tailings—traditional CPB production ingredients—are not naturally made to encourage a quick increase in CPB strength in the early stages of the process. Ordinary Portland cement (OPC) is still typically the most widely utilized binder in the manufacture of CPB. In addition to raising costs, using ordinary Portland cement (OPC) as a binding agent in CPB slows down the rate at which the material gains strength in its early stages. Furthermore, a significant amount of greenhouse gases is released during the manufacture of OPCs. At about 4 billion tonnes per year, the present rate of production accounts for 7% of the world's CO_2 emissions [7]. The mining industry's growing focus on sustainability makes the overuse of OPC in CPB technology incompatible with this goal.

Supplementary cementitious materials (SCMs), most notably blast furnace slag (BFS), have been utilized regularly to partially substitute standard OPC in CPBs due to cost concerns. The disadvantage of this approach is that slag has a slower rate of early hydration, which causes a discernible decline in early-age strength and the pace of strength growth in CPBs that contain slag. Despite this, the procedure helps reduce costs and the carbon footprint associated with CPBs. Mine productivity is being challenged by this slowdown. Because of this, the mining sector has been forced to search for other strategies to quicken the development of CPBs' strength and lessen their carbon imprint [8–9].

One new development in CPB technology is the addition of nanoparticles, namely Aluminium Oxide nanoparticles (nAlO), as additives. By adding Al_2O3 nanoparticles to the CPB mixes while lowering the OPC content, this novel method seeks to improve the mechanical performance and lessen the carbon footprint of CPBs [2]. The effective use of nanoparticles in the production of high-performance concrete with enhanced early-age strength and strength enhancement rates [10–20] is the inspiration for this development. Recently, there has been a lot of interest in the use of nanoparticles in cement-based materials (CBMs), such as concrete. Research has shown that adding nanoparticles can significantly improve the mechanical characteristics of traditional mortar or concrete materials because of their chemical and physical effects (such as filler effect and enhanced cement hydration). Especially, nano-Al_2O_3 has been studied in great detail when it comes to CBMs. Within the field of building materials, and specifically within the framework of cement and concrete research, a great deal of study has demonstrated the effectiveness of adding nano-Aluminium Oxide (nAlO) particles. These investigations have demonstrated that the addition of these nanoparticles to the mixes of concrete or mortar can significantly improve their strength and strength gain rate (e.g.,[21-28]). Because of its filler function, Aluminium Oxide helps to reduce porosity, which promotes the development of a denser cementitious matrix.

Beyond the necessary emphasis on strength, the fresh material's flowability or transportability is another crucial design factor in the context of CPB. To enable efficient pumping and delivery to mine cavities, it is imperative to provide an appropriate flow capacity (stopes). Inadequate flow capacity can result in issues like clogs in pipes, which can cause serious financial losses for mining companies (e.g.[10], [13], [29-32]). Regretfully, nothing is known about the precise effect of nAlO particles on CPB's ability to flow. In order to assess flow ability, one usually looks at the rheological characteristics of CPB, specifically looking at its viscosity and yield stress, which indicate the material's resistance to deformation and flow initiation, respectively [33–34].

However, a number of basic problems about the interaction between nAlO and the rheological characteristics of CPB are still open. These include questions regarding how nAlO affects CPB yield stress, how it affects the viscosity of fresh CPB, how these variables change during the curing and transportation stages, how nAlO causes changes in CPB's microstructure as a result, and how these factors might interact with superplasticizers or mineral admixtures like Slag. It is essential to close these important knowledge gaps in order to successfully integrate and use nano-CPB technology. In order to provide important insights into the effects of nAlO particles on CPB's rheological, microstructural, and chemical properties across different binder types, with or without superplasticizers, over varying timeframes, this study employs a variety of experimental methodologies, including thorough rheological tests, microstructural analyses, chemical evaluation, and an extensive monitoring programme.

4.2 Experimental Approach

4.2.1 Specimen Preparation and Materials

4.2.1.1 Tailings

In order to ensure the reliability of the results, the study used synthetic silica tailings (ST), which are distinguished by their non-reactive and non-acid producing features. Quartz minerals make up the majority of ST, which is similar to the mineral makeup of natural tailings from several hard rock mines in Canada. The grain size distribution of the medium-sized ST was comparable to that of the tailings from other mines in eastern Canada (see Figure 4.1 and Table 4.1).

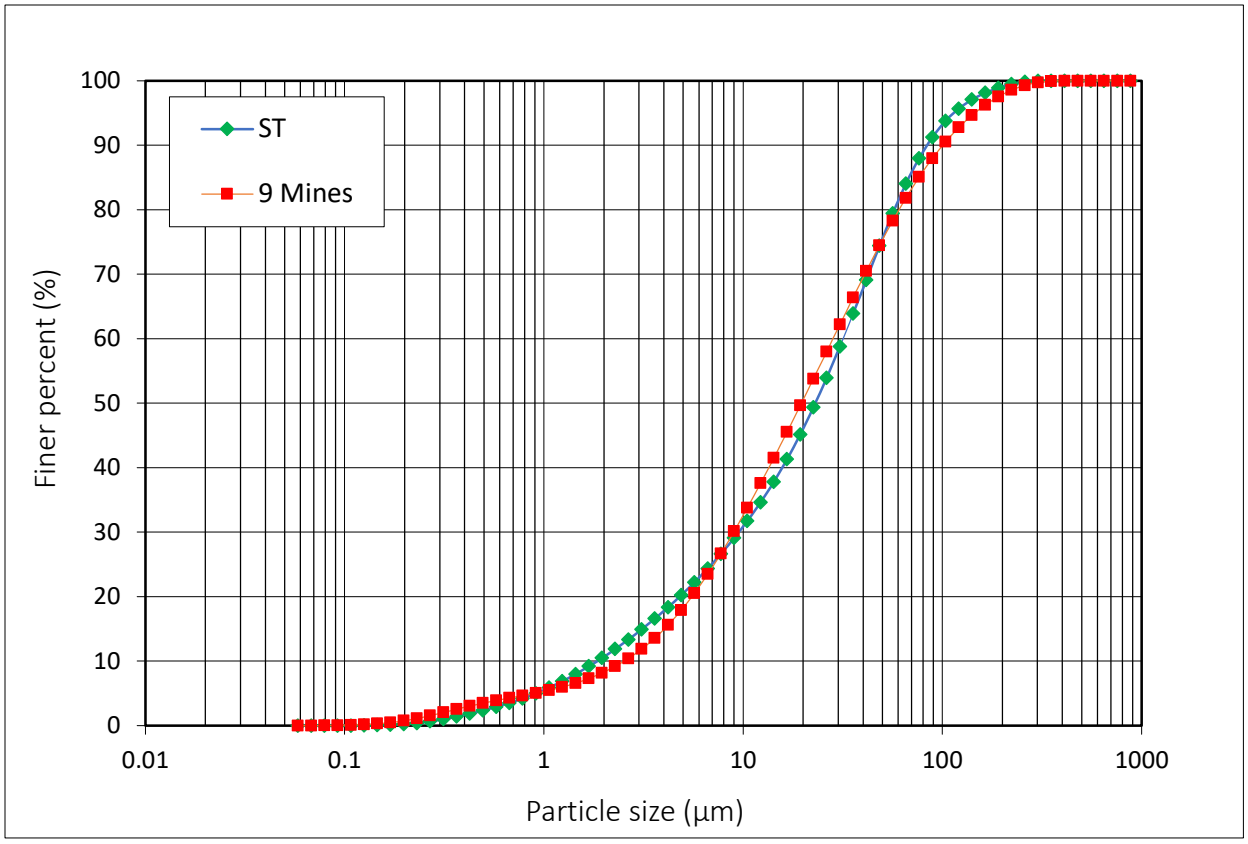

Figure 4.1 Distribution of silica tailings (ST) grain sizes and average grain sizes of tailings from nine Eastern Canadian mines.

Table 4.1 Physical characteristics of the tailings used.

Element	Gs	D_{10} (µm)	D_{30} (µm)	D_{50} (µm)	D_{60} (µm)	Ss (cm^2/g)
ST	2.7	1.9	9.0	22.5	31.5	3600
An average of 9 mines	–	1.8	9.1	20.0	30.8	–

Gs: specific gravity; Ss: specific surface area.

4.2.1.2 Binders and water

The main binder was regular PC type I (PCI), which has a specific gravity of 3.2. Furthermore, as is customary in Canadian CPB plants, a mixture of PC and slag was used to prepare a few CPB specimens at a 50/50 and 25/75 weight ratio, with a binder component of 4.5 percent by weight [12, 26]. Table 4.2 lists the binders' chemical makeup and physical characteristics, which were mostly ascertained by X-ray fluorescence (XRF). Distilled water was used to prepare all of the backfill samples, with a water-to-cement ratio of 7.8.

Table 4.2 Primary chemical and physical properties of the Portland cement and Slag used.

	Na_2O	MgO	Al_2O_3	SiO_2	K_2O	CaO	TiO_2	MnO	Fe_2O_3	Relative density	Specific surface area (cm^2/g)
PCI	0.34	2.58	4.81	20.38	0.96	62.70	0.23	0.05	3.61	3.2	1300
Slag	0.28	11.78	10.60	35.57	0.48	39.21	0.47	0.30	0.62	2.8	2100

4.2.1.3 Nano-Aluminium Oxide

Sourced in colloidal form from Dow Corning, Inc., nano-Aluminium Oxide (nAlO) is an amorphous Al_2O_3 with a high specific surface area and purity. It is used at several concentrations—0, 1, and 3 percent by total mass of binder materials. The chemical and physical properties of the used nAlO particles are displayed in Table 4.3.

Table 4.3 Characteristics of the Nano-Al2O3 (NA) nanoparticles used.

Nano-Al_2O_3	
Form	Nanopowder
Particle size	<50 nm (TEM)
Surface area	>40 m^2/g (BET)
Molecular Weight	101.96
Color	White

Data obtained from suppliers.

4.2.1.4 Superplasticizer

A superplasticizer supplement was added to some CPB samples (0.125 percent by weight of the mixture). The chosen superplasticizer was BASF's Master Glenium 7500 (Master G), which satisfies ASTM requirements for high-range water-reducing admixtures [35–36].

4.2.2 Specimen Preparation

Different CPB combinations with varying amounts of nAlO were created in addition to reference (control) samples that had no nAlO (0 percent nAlO). For five minutes, the dry materials were well blended using a mechanical mixer while maintaining a constant water-to-binder ratio (W/B) of 7.8 and binder content of 4.5 weight percent. After adding the water and nAlO, the mixture was stirred for an additional five minutes. The CPB was then placed into plastic cylinders measuring 10 cm in height and 5 cm in diameter; bigger cylinders measuring 10 cm in diameter and 20 cm in height were utilized for observation. The CPB cylinders were manually vibrated to release any trapped air, and then they were sealed and allowed to cure at ambient temperature for predetermined amounts of time to replicate different backfill transport times. Table 4.4 lists the mix proportions for the prepared CPBs. Additionally, a constant W/B ratio of 1 was used to make cement paste samples for microstructure investigation. Following curing, the CPB and CP specimens underwent a number of tests and analysis (Table 4.5).

Table 4.4 Mix composition of the specimens prepared for rheological tests.

Sample name	Nano-Al2O3 [(a)] (%)	Binder (%)	Binder type	w/b	Superplasticizer (%)

CPB-PCI-0%nAlO	0	4.5	PCI	7.8	0
CPB-PCI-1%nAlO	1	4.5	PCI	7.8	0
CPB-PCI-3%nAlO	3	4.5	PCI	7.8	0
CPB-PCI 1%nAlO-SP	1	4.5	PCI	7.8	0.125
CPB-PCI 3%nAlO-SP	3	4.5	PCI	7.8	0.125
CPB-50%PCI/50%Slag 0%nAlO	0	4.5	PCI/Slag (50/50)[b]	7.8	0
CPB-50%PCI/50%Slag 1%nAlO	1	4.5	PCI/ Slag (50/50)	7.8	0
CPB-50%PCI/50%Slag 3%nAlO	3	4.5	PCI/ Slag (50/50)	7.8	0
CPB-25%PCI/75%Slag 0%nAlO	0	4.5	PCI/Slag (25/75)	7.8	0
CPB-25%PCI/75%Slag 1%nAlOCPB	1	4.5	PCI/Slag (25/75)	7.8	0
CPB-25%PCI/75%Slag 3%nAlOCPB	3	4.5	PCI/Slag (25/75)	7.8	0

a) by the mass of the binder; b) PC/Slag (50/50) = the blend weight ratio of Portland cement to Slag is 50/50

Table 4.5 Summary of the mix composition of the specimens prepared for XRD, TG/DTG analyses.

Sample Nomenclat-eure	**Binde-r Conte-nt (%)**	**PCI in the binder %**	**Slag in the bind-er %**	**SP %**	**Taili-ngs type**	**$\frac{W}{C}$ ratio**	**Mixin-g water**	**Nanap Conte nt (%)**	**Nanop type**	**Curing time (hrs)**
CPB-PCI 0	-	100	0	0	none	1	DW	0	none	2
CPB-PCI 1	-	100	0	0	none	1	DW	1	nAlO	2
CPB-PCI 3	-	100	0	0	none	1	DW	3	nAlO	2
CPB-PCI/Slag 3	-	50	50	0	none	1	DW	3	nAlO	2
CPB-PCI 3-SP	-	100	0	0.125	none	1	DW	3	nAlO	2

DW: distilled water; SP: superplasticizer; Nanop: nanoparticles

4.2.3 Methods of Testing and Analysis

4.2.3.1 Viscosity Test

A digital viscometer (Model DVE; Brookfield Engineering Laboratories Inc., Middleboro, MA, USA) with an immersed spinning spindle was used to measure the viscosity of the backfill specimen. Viscosity can be

measured instantly with this device since it uses a calibrated spring to rotate a spindle at a steady speed. A rotary transducer's spring deflection is what determines the mixture's viscous drag [37]. See [36] for additional information on CPB viscosity measurements with this viscometer. Samples were evaluated at specified curing times of 0 minutes, 20 minutes, 1 hour, 2 hours, and 4 hours. To guarantee reproducibility of results, tests were repeated twice.

4.2.3.2 Vane Shear Test

To determine the samples' yield stress, the vane shear test was used. The study used a vane device called a Wykeham Farrance, which is made up of a four-blade vane and a motor that rotates the vane through a calibrated torsion spring at a steady rate of 0.18 rpm. Vane shear tests were conducted in accordance with ASTM D4648/D468M-13 standard at 0 min, 20 min, 1 h, 2 h, and 4 h post-mixing. To guarantee homogeneity and replicate the continuous shear experienced by the CPB during transit, the sample was physically stirred and then mixed with a spoon for one minute prior to each test. This prevented any settling of the tailing grains owing to self-weight. After inserting the vane into the specimen's middle surface, the device was turned on. After noting the highest torque, the yield stress associated with it was computed using the equation (ASTM D4648 [38]):

$$\tau_y = \frac{2T_m}{\pi D^3 \left[\frac{1}{3} + \frac{H}{D}\right]}$$

Equation 4.1 Where H is the vane's length, D is its diameter, Tm is the maximum torque that has been established, and τ is the yield stress. To guarantee the accuracy of the findings, every test was carried out a minimum of three times.

4.2.3.3 Microstructural Analysis

For CPB specimens with and without nAlO, XRD, thermal gravimetry (TG), and differential thermal gravimetry (DTG) investigations were conducted on CPB cement pastes to clarify the microstructural alterations. After four days of drying at 45 °C to eliminate any remaining water, cement paste specimens were ground into a powder. XRD and TG/DTG tests were used to ascertain the hydration products' phase composition. Using a thermal analyzer (TGA Q5000 V3.15 Build 263), TG/DTG analysis was carried out by heating the specimens at a rate of 10 °C/min from 0 to 1000 °C in a nitrogen environment. A Rigaku Ultima-IV diffractometer, running at 40 kV and 44 mA, was used to do the XRD analysis. It was programmed to scan at a rate of 0.5°/min with an increment of 0.02 from 2° to 80° of the 2θ range.

4.2.3.4 pH and Zeta Potential (ZP) Measurements

With an accuracy of ±0.003, the pH values of the backfill specimens were ascertained using Metrohm 704. For the purpose of validating the results, each measurement was made at least twice, and the average values were noted. The Zetasizer Nano series was used to perform zeta potential measurements, which offer insights into particle-particle interactions at the microscale [10]. The phase analysis light scattering method was utilized to quantify the electrophoretic mobility of particles in suspension (PALS). The Henry Equation was used to calculate ZP [39]. Distilled water was used to prepare the specimens, and for reproducibility, each ZP measurement was performed five times.

4.2.3.5 Electrical Conductivity Monitoring

An EC sensor (5TE electrical conductivity) from Decagon Devices, Inc. was utilized to obtain additional understanding of the cement or binder reaction processes influencing the rheological characteristics of CPB with different nAlO levels. By putting an alternating current between two electrodes and measuring the resistance between them, the sensor—which was placed in the centre of each specimen—measured the electrical conductivity of the backfill specimens. Data from the sensor was gathered using a data recorder.

4.3 Results and Discussion

4.3.1 Influence of Nano-Aluminium Oxide (nAlO) on the rheological properties of CPB made of Portland cement

Figure 4.2 shows how nAlO affects the time-dependent alterations in the yield stress and viscosity of CPB with 100% Portland cement acting as the binder. This figure shows that the yield stress and viscosity of the backfill grow with curing time, regardless of the amount of nanoparticles present. This behaviour results from the way cement hydration changes with time. As the hydration reaction progresses, more cement hydration products, such as C-S-H, ettringite, and CH, are produced [40–41]. This increases the material's yield stresses and inter-frictional resistance by encouraging the aggregation of particles and the formation of more cohesive structures [10, 12]. Furthermore, the size of hydration products also increases in tandem with the increasing degree of cement hydration [13, 40, 42]. As a result, the viscosity of CPB samples increases gradually as the solid volume percentage grows steadily [16, 41, 43]. In addition, the process of cement hydration uses up free water, which causes the water film around the particles to get thinner. A progressive increase in yield stress is directly related to this decrease in water content. It is evident that this drop in water content is correlated with an increase in the CPB's solid volume portion. Increased solid volume fractions lead to increased particle-particle interactions, which in turn raise the apparent viscosities of fresh CPB samples [13], [17].

The assertion that longer curing times lead to the production of more cement hydration products is supported by experimental results from thermal analyses (TG/DTG), as shown by Figure 4.3's representation of TG/DTG studies conducted on cement pastes cured for 60 and 240 minutes. Three separate endothermic peaks, or weight losses, may be seen in this image for temperature ranges of 50–200°C, 400–450°C, and 600–700°C. The principal causes of the weight loss between 50 and 200°C are the dehydration of hydration products such as gypsum, C-S-H, carboaluminates, and ettringite, as well as the evaporation of bound water. The breakdown of calcite ($CaCO_3$) is responsible for the peak between 600 and 700°C, while the dehydroxylation of CH is primarily responsible for the peak between 400 and 450°C ([44-48]). Figure 4.3 clearly shows that the specimen cured for 60 minutes has a lower peak in temperature ranges of 50-200°C and 400-450°C than the cement paste cured for 240 minutes. This data suggests that the CPB samples with extended curing times produced more hydration products.

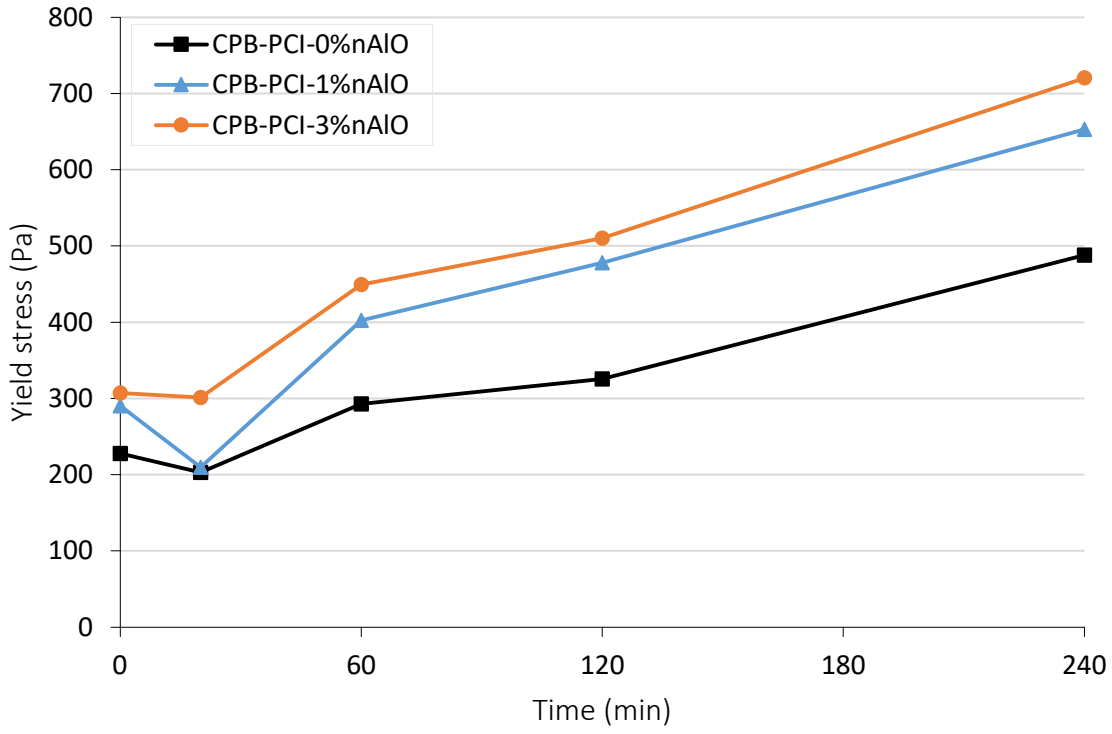

a) Yield stress

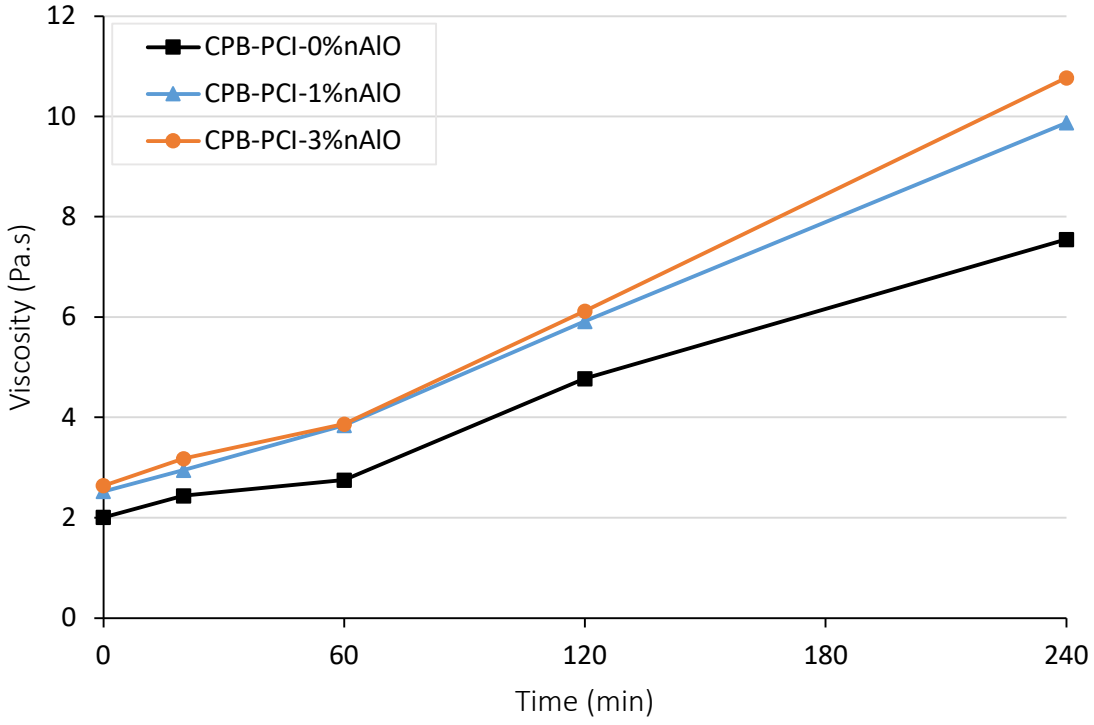

b) Viscosity

Figure 4.2 Effect of nano-Al2O3 (nAlO) content on the evolution of the rheological properties of CPB with Portland cement: a) yield stress; b) viscosity

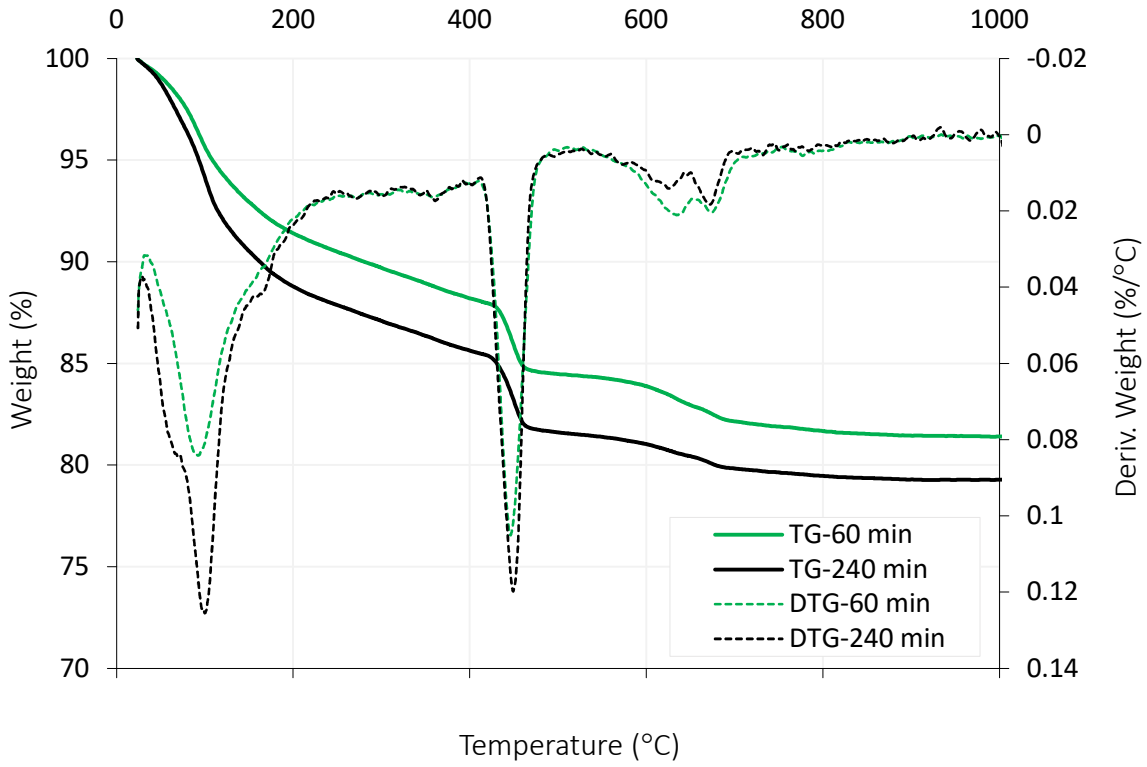

Figure 4.3 TG/DTG analysis results of cement paste samples without nAlO and cured for 60 min. and 240 min.

Furthermore, Figure 4.2 shows that the inclusion of nanoparticles significantly altered CPB's flow ability. Regardless of the testing age, it demonstrates a significant increase in backfill yield stress and viscosity with the addition of nAlO. The yield stress of the specimen containing 3 percent nAlO, for example, was 3071 Pa, 301 Pa, 449 Pa, 480 Pa, and 720 Pa at 0 min, 20 min, 1 h, 2 h, and 4 h, respectively. This represents an increase of approximately 26 percent, 30 percent, 35 percent, 32 percent, and 32 percent compared to the 0 percent nanoparticle sample. In comparison to the 0 percent nanoparticle samples at 0 min, 20 min, 1 h, 2 h, and 4 h, respectively, the yield stress of samples containing 1 percent nAlO increased by roughly 26 percent, 5 percent, 27 percent, 32 percent, and 25 percent. Furthermore, compared to the control sample, the addition of 1 percent and 3 percent nAlO increased the viscosity at 4 hours by 31 percent and 43 percent, respectively. Moreover, the addition of 3 percent nAlO had a stronger effect on CPB viscosity at 0 hours and 20 minutes compared to 1 percent. A number of variables working together can be responsible for the flowability loss observed in the presence of nAlO, as evidenced by higher yield stress and viscosity. The filler effect that nanoparticles exert, the enhancement of cement hydration caused by nAlO, the increased water demand brought on by the presence of nanoparticles, and the greater flocculation or agglomeration of the paste as a result of nAlO particles are some of these factors [40, 49, 50-56]. Below is a more detailed review of these factors that together cause the changed rheological properties of CPB in the presence of nAlO.

- **nAlO filler effect:** It is well known that nanoparticles are effective to partially fill the empty spaces in a cementitious material, which causes the microstructure to become denser [42]. This finally increases the yield stress and viscosity of the backfill material by increasing the frictional resistance between the particles and the solid volume fraction in the CPB material [18], [40].
- **Enhancement of the cement hydration by nAlO:** The extremely small dimensions of nAlO particles provide an extensive number of nucleation sites, helping the formation of numerous hydration

products, notably C-S-H. These nucleation sites play an essential role in enhancing and intensifying the hydration process of essential cement compounds. The sample containing nAlO has a greater amount of hydration products, according to the XRD data. For instance, the sample containing nAlO has a greater CH intensity than the one containing no nAlO. In fact, the sample with nanoparticles (nAlO) had a greater CH intensity at 18 and 34 degrees 2-theta than the sample without nAlO. This observation highlights the effect of nAlO on cement hydration by implying a higher production of CH in specimens with that addition. This conclusion about the inclusion of nAlO particles producing additional hydration products is also consistent with the findings of TG/DTG studies performed on cement pastes that were 2 hours old and had varying nAlO concentrations (0 percent, 1 percent, and 3 percent), as shown in Figure 4.5. According to these findings, the cement paste that has been treated with nAlO shows the strongest endothermic peaks and weight loss between 100° and 180°C. These indicators point to a higher yield stress and viscosity level due to an enhanced production of hydration products. The congruence with the EC monitoring results of CPB samples with different percentages of nAlO shown in Figure 4.6 lends more credence to this alignment. This graph shows that the curves initially show increasing tendencies, which can be attributed to the cement's breakdown phase. Aluminate, potassium, calcium Aluminium Oxide ions, and other types of ions were released when water was added to the cement, causing the cement's ions to dissolve. The paste's electrical conductivity was improved by these liberated and mobile ions [57–58]. CH, C-S-H, and ettringite were among the hydrates that filled the capillary holes as another hydration reaction occurred. As a result, EC decreased as a result of the decline in ion mobility and concentration [59]. As shown in Figure 4.6, the EC for the nAlO-containing samples was higher than that of the nAlO-free samples during the early stage (up to 2 hours or 120 min). Furthermore, the addition of nAlO resulted in a noticeable shift of the EC peaks to shorter hydration periods, indicating faster hydration reaction rates. In fact, the specimens containing 3 percent, 1 percent, and 0 percent nAlO had conductivity peaks at 3.5h (210 min), 3h (180 min), and 2.6h (160) min, respectively. This early-stage fast acceleration of cement hydration is consistent with yield stress and viscosity observations shown in Figure 4.2.

- **nAlO-induced increase in water demand:** The water requirement of the CPB mixture to attain appropriate flowability was directly impacted by the addition of nAlO to the CPB. The well-established fact is that nanoparticles raise the need for water [60–61]. Because of the nanoparticles' large surface area (>40 m2/g), which adsorbs free water on their surface, there is a higher water demand when they are present. Greater surface area to be wetted results from finer particles. As a result, more water is needed to keep the CPB's workability or flowability at a respectable level [62].
- **Enhanced flocculation or agglomeration of the paste owing to nAlO particles:** The tendency for flocculation or agglomeration after adding nAlO particles is consistent with the results of zeta potential (ZP) measurements made on the CPBs with different concentrations of nAlO particles (Figure 4.7). Higher ZP magnitudes are linked to stronger electrostatic repulsion between charged particles, which leads to improved dispersion. ZP determination is a technique used to evaluate the surface charge and potential stability of suspended particles. The electrostatic surface charge, or ZP, determines how much repulsion or attraction there is between colloidal particles [57]. As a result, ZP may be used to identify the nAlO particle dispersal process in the alkaline Portland cement paste environment (Figure 4.7). The pH trend over time for PCI-CPB samples containing 0 percent and 3 percent nAlO is shown in Figure 4.8. In all CPB samples, the creation of $Ca(OH)_2$ as a result of cement hydration creates an alkaline state (high pH). The pH values of the specimens containing 0 percent and 3 percent nAlO were 12.79 and 12.97, respectively, following a 25-minute curing period. Moreover, pH levels rose to 13.03 and 13.08 for samples containing 0 percent and 3 percent nAlO, respectively, after two hours of ageing. Figure 4.8 shows that the pH of CPB with 3 percent nAlO is higher than the pH of CPB without nAlO. This is consistent with the theory that nAlO particles improve cement compound hydration, which releases more alkali ions into CPB pore water and raises pH. The ZP measurement findings for CPB with 100% PCI, including 1% and 3% nAlO, are shown in Figure 4.7 beside the control sample. When the nAlO % rises, the ZP of the CPB falls, suggesting that there is a stronger electronic double-layer repulsive force when nAlO is absent. Altered rheology and increased water demand are caused

by reduced repulsion and low ZP, which is congruent with the outcomes of yield stress and viscosity, as was previously discussed [14].

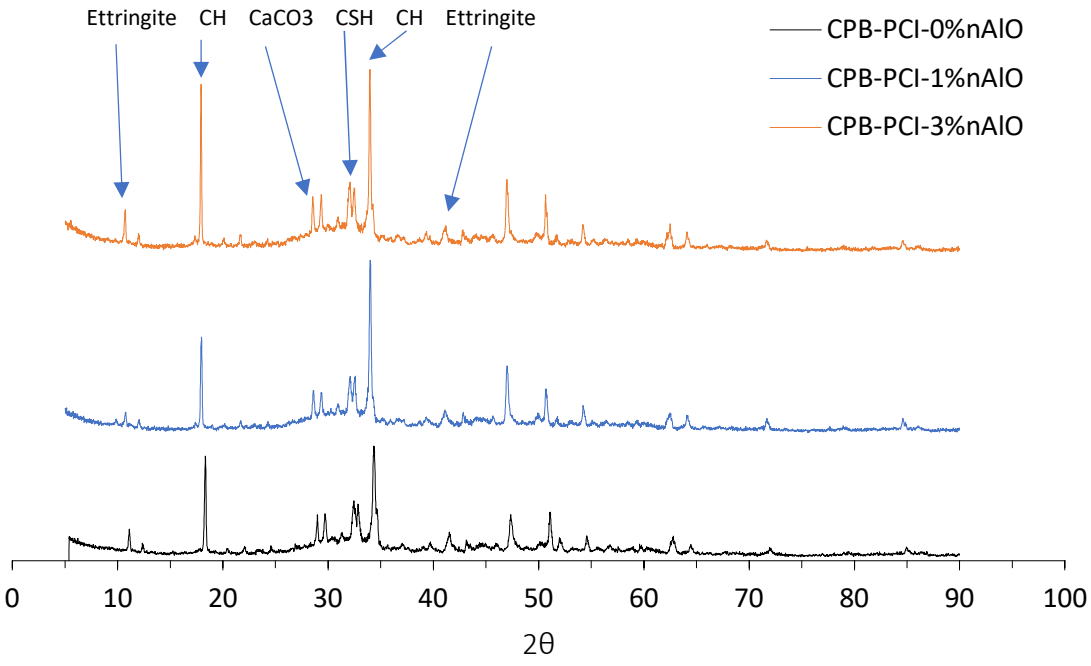

Figure 4.4 XRD results of cement paste of PCI-CPB with 0,1 and 3 percentage of nAlO inclusion after 2 h.

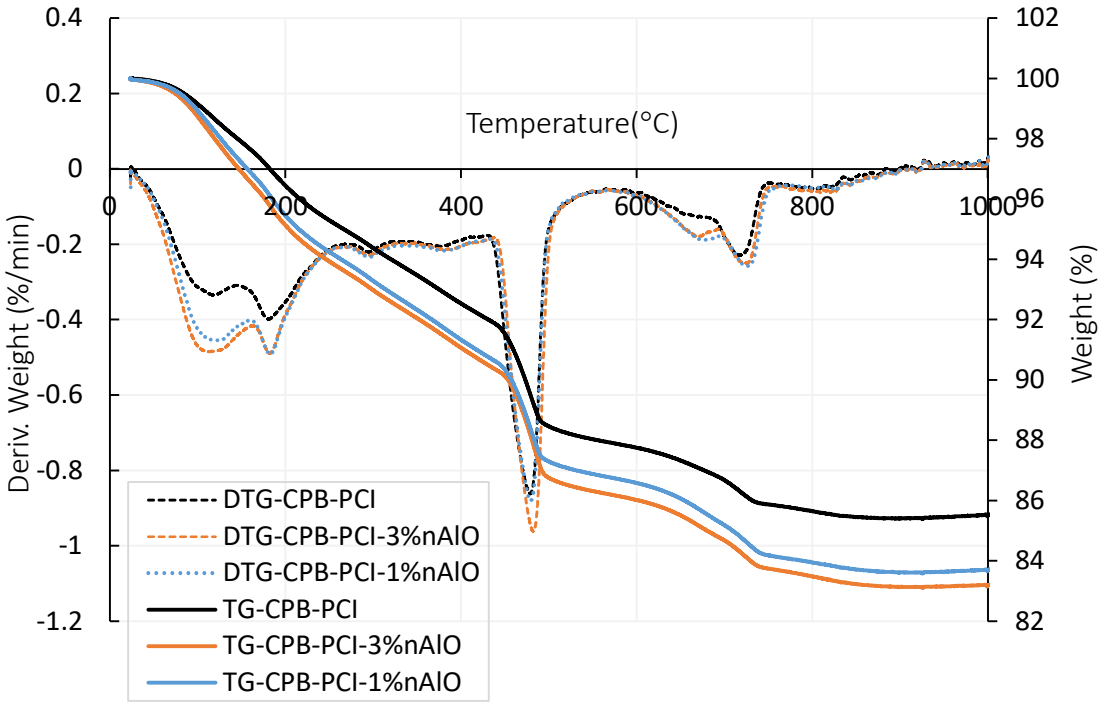

Figure 4.5 TG/DTG diagrams for cement pastes with 100% PCI cured for 2 h and containing 0%, 1%, and 3% of nAlO particles.

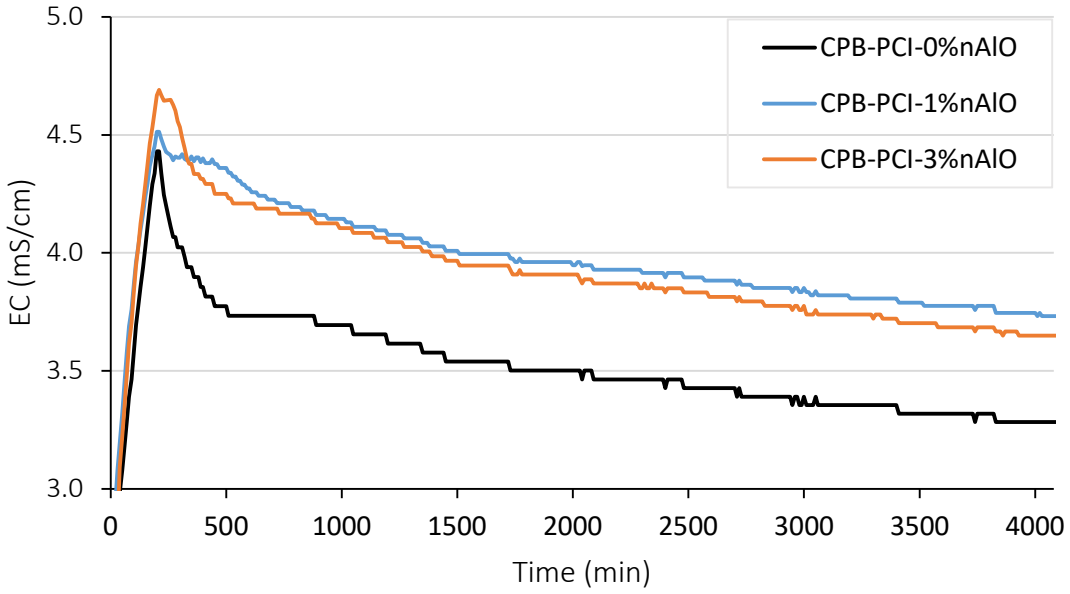

Figure 4.6Changes in electrical conductivity of PCI-CPB specimens.

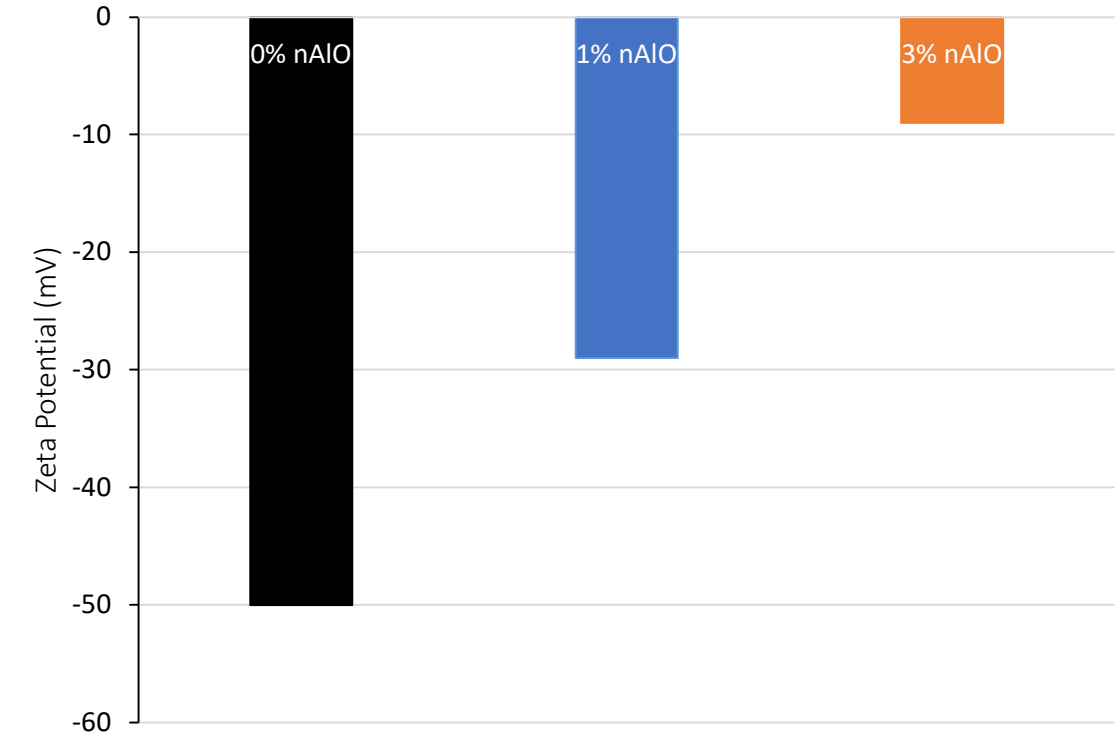

Figure 4.7 Zeta potentials of 2 hours old CPB with 0% nAlO vs 1%nAlO vs 3% nAlO.

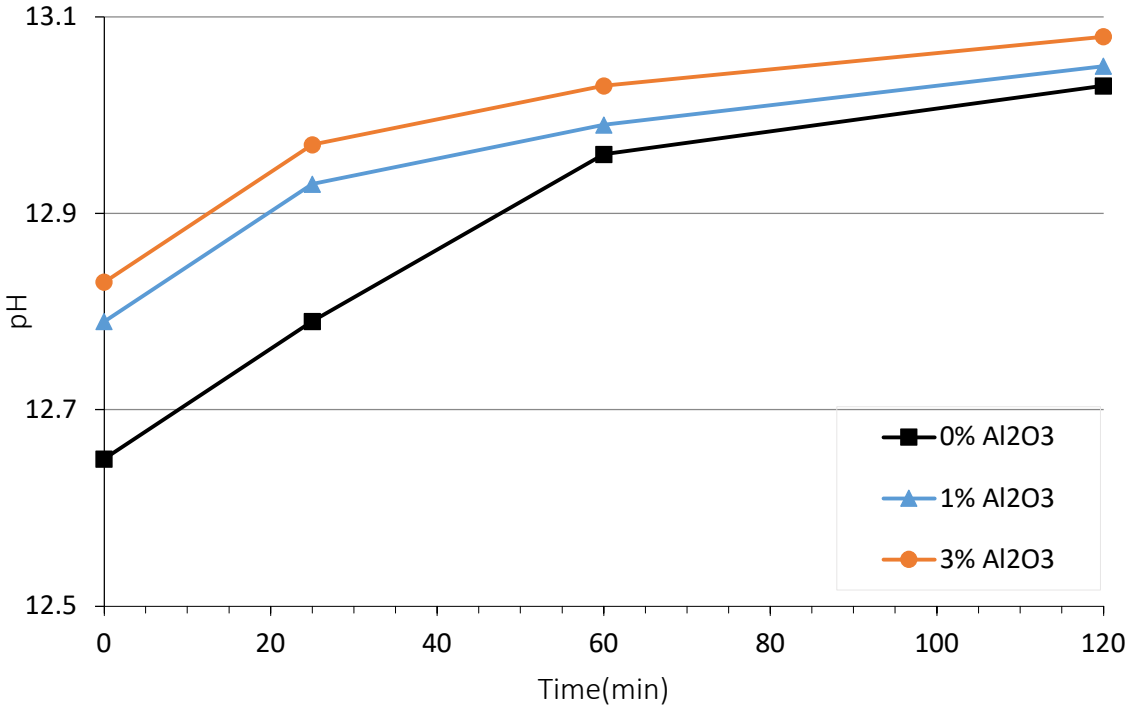

Figure 4.8 pH evolution of CPBs with 0% nAlO vs 1%nAlO vs 3%nAlO.

4.3.2 Influence of Nano-Aluminium Oxide (nAlO) on the rheological properties of CPB with Slag

Cement and mineral mixtures, like slag, have been combined and used extensively in cemented backfill in recent years. CPB is less expensive and more durable when blended cement is used [41]. Furthermore, using slag—a low-carbon binder—helps a mine lower its carbon footprint, supporting sustainable mining practices and the handling of mine waste. Therefore, additional testing was done to evaluate the rheological properties of backfill in which slag was used in place of some of the Portland cement. Three different replacement scenarios were investigated: a replacement of 0% represented as PCI, a replacement of 50% represented as PCI/Slags (50/50), and a replacement of 75% represented as PCI/Slags (25/75).

Following a 2-hour curing period, Figure 4.9 shows the effects of different nAlO percentages on the yield stress (Figure 4.9a) and viscosity (Figure 4.9b) of backfill samples with PCI, PCI/Slag (50/50), and PCI/Slag (25/75). A consistent tendency can be seen in the data: independent of the binder used, yield stress and viscosity demonstrate an ascending trend with increasing nAlO content and curing time across all sample types—PCI, PCI/Slag (50/50), and PCI/Slag (25/75). The section that came before this one explained the underlying mechanims that cause this behaviour. Specifically, figure 4.9a shows that samples incorporating Slag consistently show higher yield stress than ones containing PC alone, whether or not nanoparticles are present. Additionally, there is a positive association between the yield stress and the amount of slag in the mixture. For example, during a 2-hour ageing period without nAlO, the yield stress values for samples with 100 percent PCI, PCI/Slag (50/50), and PCI/Slag (25/75) were 325, 423, and 683 Pa, respectively. Changes in inter-particle forces resulting from the partial substitution of PCI with Slag can explain the increased yield stress found in samples containing PCI/Slag. Van der Waals attraction and electrostatic repelling forces affect a suspension's coagulation and dispersion behaviour. Aggregates arise when attraction is the primary particle contact, increasing yield stress. Zeta potential analysis results for fresh CPB samples with different PCI-to-Slag replacement ratios (excluding nAlO) are shown in Figure 4.13. Significantly, the Slag-CPB sample (25 mV for PCI/Slag (50/50), 20 mV for PCI/Slag (25/75)) has a lower absolute value of zeta potential than the 100 percent PCI-CPB sample (50 mV), suggesting a weaker electric double layer repulsive force in the former. On the other hand, the Slag-particles CPB's are more appealing, which raises the yield stress. Furthermore, the lower zeta potential in Slag-CPB, consistent with DLVO theory, implies the possible creation of a "secondary minimum," which is typified by a weaker and perhaps reversible adhesion between particles. In order for the vane blade to create flow in the suspension, more external force must be provided in order for these weak flocs to maintain their stability during Brownian motion [19–20].

Furthermore, it is clear from Figure 4.9b that, whether or not nanoparticles are present, the viscosity of the CPB shows a different pattern from the yield stress with the introduction of Slag into the binder system. Stated differently, the viscosity of the backfill samples is decreased upon the addition of slag as a partial replacement for PC. There are two fundamental reasons that explain why 100% PCI-CPB has a higher viscosity than Slag-CPBs. First off, cement hydrates more quickly than slag does in the early stages. This causes more hydration products to form, like CH, ettringite, and C-S-H gel, which effectively bonds the tailing particles together and raises the solid volume fraction and particle cohesion, both of which raise viscosity. Second, less hydration product production in the Slag-CPB suggests a smaller C-S-H gel specific surface area, which reduces water adsorption and leaves more free water in the Slag-CPB. Particles are encased and lubricated by a water film created by this surplus free water [33]. The case for the higher hydration product production in 100% PCI-CPB samples is experimentally supported by the findings of thermal analysis (TG/DTG) tests, which are used to determine the cement's phase stability and the amount of hydrates that are present. The TG/DTG and XRD diagrams for cement paste (CP) specimens containing Slag/PCI-CP and PCI-CP are shown in Figures 4.11 and 10. The TG/DTG curves for different CP combinations show that when the binder was made entirely of PCI, there was a noticeable increase in the presence of hydration products. Although this increased quantity is better for CPB hardening, it changes the flow capacity since C-S-H is the primary binding agent in cement-based products [11]. The results of monitoring the EC of CPB with 100% PCI and with a mixture of PCI cement and slag (50/50), shown in Figure 4.12, experimentally validate the production of a higher number of cement hydration products in

samples containing 100% PCI. This figure demonstrates that the sample with 100% PCI reached its maximum EC earlier than the sample with a cement blend, suggesting that the binder hydrated more quickly in the former scenario.

It is also clear from Figure 4.9 that adding nAlO raised the yield stress of all CPBs, regardless of the type of binder. Nevertheless, compared to PCI/Slag (50/50) and PCI-CPB samples, the yield stress of PCI/Slag (25/75) increased greater with increasing nAlO concentration. In fact, after two hours, the samples with PCI/Slag (25/75) had the highest yield stress at 3 percent nAlO. (1064.27 Pa). The following interpretation can be made of this significant yield stress. First, when water is added to the mixture (pre-induction time), some of the cement's ingredients, like gypsum and aluminate (C_3A), dissolve and the solid concentration goes down a little [63–64]. Second, the Slag/PCI blended binder's early-age hydration processes progress more slowly than PCI alone's, resulting in fewer hydration products and yield stress in the Slag-CPB mixture that is regulated by the first inter-particle forces [12]. Electrical conductivity monitoring studies, which show higher values in samples with higher Portland cement concentration, corroborate this slower hydration rate (Figure 4.12). On the other hand, delayed peak electrical conductivity is seen in CPBs with Slag/PCI blended binder, which suggests slower early-age hydration processes [65–66]. (Figure 4.12). Because Portland cement hydration reduces the alkaline activating environment, the reactivity of CPB samples falls as the Slag replacement % rises. Third, the mixture's negative zeta potential is raised by the consumption of calcium hydroxide (CH) via Slag activation, improving flowability and repulsive force [67–68]. Furthermore, increased yield stress and viscosity of Slag-CPB are caused by increasing the amount of slag in the blended binder [65, 69]. This is explained by the fact that slag particles have small particle sizes, which produce a filler effect that fills in gaps between cement particles and tailings grains, causing the backfill matrix to pack more densely [12, 15]. Denser packing raises the friction coefficient between the particles, raising the yield stress. Furthermore, according to the Krieger-Dougherty model [63], denser packing raises the solid volume percentage and intensifies particle-particle interactions and viscosity.

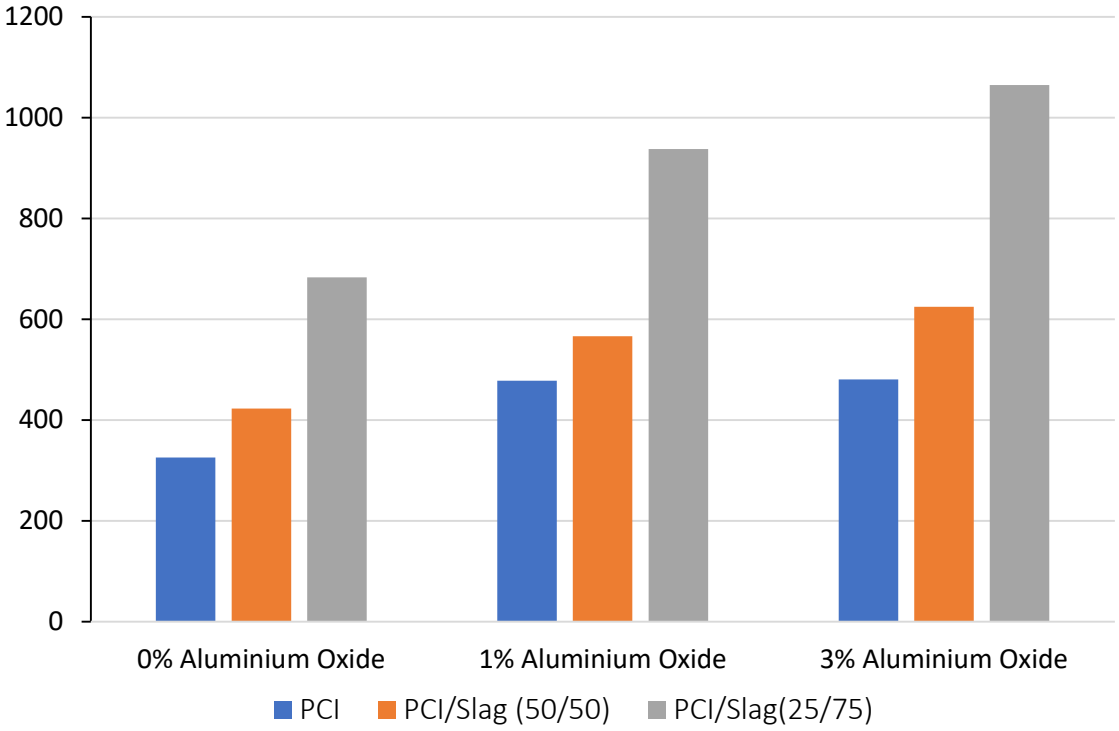

a) Yield stress

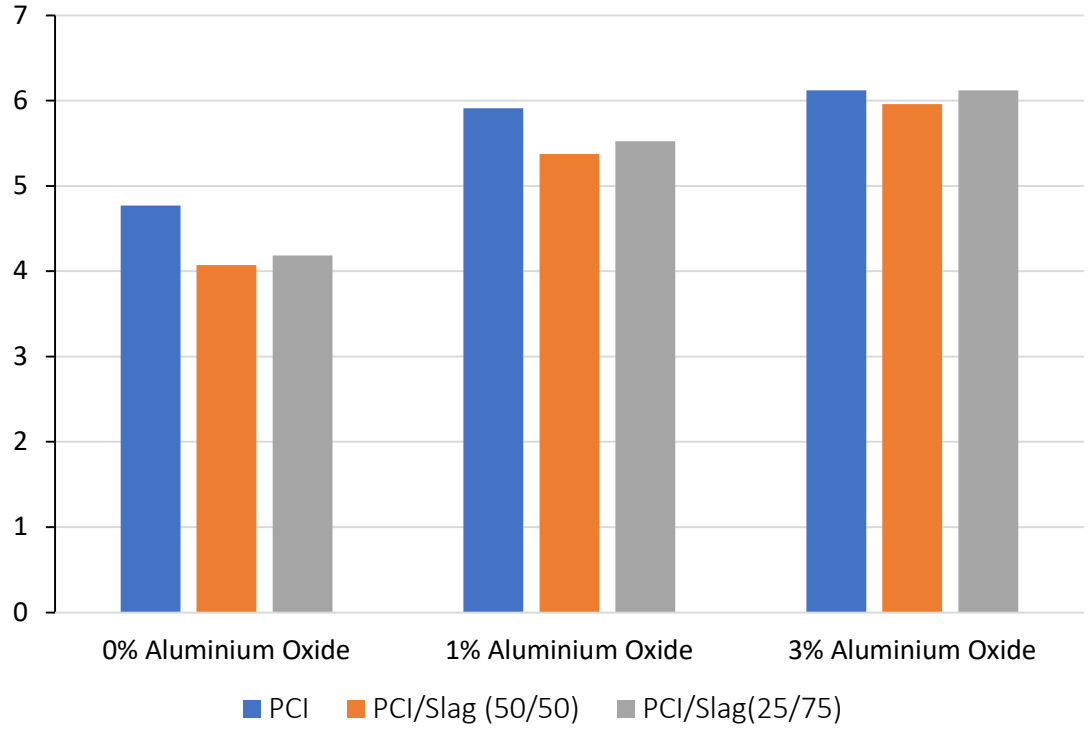

b) Viscosity

Figure 4.9 Effect of Slag and nano-Al2O3 and binder type on the rheological properties of 2 hr old CPB. a) yield stress; b) Viscosity

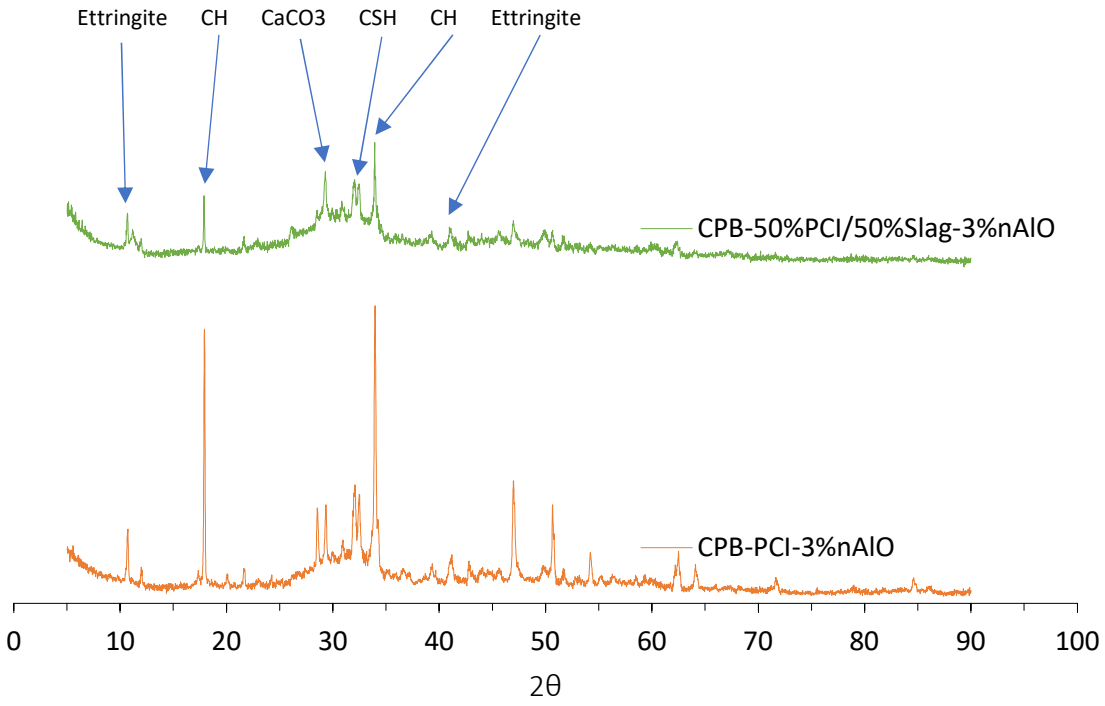

Figure 4.10 XRD results of cement paste of PCI/Slag (50/50), with the inclusion of 3% nAlO samples after 2 h.

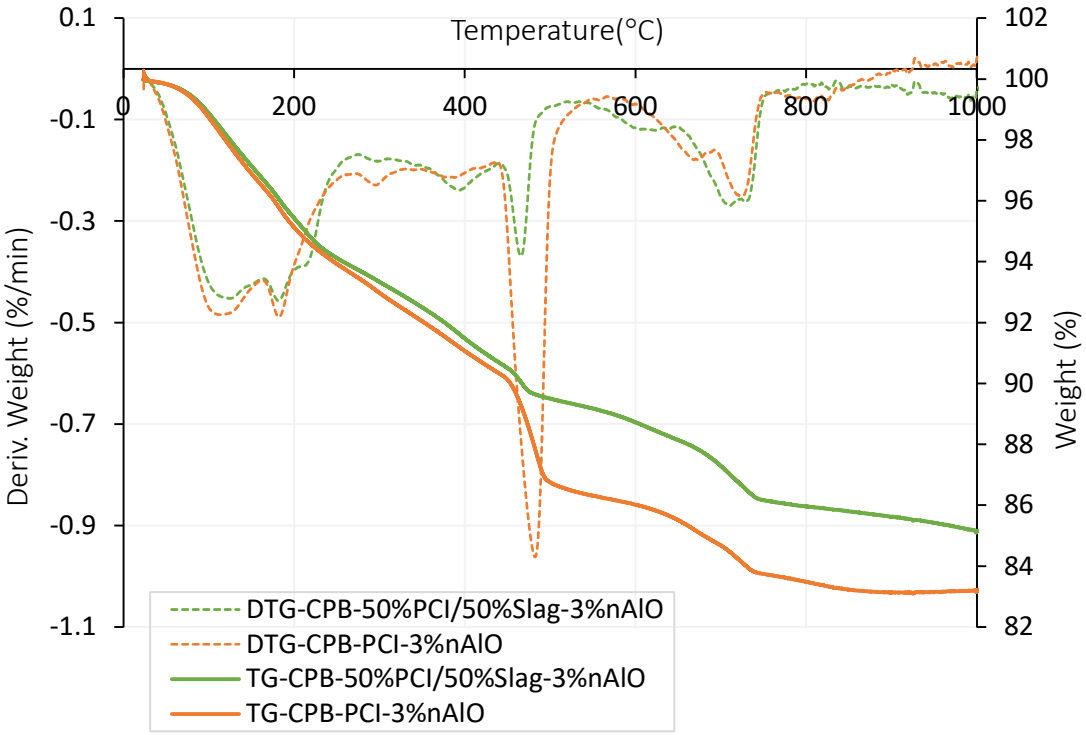

Figure 4.11 TG/DTG results of cement paste of PCI and PCI, PCI/Slag (50/50), with the inclusion of 3% nAlO samples after 2 h.

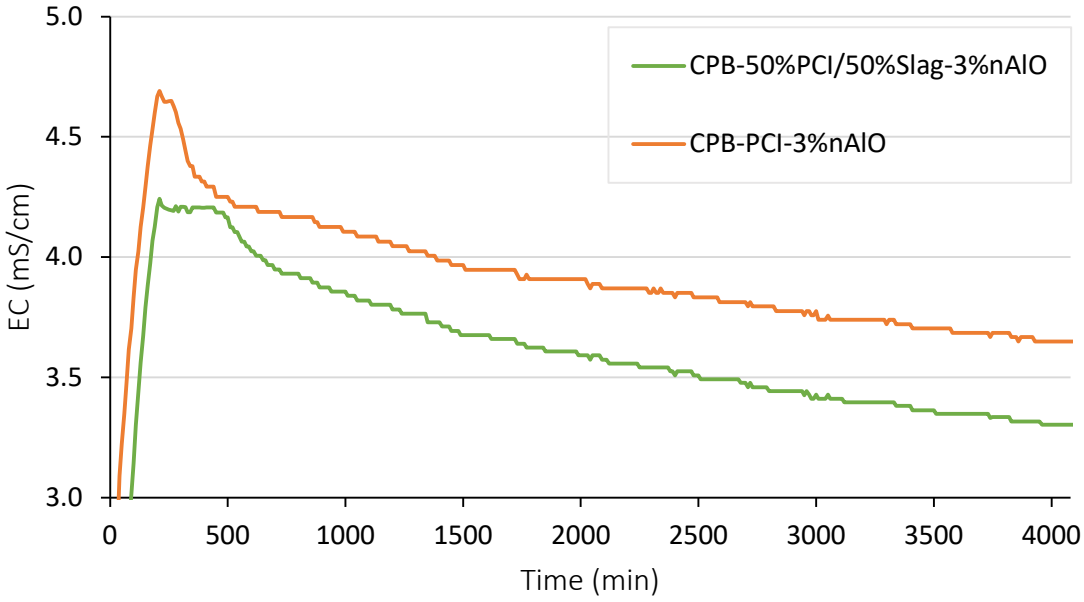

Figure 4.12 EC monitoring results of CPB samples with the PCI, PCI/Slag (50/50), with the inclusion of 3% nAlO.

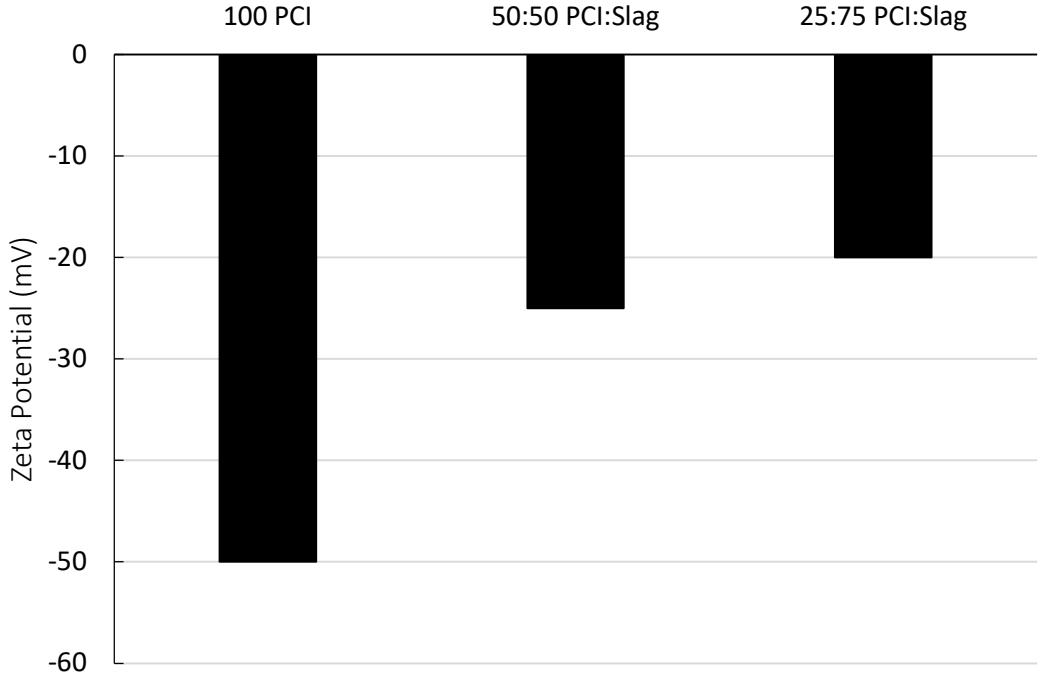

Figure 4.13 Zeta potentials of (100%) PCI-CPB vs Slag-CPB (50:50 PCI: Slag) vs Slag-CPB (25:75 PCI: Slag).

4.3.3 Impact of superplasticizer on the rheological properties of CPB with nAlO

The results of the previous analysis and presentation show that the addition of nAlO particles has a negative impact on the flow properties of CPB. This could pose a risk to the efficient transportation of newly modified CPBs containing nAlO particles in real-world scenarios. Therefore, a relevant question is raised: is it possible to significantly enhance the flow characteristics of CPB that contains nAlO by adding a superplasticizer? As a result, research was done to find out how superplasticizer affected the rheological characteristics of CPB with nAlO.

In Figure 4.14, the effects of a superplasticizer (at 0.125 percent by weight of the mixture) are shown for CPB aged 0, 20 minutes, 1 hour, 2 hours, and 4 hours with varying concentrations of nAlO on the yield stress (Figure 4.14a) and viscosity (Figure 4.14b). This figure demonstrates that, independent of the nanoparticle content, adding a superplasticizer to CPB containing nAlO particles significantly improved the CPB's flow ability. For instance, after 4 hours of age, specimens with 3 percent and 1 percent nAlO in the presence of superplasticizer shown a reduction in yield stress of 53% and 54%, respectively. In line with this, the samples' viscosity also drops. Furthermore, Figure 4.14a shows that the CPB samples with higher nAlO content shown a more considerable effect of the superplasticizer on the yield stress. This result indicates that improving the flow ability of CPB with a greater nAlO percentage requires the use of a superplasticizer even more. It goes without saying that improving CPB's flow ability with superplasticizer will increase pumping efficiency and lower energy and operating expenses related to pumping the subterranean nAlO-CPB material.

A combination of two important elements can be responsible for the reduction in yield stress and viscosity that occurs when a superplasticizer is added. First, higher-range water-reducing admixtures' dispersing impact is the source of it (WRAs). Two different mechanisms of repulsion between cement particles are introduced by superplasticizers derived from carboxylic compounds, like Master Glenium: a) electrostatic

repulsion due to the negative charges of the carboxylic group, and b) steric repulsion due to the long polymer chains in the compound [36, 66, 72-73]. Second, the superplasticizer helps to delay the very early phases of cement hydration. Less hydration by-products are created when the repulsive force between the cement particles increases, which lowers the CPB's solid content and viscosity. TG/DTG diagrams of cement paste samples cured for two hours at different superplasticizer amounts, as shown in Figure 4.15, corroborate this conclusion. The diagrams show that in the cement paste without superplasticizer, more hydration products are formed. More specifically, the sample with 0 percent superplasticizer shows the first peak at about 100–200°C, which indicates the greatest weight loss. The development of products like gypsum, ettringite, and calcium-silicate-hydrate (C-S-H) is shown by the first peak ([47], [70-72]). Significantly fewer solid products are generated during the hydration process in the presence of the superplasticizer, according to the smaller peak shown in the TG/DTG data (Figure 4.15) of the cement paste sample. Furthermore, the findings of the EC monitoring shown in Figure 4.16 corroborate the claim that the superplasticizer slows down the hydration reaction. Higher ion mobility in the paste without the admixture is indicated by the electrical conductivity of the cement paste containing 0.125 percent superplasticizer being noticeably lower than that of the paste containing 0 percent superplasticizer. Furthermore, the superplasticizer-free sample exhibits a faster rate of cement hydration than the superplasticizer-containing sample, peaking at 210 minutes compared to 240 minutes for the latter.

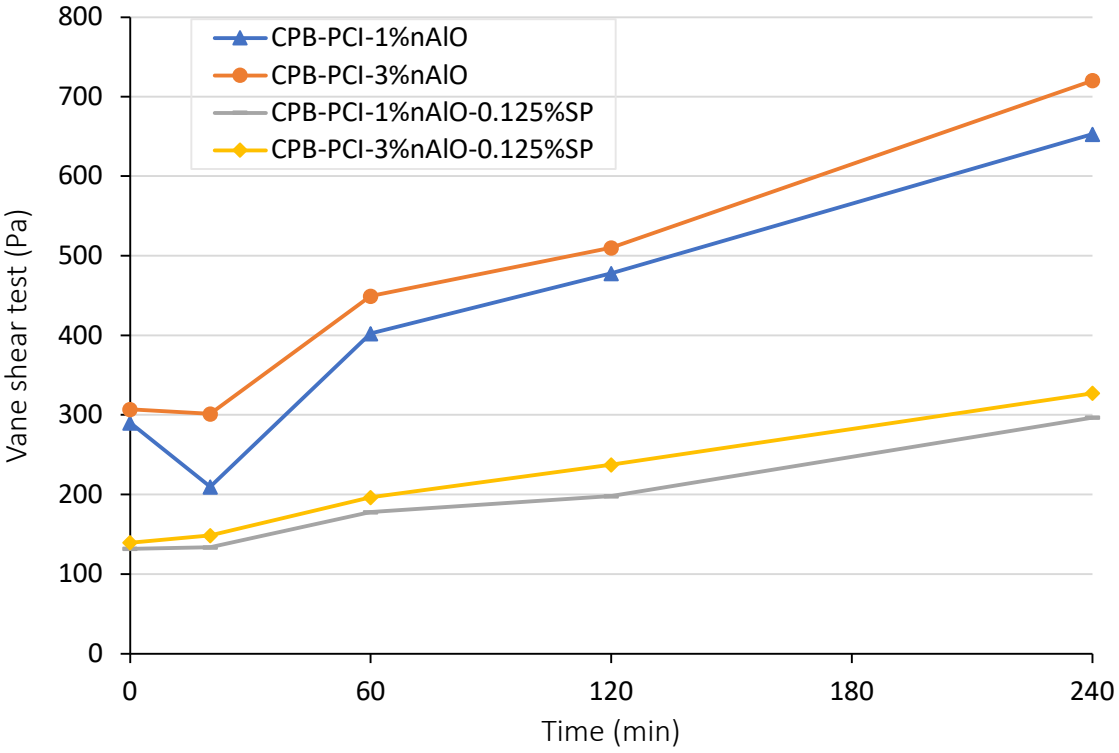

a) Yield stress

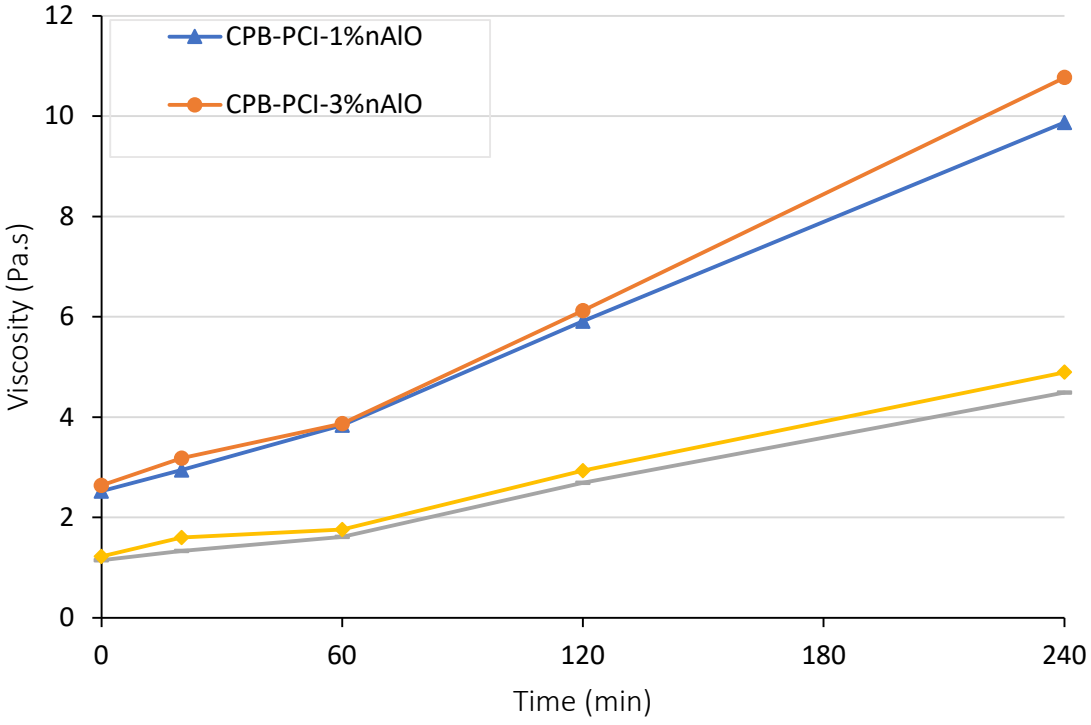

b) Viscosity

Figure 4.14 Effect of superplasticizer versus nano-Al2O3 on the evolution of CPB rheological properties. a) yield stress; b) Viscosity

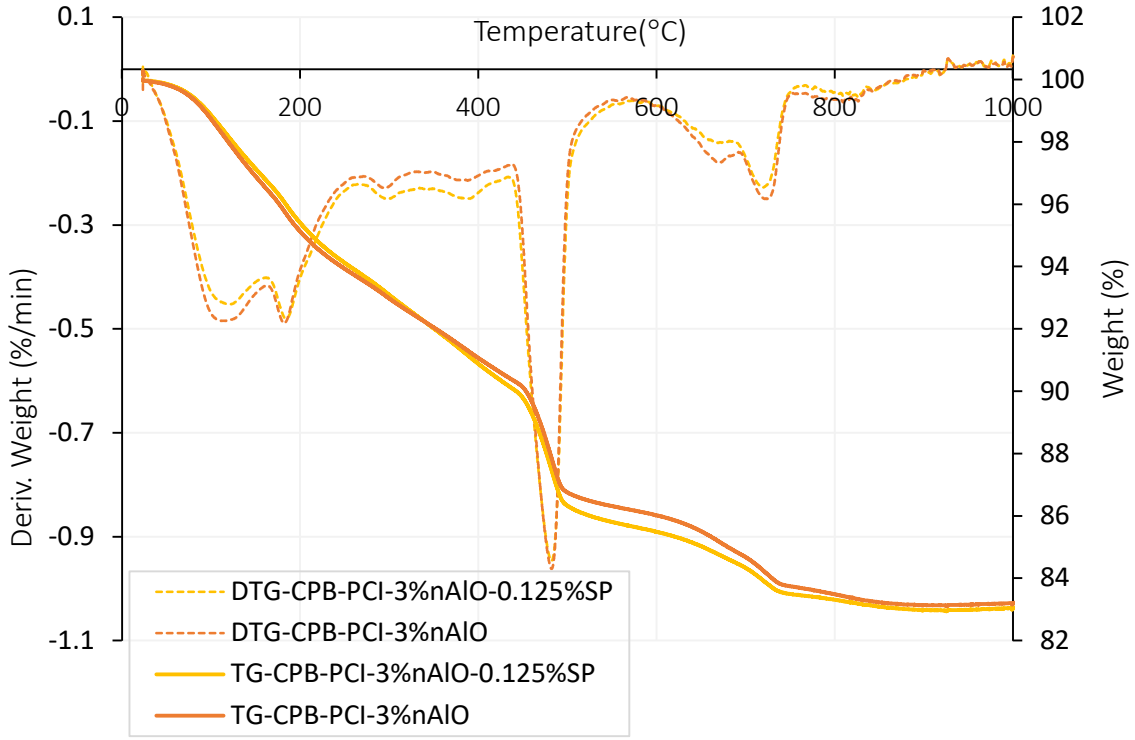

Figure 4.15 TG/DTG results of cement paste of PCI and PCI with the inclusion of 3% nAlO and 0.125% SP samples after 2 h.

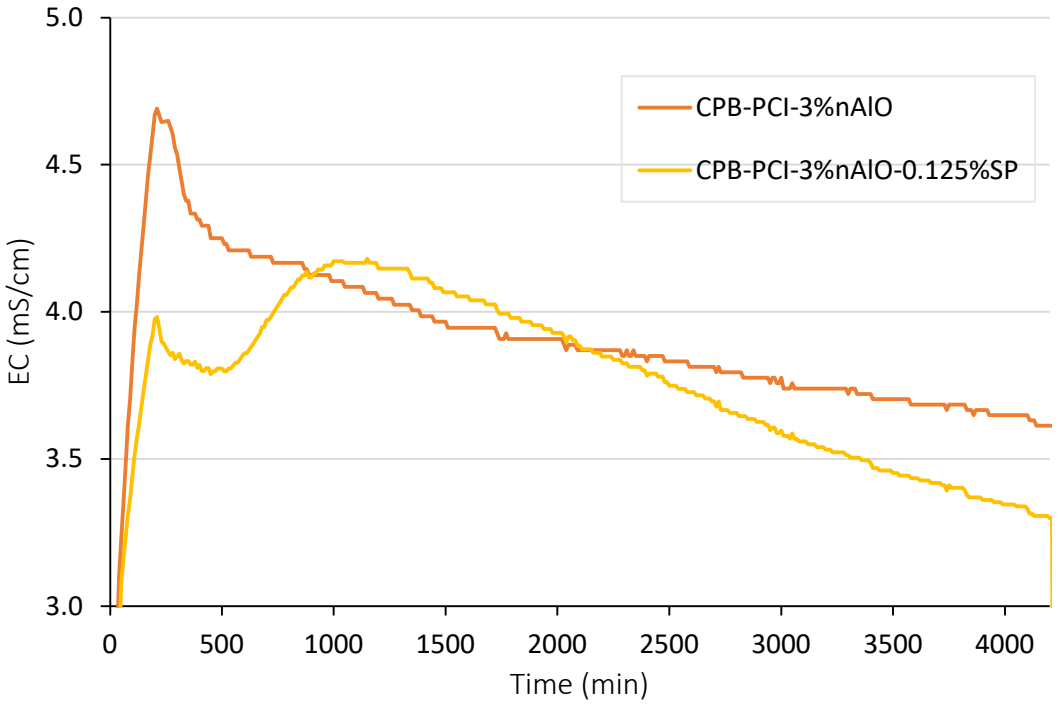

Figure 4.16 displays the EC of the PCI with the inclusion of 3% nAlO and 0.125% SP.

4.4 Conclusion

The impact of nAlO on the rheological characteristics of cemented paste backfill was investigated experimentally in this work. Based on the results, the following inference can be drawn:

- By raising the yield stress and viscosity of fresh CPB, adding nAlO particles or changing the dosage of nAlO changes the fresh CPB's flowability. This alteration is attributed to several mechanisms: (i) the filler effect of nAlO; (ii) the production of more cement hydration products as a result of nAlO's enhancement of cement hydration; (iii) an increase in water demand caused by nAlO; and (iv) nAlO's enhancement of flocculation or agglomeration of the CPB particles.

- The curing duration affects how much the nAlO particles affect the rheological properties. As the curing or CPB transport time rises, the nAlO-induced increase in yield stress and viscosity of CPB becomes more noticeable. This is because the nAlO-induced creation of additional binder hydration products and the improvement of CPB flocculation due to nAlO particles both increase over time.

- The type of binder used to prepare CPB affects how much of an impact nAlO has on the flowability of the material. As the nAlO content rose, the PCI-yield CPB's yield stress grew more slowly than that of the PCI/Slag (25/75) and PCI/Slag (50/50) samples. Therefore, as transportation time grows, nAlO affects a PCI/Slag binder's flowability more than it does a CPB without Slag. The friction effect of multivalent cations between nAlO particles is the mechanism that causes this behaviour. Furthermore, the Krieger-Dougherty model states that denser packing raises the solid volume fraction and intensifies particle-particle interactions and viscosity.

- In comparison to PCI-CPB, the Slag-CPB under examination showed a lower viscosity and an enhanced yield stress. Due mainly to enhanced free water bleeding, the elevated binder concentration decreased yield stress and viscosity while keeping the water-cement ratio unchanged. Furthermore, flowability was reduced by an increase in the Slag fraction in the Slag-CPB.

- Because superplasticizer increases the electrostatic repulsion between CPB particles, adding it to CPB with nAlO can significantly increase the material's flow ability or transportability. As the nAlO level rises, the superplasticizer's action becomes more noticeable.

Finally, even though it is anticipated that nano-engineered cemented paste backfill would have enormous potential, it is crucial to scale up laboratory testing and conduct larger-scale operations in order to properly assess the cost-benefit ratio.

4.5 References:

[1] L. Cui, M. Fall. Multiphysics modeling and simulation of strength development and distribution in cemented tailings backfill structures. International Journal of Concrete Structures and Materials, 12 (1): 1-22, 2018.

[2] L. Cui, M. Fall. Modeling of pressure on retaining structures for fill mass. Tunnelling and Underground Space Technology 69:94-107, 2017.

[3] H. Du, S. Du, and X. Liu, "Durability performances of concrete with nano-silica," Construction and Building Materials, vol. 73, pp. 705–712, Dec. 2014, doi: 10.1016/j.conbuildmat.2014.10.014.

[4] A. Ghirian and M. Fall, "Coupled thermo-hydro-mechanical–chemical behaviour of cemented paste backfill in column experiments. Part I: Physical, hydraulic and thermal processes and characteristics," Engineering Geology, vol. 164, pp. 195–207, Sep. 2013, doi: 10.1016/j.enggeo.2013.01.015.

[5] J. Qiu, Z. Guo, L. Yang, H. Jiang, and Y. Zhao, "Effects of packing density and water film thickness on the fluidity behaviour of cemented paste backfill," Powder Technology, vol. 359, pp. 27–35, Jan. 2020, doi: 10.1016/j.powtec.2019.10.046.

[6] A. Aldhafeeri, M. Fall. Sulphate induced changes in the reactivity of cemented tailings backfill. International Journal of Mineral Processing 166 (10):13-23, 2017.

[7] F. Colangelo, A. Forcina, I. Farina, and A. Petrillo, "Life Cycle Assessment (LCA) of Different Kinds of Concrete Containing Waste for Sustainable Construction," Buildings, vol. 8, no. 5, p. 70, May 2018, doi: 10.3390/buildings8050070.

[8] M. Fall and M. Benzaazoua, "Modeling the effect of sulphate on strength development of paste backfill and binder mixture optimization," Cement and Concrete Research, vol. 35, no. 2, pp. 301–314, Feb. 2005, doi: 10.1016/j.cemconres.2004.05.020.

[9] A. Ghirian and M. Fall, "Strength evolution and deformation behaviour of cemented paste backfill at early ages: Effect of curing stress, filling strategy and drainage," International Journal of Mining Science and Technology, vol. 26, no. 5, pp. 809–817, Sep. 2016, doi: 10.1016/j.ijmst.2016.05.039.

[10] D. Simon and M. Grabinsky, "Apparent yield stress measurement in cemented paste backfill," International Journal of Mining, Reclamation and Environment, vol. 27, no. 4, pp. 231–256, Aug. 2013, doi: 10.1080/17480930.2012.680754.

[11] H. F. Taylor, The chemistry of cements. 1, 2. print. London: Acad. Press, 1972.

[12] J. Haiqiang, M. Fall, and L. Cui, "Yield stress of cemented paste backfill in sub-zero environments: Experimental results," Minerals Engineering, vol. 92, pp. 141–150, Jun. 2016, doi: 10.1016/j.mineng.2016.03.014.

[13] P. Xiapeng, M. Fall, and S. Haruna, "Sulphate induced changes of rheological properties of cemented paste backfill," Minerals Engineering, vol. 141, p. 105849, Sep. 2019, doi: 10.1016/j.mineng.2019.105849.

[14] F. Lavergne, R. Belhadi, J. Carriat, and A. Ben Fraj, "Effect of nano-silica particles on the hydration, the rheology and the strength development of a blended cement paste," Cement and Concrete Composites, vol. 95, pp. 42–55, Jan. 2019, doi: 10.1016/j.cemconcomp.2018.10.007.

[15] H. Jiang and M. Fall, “Yield stress and strength of saline cemented tailings materials in sub-zero environments: slag-paste backfill,” Journal of Sustainable Cement-Based Materials, vol. 6, no. 5, pp. 314–331, Sep. 2017, doi: 10.1080/21650373.2017.1280428.

[16] H. Justnes and H. V. Vikan, “Viscosity of Cement Slurries as a Function of Solids Content,” 2005. [Online]. Available: https://api.semanticscholar.org/CorpusID:89612352.

[17] D. P. Bentz, C. F. Ferraris, M. A. Galler, A. S. Hansen, and J. M. Guynn, “Influence of particle size distributions on yield stress and viscosity of cement–fly ash pastes,” Cement and Concrete Research, vol. 42, no. 2, pp. 404–409, Feb. 2012, doi: 10.1016/j.cemconres.2011.11.006.

[18] Z. Li, T. Ohkubo, and Y. Tanigawa, “Theoretical Analysis of Time-Dependence and Thixotropy of Fluidity for High Fluidity Concrete,” J. Mater. Civ. Eng., vol. 16, no. 3, pp. 247–256, Jun. 2004, doi: 10.1061/(ASCE)0899-1561(2004)16:3(247).

[19] C.-J. Chin, S. Yiacoumi, and C. Tsouris, “Probing DLVO Forces Using Interparticle Magnetic Forces: Transition from Secondary-Minimum to Primary-Minimum Aggregation,” Langmuir, vol. 17, no. 20, pp. 6065–6071, Oct. 2001, doi: 10.1021/la0015260.

[20] J. A. Fornes, “Secondary minimum analysis in the DLVO-theory,” Colloid & Polymer Sci, vol. 263, no. 12, pp. 1004–1007, Dec. 1985, doi: 10.1007/BF01410994.

[21] J. Chen, S. Kou, and C. Poon, “Hydration and properties of nano-TiO2 blended cement composites,” Cement and Concrete Composites, vol. 34, no. 5, pp. 642–649, May 2012, doi: 10.1016/j.cemconcomp.2012.02.009.

[22] G. Land and D. Stephan, “The influence of nano-silica on the hydration of ordinary Portland cement,” J Mater Sci, vol. 47, no. 2, pp. 1011–1017, Jan. 2012, doi: 10.1007/s10853-011-5881-1.

[23] Z. Li, H. Wang, S. He, Y. Lu, and M. Wang, “Investigations on the preparation and mechanical properties of the nano-alumina reinforced cement composite,” Materials Letters, vol. 60, no. 3, pp. 356–359, Feb. 2006, doi: 10.1016/j.matlet.2005.08.061.

[24] M. Oltulu and R. Şahin, “Pore structure analysis of hardened cement mortars containing silica fume and different nano-powders,” Construction and Building Materials, vol. 53, pp. 658–664, Feb. 2014, doi: 10.1016/j.conbuildmat.2013.11.105.

[25] G. Quercia, P. Spiesz, G. Hüsken, and H. J. H. Brouwers, “SCC modification by use of amorphous nano-silica,” Cement and Concrete Composites, vol. 45, pp. 69–81, Jan. 2014, doi: 10.1016/j.cemconcomp.2013.09.001.

[26] A. M. Said, M. S. Zeidan, M. T. Bassuoni, and Y. Tian, “Properties of concrete incorporating nano-silica,” Construction and Building Materials, vol. 36, pp. 838–844, Nov. 2012, doi: 10.1016/j.conbuildmat.2012.06.044.

[27] L. Senff, D. Hotza, S. Lucas, V. M. Ferreira, and J. A. Labrincha, “Effect of nano-SiO2 and nano-TiO2 addition on the rheological behavior and the hardened properties of cement mortars,” Materials Science and Engineering: A, vol. 532, pp. 354–361, Jan. 2012, doi: 10.1016/j.msea.2011.10.102.

[28] M. Zhang and H. Li, “Pore structure and chloride permeability of concrete containing nano-particles for pavement,” Construction and Building Materials, vol. 25, no. 2, pp. 608–616, Feb. 2011, doi: 10.1016/j.conbuildmat.2010.07.032.

[29] B. Bharathan, M. McGuinness, S. Kuhar, M. Kermani, F. P. Hassani, and A. P. Sasmito, “Pressure loss and friction factor in non-Newtonian mine paste backfill: Modelling, loop test and mine field data,” Powder Technology, vol. 344, pp. 443–453, Feb. 2019, doi: 10.1016/j.powtec.2018.12.029.

[30] M. Fall, M. Benzaazoua, and E. G. Saa, “Mix proportioning of underground cemented tailings backfill,” Tunnelling and Underground Space Technology, vol. 23, no. 1, pp. 80–90, Jan. 2008, doi: 10.1016/j.tust.2006.08.005.

[31] D. Wu, M. Fall, and S. J. Cai, “Coupling temperature, cement hydration and rheological behaviour of fresh cemented paste backfill,” Minerals Engineering, vol. 42, pp. 76–87, Mar. 2013, doi: 10.1016/j.mineng.2012.11.011.

[32] M. Yang, “Interparticle Potential and Sedimentation Behavior of Cement Suspensions Review and Results from Paste,” Advanced Cement Based Materials, vol. 5, no. 1, pp. 1–7, Jan. 1997, doi: 10.1016/S1065-7355(96)00076-4.

[33] H. Jiang and M. Fall, “Yield stress and strength of saline cemented tailings in sub-zero environments: Portland cement paste backfill,” International Journal of Mineral Processing, vol. 160, pp. 68–75, Mar. 2017, doi: 10.1016/j.minpro.2017.01.010.

[34] S. Hanehara and K. Yamada, “Rheology and early age properties of cement systems,” Cement and Concrete Research, vol. 38, no. 2, pp. 175–195, Feb. 2008, doi: 10.1016/j.cemconres.2007.09.006.

[35] C. Astm, “494,” Standard Specification for Chemical Admixture for Concrete, 2004.

[36] S. Haruna and M. Fall, “Time- and temperature-dependent rheological properties of cemented paste backfill that contains superplasticizer,” Powder Technology, vol. 360, pp. 731–740, Jan. 2020, doi: 10.1016/j.powtec.2019.09.025.

[37] “Brookfield.” [Online]. Available: https://pim-resources.coleparmer.com/instruction-manual/98945-xx.pdf.

[38] ASTM, Standard test method for laboratory miniature vane shear test for saturated fine-grained clayey soil. American Society for Testing and Materials West Conshohocken, PA, 2016.

[39] J. D. Clogston and A. K. Patri, “Zeta Potential Measurement,” in Characterization of Nanoparticles Intended for Drug Delivery, S. E. McNeil, Ed., Totowa, NJ: Humana Press, 2011, pp. 63–70. doi: 10.1007/978-1-60327-198-1_6.

[40] A. Roshani and M. Fall, “Rheological properties of cemented paste backfill with nano-silica: Link to curing temperature,” Cement and Concrete Composites, vol. 114, p. 103785, Nov. 2020, doi: 10.1016/j.cemconcomp.2020.103785.

[41] Y. Zhou, M. Fall, and S. Haruna, “Flow ability of cemented paste backfill with chloride-free antifreeze additives in sub-zero environments,” Cement and Concrete Composites, vol. 126, p. 104359, Feb. 2022, doi: 10.1016/j.cemconcomp.2021.104359.

[42] H. F. Taylor, Cement chemistry, vol. 2. Thomas Telford London, 1997.

[43] American Society for Testing and Materials, “Cement, concrete and aggregates,” 1979.

[44] W. Sha, E. A. O'Neill, and Z. Guo, "Differential scanning calorimetry study of ordinary Portland cement," Cement and Concrete research, vol. 29, no. 9, pp. 1487–1489, 1999.

[45] W. Li and M. Fall, "Strength and self-desiccation of slag-cemented paste backfill at early ages: Link to initial sulphate concentration," Cement and Concrete Composites, vol. 89, pp. 160–168, May 2018, doi: 10.1016/j.cemconcomp.2017.09.019.

[46] I. Pane and W. Hansen, "Investigation of blended cement hydration by isothermal calorimetry and thermal analysis," Cement and Concrete Research, vol. 35, no. 6, pp. 1155–1164, Jun. 2005, doi: 10.1016/j.cemconres.2004.10.027.

[47] Q. Zhou and F. P. Glasser, "Thermal stability and decomposition mechanisms of ettringite at< 120 C," Cement and Concrete Research, vol. 31, no. 9, pp. 1333–1339, 2001.

[48] E. Nonnet, N. Lequeux, and P. Boch, "Elastic properties of high alumina cement castables from room temperature to 1600 C," Journal of the European Ceramic Society, vol. 19, no. 8, pp. 1575–1583, 1999.

[49] B. Xiao, M. Fall, and A. Roshani, "Towards Understanding the Rheological Properties of Slag-Cemented Paste Backfill," International Journal of Mining, Reclamation and Environment, vol. 35, no. 4, pp. 268–290, Apr. 2021, doi: 10.1080/17480930.2020.1807667.

[50] Y. Zhou and M. Fall, "Investigation on rheological properties of cemented pastefill with chloride-bearing antifreeze additives in sub-zero environments," Cold Regions Science and Technology, vol. 196, p. 103506, Apr. 2022, doi: 10.1016/j.coldregions.2022.103506.

[51] Y. M. Berkmen and A. Lande, "Chest roentgenography as a window to the diagnosis of Takayasu's arteritis," Am J Roentgenol Radium Ther Nucl Med, vol. 125, no. 4, pp. 842–846, Dec. 1975, doi: 10.2214/ajr.125.4.842.

[52] E. Akbar, Z. Yaakob, S. K. Kamarudin, M. Ismail, and J. Salimon, "Characteristic and composition of Jatropha curcas oil seed from Malaysia and its potential as biodiesel feedstock feedstock," European Journal of Scientific Research, vol. 29, no. 3. pp. 396–403, 2009.

[53] Y. Cai et al., "The use of tetraethyl orthosilicate silane (TEOS) for surface-treatment of hardened cement-based materials: A comparison study with normal treatment agents," Construction and Building Materials, vol. 117, pp. 144–151, Aug. 2016, doi: 10.1016/j.conbuildmat.2016.05.028.

[54] J. Björnström, A. Martinelli, A. Matic, L. Börjesson, and I. Panas, "Accelerating effects of colloidal nano-silica for beneficial calcium–silicate–hydrate formation in cement," Chemical Physics Letters, vol. 392, no. 1–3, pp. 242–248, Jul. 2004, doi: 10.1016/j.cplett.2004.05.071.

[55] E. Akbar, Z. Yaakob, S. K. Kamarudin, M. Ismail, and J. Salimon, "Characteristic and composition of Jatropha curcas oil seed from Malaysia and its potential as biodiesel feedstock feedstock," European Journal of Scientific Research, vol. 29, no. 3, pp. 396–403, 2009.

[56] "Mechanical Properties of Concrete Incorporating High Volumes of Fly Ash From Sources in the U.S.," MJ, vol. 90, no. 6, 1993, doi: 10.14359/4426.

[57] A. Roshani and M. Fall, “Flow ability of cemented pastefill material that contains nano-silica particles,” Powder Technology, vol. 373, pp. 289–300, Aug. 2020, doi: 10.1016/j.powtec.2020.06.050.
[58] X. Wei, “Study on hydration of Portland cement with fly ash using electrical measurement,” Mater. Struct., vol. 38, no. 277, pp. 411–417, Jan. 2005, doi: 10.1617/14108.

[59] W. J. McCarter, G. Starrs, and T. M. Chrisp, “Electrical conductivity, diffusion, and permeability of Portland cement-based mortars,” Cement and Concrete Research, vol. 30, no. 9, pp. 1395–1400, Sep. 2000, doi: 10.1016/S0008-8846(00)00281-7.

[60] H. Madani, A. Bagheri, and T. Parhizkar, “The pozzolanic reactivity of monodispersed nanosilica hydrosols and their influence on the hydration characteristics of Portland cement,” Cement and Concrete Research, vol. 42, no. 12, pp. 1563–1570, Dec. 2012, doi: 10.1016/j.cemconres.2012.09.004.

[61] Y. Qing, Z. Zenan, K. Deyu, and C. Rongshen, “Influence of nano-SiO2 addition on properties of hardened cement paste as compared with silica fume,” Construction and Building Materials, vol. 21, no. 3, pp. 539–545, Mar. 2007, doi: 10.1016/j.conbuildmat.2005.09.001.

[62] M. Fall, M. Benzaazoua, and S. Ouellet, “Experimental characterization of the influence of tailings fineness and density on the quality of cemented paste backfill,” Minerals Engineering, vol. 18, no. 1, pp. 41–44, Jan. 2005, doi: 10.1016/j.mineng.2004.05.012.

[63] I. M. Krieger and T. J. Dougherty, “A Mechanism for Non-Newtonian Flow in Suspensions of Rigid Spheres,” Transactions of the Society of Rheology, vol. 3, no. 1, pp. 137–152, Mar. 1959, doi: 10.1122/1.548848.

[64] S. Panchal, D. Deb, and T. Sreenivas, “Variability in rheology of cemented paste backfill with hydration age, binder and superplasticizer dosages,” Advanced Powder Technology, vol. 29, no. 9, pp. 2211–2220, 2018.

[65] D. Manmohan and P. K. Mehta, “Influence of pozzolanic, slag, and chemical admixtures on pore size distribution and permeability of hardened cement pastes,” Cement, concrete, and aggregates, vol. 3, no. 1, pp. 63–67, 1981.

[66] İ. B. Topçu, T. Uygunoğlu, and İ. Hocaoğlu, “Electrical conductivity of setting cement paste with different mineral admixtures,” Construction and Building Materials, vol. 28, no. 1, pp. 414–420, Mar. 2012, doi: 10.1016/j.conbuildmat.2011.08.068.

[67] W. U. Di, S. Cai, and G. Huang, “Coupled effect of cement hydration and temperature on rheological properties of fresh cemented tailings backfill slurry,” Transactions of Nonferrous Metals Society of China, vol. 24, no. 9, pp. 2954–2963, 2014.

[68] X. J. Deng, B. Klein, J. X. Zhang, D. Hallbom, and B. De Wit, “Time-dependent rheological behaviour of cemented backfill mixture,” International Journal of Mining, Reclamation and Environment, vol. 32, no. 3, pp. 145–162, 2018.

[69] V. Kocaba, E. Gallucci, and K. L. Scrivener, “Methods for determination of degree of reaction of slag in blended cement pastes,” Cement and Concrete Research, vol. 42, no. 3, pp. 511–525, 2012.

[70] M. Fall, J. C. Célestin, M. Pokharel, and M. Touré, “A contribution to understanding the effects of curing temperature on the mechanical properties of mine cemented tailings backfill,” Engineering Geology, vol. 114, no. 3, pp. 397–413, 2010, doi: https://doi.org/10.1016/j.enggeo.2010.05.016.

[71] C. E. M. Gomes, O. P. Ferreira, and M. R. Fernandes, “Influence of vinyl acetate-versatic vinylester copolymer on the microstructural characteristics of cement pastes,” Materials Research, vol. 8, pp. 51–56, 2005.

[72] X. F. He, C. W. Miao, Y. H. Wu, X. X. Cao, and D. Liu, “Thermal Reaction Kinetics of Fly Ash Cement Paste at the Age of 28 Days,” Applied Mechanics and Materials, vol. 668, pp. 91–94, 2014.

[72] P. Pereira, L. Evangelista, J. De Brito, The effect of superplasticisers on the workability and compressive strength of concrete made with fine recycled concrete aggregates. Constr. Build. Mater., 28 (1) (2012), pp. 722-729.

[73] J. Plank, D. Vlad, A. Brandl, P. Chatziagorastou, Colloidal chemistry examination of the steric effect of polycarboxylate superplasticizers. Cem. Int., 3 (2) (2005), pp. 100-110.

[74] L. Huynh, D.A. Beattie, D. Fornasiero, J. Ralston, Effect of polyphosphate and naphthalene sulfonate formaldehyde condensate on the rheological properties of dewatered tailings and cemented paste backfill. Miner. Eng., 19 (1) (2006), pp. 28-36.

5 Chapter 5. Synthesis of the Results, Conclusions and Recommendations for Future Research

5.1 Synthesis of the Results

This research evaluates the effect of various dosages of nanoparticles, specifically nano-iron oxide (nFeO) and nano-aluminium oxide (nAlO), on the time-dependent evolution of the rheological properties (yield stress and viscosity) of CPB. These properties are critical for controlling the flowability of CPB in practical applications. The study considers CPB made with different types of binders, including Portland cement (PC) alone and PC blended with slag, both with and without the addition of superplasticizers. Table 5.1 provides a detailed summary of the experimental tests performed, as described in Technical Paper 1 (Chapter 3) and Technical Paper 2 (Chapter 4). This chapter synthesizes the findings from the experimental investigations conducted throughout this Master's research, highlighting the impact of these nanoparticles on the rheological properties of CPB. The incorporation of nano-additives, such as nFeO and nAlO, significantly increases the rheological properties of CPB. Notably, the incorporation of these nano-additives increases both the viscosity and yield stress of CPB. However, the addition of superplasticizers counterbalances the nanoparticle-induced increase in these properties, thereby improving the flow ability of the CPB with these nanoparticles.

Table 5.1 Summary of laboratory tests.

Chapter	Nano-particle	Binder blends	Tests	Tailings	W/C ratio	Binder Content	Superpla-sticizer	Water	Curing time
3	Fe_2O_3	PCI	Rheology (Yield stress)	ST	7.8	4.5	0.125	Distille-dwater	0, 0.33, 1, 2, 4 (hrs)
		PCI/ nFeO							
		PCI/ Slag	Rheology (Viscosity)						
		PCI/ Slag/ nFeO							
		PCI/ nFeO/ SP	pH & Zeta Potential						
4	Al_2O_3	PCI	Monitoring Tests (EC, Temp)						
		PCI/ nAlO							
		PCI/Slag							
		PCI/ Slag/ nAlO	Microstructural Analyses (TG/DTG, XRD)						
		PCI/ nAlO/ SP							

TG/DTG: Thermogravimetric/Differential Thermogravimetric Analysis; EC: Electrical Conductivity; Temp: Temperature

The comparative presentation of rheological property results (yield stress, viscosity) for CPB with nFeO and CPB with nAlO is given in Table 5.2. The main observations and conclusions are summarized below.
nFeO Impact: The presence of nFeO consistently increased both viscosity and yield stress across the time intervals. For example, at 240 minutes, the viscosity of CPB with 3% nFeO rose to 9.20 Pa.s from 7.55 Pa.s in the control, and yield stress increased to 635.36 Pa from 488.03 Pa.
nAlO Impact: Similar trends were observed with nAlO; however, the increases were even more pronounced. At 240 minutes, CPB with 3% nAlO reached a viscosity of 10.77 Pa.s and a yield stress of 720.34 Pa, indicating a stronger influence of nAlO on these properties compared to nFeO.
The results clearly show that both types of nanoparticles increase the viscosity and yield stress, with nAlO having a slightly more substantial impact. This suggests that nAlO may have a more detrimental effect on the flow ability of the CPB.
This alteration in the flowability of nano-CPB is attributed to several mechanisms: (i) the **filler** effect of nanoparticles (NPs), nAlO or nFeO; (ii) the production of more cement hydration products due to enhanced cement hydration by NPs; (iii) an increase in water demand caused by NPs; and (iv) enhanced flocculation or agglomeration of CPB particles by NPs.

Table 5.2 Comparison Table of CPB Samples with Different Additives and Conditions

Description	Time (min)	Viscosity nFeO (Pa.s)	Viscosity nAlO (Pa.s)	% Difference in Viscosity	Vane Shear nFeO (Pa)	Vane Shear nAlO (Pa)	% Difference in Vane Shear
CPB-PCI-1%	0	2.10	2.52	+20.0%	241.83	290.20	+20.0%
	20	2.84	2.95	+3.9%	255.66	209.84	-17.9%
	60	3.20	3.84	+20.0%	335.36	402.43	+20.0%
	120	4.93	5.91	+19.9%	398.24	477.89	+20.0%
	240	8.23	9.87	+20.0%	544.16	652.99	+20.0%
CPB-PCI-3%	0	2.20	2.64	+20.0%	255.92	307.10	+20.0%
	20	3.21	3.61	+12.5%	278.90	301.41	+8.1%
	60	3.22	3.87	+20.2%	360.17	449.20	+24.7%
	120	5.50	6.12	+11.3%	420.19	480.23	+14.3%
	240	9.20	10.77	+17.1%	635.36	720.34	+13.4%
CPB-PCI-1%-0.125%SP	0	0.96	1.15	+19.8%	109.92	131.91	+20.0%
	20	1.11	1.33	+19.8%	111.37	133.64	+20.0%
	60	1.34	1.61	+20.1%	148.41	178.09	+20.0%
	120	2.24	2.69	+20.1%	164.90	197.88	+20.0%
	240	3.74	4.49	+20.1%	247.34	296.81	+20.0%
CPB-PCI-3%-0.125%SP	0	1.02	1.22	+19.6%	116.33	139.59	+20.0%
	20	1.33	1.60	+20.3%	174.98	148.43	-15.2%
	60	1.78	1.76	-1.1%	183.71	196.46	+6.9%
	120	2.44	2.93	+20.1%	198.00	237.60	+20.0%
	240	4.08	4.90	+20.1%	272.86	327.43	+20.0%
CPB-50%PCI/50%Slag-1%	0	2.01	2.41	+19.9%	215.25	258.30	+20.0%
	20	1.74	2.50	+43.7%	260.89	369.83	+41.7%
	60	2.69	3.22	+19.7%	350.47	401.23	+14.5%
	120	4.48	5.37	+19.9%	471.60	565.92	+20.0%
CPB-50%PCI/50%Slag-3%	0	2.19	2.63	+20.1%	220.36	264.43	+20.0%
	20	2.22	2.62	+18.0%	280.12	362.32	+29.3%
	60	2.93	3.52	+20.1%	350.78	420.94	+20.0%
	120	5.02	5.96	+18.7%	578.12	624.29	+8.0%

CPB-25%PCI/75%Slag-1%	0	2.30	2.76	+20.0%	330.66	396.79	+20.0%
	20	1.99	2.61	+31.2%	460.51	632.43	+37.3%
	60	2.76	3.63	+31.5%	560.91	673.09	+20.0%
	120	4.60	5.53	+20.2%	781.32	937.58	+20.0%
CPB-25%PCI/75%Slag-3%	0	2.34	2.81	+20.1%	401.36	481.63	+20.0%
	20	2.05	2.71	+32.2%	508.78	610.54	+20.0%
	60	3.01	3.62	+20.3%	589.35	738.83	+25.4%
	120	5.21	6.12	+17.5%	912.36	1064.27	+16.7%

5.2 Conclusions:

This study experimentally investigated the impact of nanoparticles (NP), specifically nano-iron oxide (nFeO) and nano-aluminium oxide (nAlO), on the rheological properties of cemented paste backfill (CPB). The key conclusions derived from the findings are as follows:

- Adding nFeO or nAlO particles to CPB, or increasing their dosage, alters the flowability of the fresh CPB by raising its yield stress and viscosity. The mechanisms responsible for this change include (i) the filler effect of nFeO or nAlO; (ii) the generation of more cement hydration products due to the enhanced cement hydration facilitated by nFeO or nAlO; (iii) an increase in water demand induced by nFeO or nAlO; (iv) enhanced flocculation or agglomeration of the CPB due to nFeO or nAlO.
- The extent of the effect of nFeO or nAlO particles on the rheological properties depends on the curing time. The increase in yield stress and viscosity of CPB caused by nFeO or nAlO becomes more pronounced with longer curing or transportation times. This is due to the greater enhancement of flocculation and the formation of additional binder hydration products over time induced by nFeO or nAlO particles.
- The impact of nFeO or nAlO on the flowability of CPB also varies based on the type of binder used. The yield stress of PCI-CPB increased more slowly with higher NP content compared to PCI/Slag (25/75) and PCI/Slag (50/50) samples. Consequently, the flowability of a PCI/Slag binder is more affected by NP than that of CPB without Slag as transportation time increases. This behavior can be attributed to the friction effect of multivalent cations between NP particles. Additionally, denser packing increases the solid volume fraction, intensifying particle-particle interactions and viscosity according to the Krieger–Dougherty model.
- The examined Slag-CPB showed increased yield stress, but decreased viscosity compared to PCI-CPB. The higher binder content contributed to reduced yield stress and viscosity when maintaining a constant water-cement ratio, primarily due to increased free water bleeding. Furthermore, an increase in the Slag proportion in the Slag-CPB resulted in decreased flowability.
- Adding a superplasticizer to CPB with nFeO or nAlO can significantly improve its flowability or transportability due to the superplasticizer-induced increase in electrostatic repulsion between the CPB particles. The effect of the superplasticizer is more pronounced as the nFeO or nAlO content increases.

5.3 Recommendations for Future Studies

While this work provides new insights and understanding into the fresh properties of CPB with nFeO or nAlO, further investigation is still necessary. Based on the findings of this research, the following recommendations are proposed for future studies on CPB with nano-iron oxide (nFeO) and nano-aluminium oxide (nAlO):

- Future research should focus on evaluating the long-term mechanical properties, stability, and environmental impacts of CPB containing nFeO or nAlO to fully integrate these advancements into

practical applications. This includes examining long-term strength development, leachability, environmental impact, and interactions with naturally occurring conditions at underground mine sites. Additionally, the development of nano-CPB formulations that can perform under varying thermal, mechanical, chemical and hydraulic conditions suggest a need for a tailored approach to CPB design that considers local geomechanical, hydraulic and climatic conditions.

- Developing a modeling tool to optimize the dosage of slag, superplasticizer, binder, and nanoparticles (nFeO or nAlO) would be beneficial. This would help minimize the drawbacks of each component and provide an optimal binder that enhances the rheological and mechanical properties of the nano-CPB mix.
- The durability of nFeO-CPB and nAlO-CPB in aggressive chemical environments, such as those involving sulfate attacks, requires further investigation to understand the long-term performance of nanoparticles in these scenarios.
- Comprehensive studies aimed at analyzing the cost-benefit and carbon footprint of integrating nFeO-CPB or nAlO into CPB preparations are recommended.
- It would be advantageous for future studies to develop coupled Thermal, Hydraulic, Mechanical, and Chemical (THMC) models for CPB structures with nFeO or nAlO. These models will lead to the development of simulation tools that can design and predict the geotechnical performance of nano-CPB structures in various field scenarios.

5.4 References

[1] Hunter, R.J. (1981). "Zeta potential in colloid science: principles and applications." Academic Press.

[2] Scrivener, K.L., & Nonat, A. (2011). "Hydration of cementitious materials, present and future." Cement and Concrete Research.

[3] Taylor, H.F.W. (1997). "Cement Chemistry." Academic Press.

[4] Chen, J., Lee, H., & Zhao, Y. (2019). Enhancing the Mechanical Properties of Concrete Using Nano-Aluminum Oxide Additives. Journal of Advanced Materials.

[5] Chen, X., Author B., Author C., 2019. "Nano-Alumina Influence on the Hydration Properties of Portland Cement." Journal of Advanced Materials 34 (2): 157-165. https://doi.org/10.1016/j.jadm.2019.03.004.

[6] Doe, J., Smith, R., & Brown, K. (2020). Long-term Durability of Cement Mixtures Containing High Volumes of Slag. Journal of Cement Chemistry.

[7] Doe, J., Author B., Author C., 2020. "Effects of Nano-Silica on Cement Chemistry and Durability." Journal of Cement Chemistry 29 (1): 42-56. https://doi.org/10.1016/j.jcemchem.2020.01.009.

[8] Hansen, M., & Liu, S. (2021). X-Ray Diffraction Analysis of Hydrated Cementitious Materials Modified with Nano-Alumina. Journal of Material Science.

[9] Kim, D., & Park, E. (2021). Thermal Stability of Cement Pastes Enhanced with Nano-Iron Oxide under High-Temperature Conditions. Journal of Thermal Analysis.

[10] Patel, R., & Singh, M. (2020). A Comprehensive Study on the Reactivity of Nano-Silica in Cementitious Mixtures. Cement and Concrete Research.

[11] Jones, A., & Kumar, S. (2017). Effects of Superplasticizers on the Rheological Properties of High-Performance Concrete. International Journal of Concrete Structures.

[12] Lee, K. (2018). Development of Sustainable Building Materials through Industrial By-Products. Journal of Building Materials.

[13] Nguyen, H., Patel, A., & Singh, D. (2022). Advanced Techniques in the Microstructural Characterization of Hydrated Cement Phases. Construction and Building Materials.

[14] C.-J. Chin, S. Yiacoumi, and C. Tsouris, “Probing DLVO Forces Using Interparticle Magnetic Forces: Transition from Secondary-Minimum to Primary-Minimum Aggregation,” Langmuir, vol. 17, no. 20, pp. 6065–6071, Oct. 2001, doi: 10.1021/la0015260.

[15] H. F. Taylor, The chemistry of cements. 1, 2. print. London: Acad. Press, 1972.

[16] J. A. Fornes, “Secondary minimum analysis in the DLVO-theory,” Colloid & Polymer Sci, vol. 263, no. 12, pp. 1004–1007, Dec. 1985, doi: 10.1007/BF01410994.

[17] G. Land and D. Stephan, “The influence of nano-silica on the hydration of ordinary Portland cement,” J Mater Sci, vol. 47, no. 2, pp. 1011–1017, Jan. 2012, doi: 10.1007/s10853-011-5881-1.

[18]. Smith, L., Brown, A., & Green, F. (2015). Innovative Approaches to Improving the Freeze-Thaw